CELLULAR MECHANISMS OF ADULT NEUROGENESIS

by

Gerald Jan-Yu Sun

A dissertation submitted to Johns Hopkins University

In conformity with the requirements for the degree of Doctor of Philosophy

Baltimore, Maryland

August, 2014

Abstract

The adult mammalian brain possesses the remarkable capacity for generating new neurons throughout life. Adult mouse hippocampal neurogenesis is thought to recapitulate many hallmarks of neurodevelopment and occurs in a spatially-defined, temporally-dilated manner. Because the mature central nervous system context is often thought of as inhospitable to cell growth or genesis, it is important to understand how the complex adult neurogenesis and neurodevelopmental processes can occur, and in what ways these processes may differ from those of embryonic neurogenesis. The thesis research presented here examines how adult mouse hippocampal neurogenesis occurs at a cellular level throughout neural development from stem cell to nerve cell.

The first part of my thesis examines the regulation of cell fate decisions made by neural stem cells to generate diverse cell types in the adult mouse hippocampus. Under normal conditions, neural stem cells generate cells of only the neuronal and astroglial lineages. However, conditional inactivation of an important negative regulator of Ras signaling, neurofibromin 1 (*NF1*), revealed an intrinsic capacity of adult hippocampal neural stem cells to generate the oligodendroglial lineage. This finding suggests a novel, non-canonical paradigm of stem cell regulation via active limitation of stem cell plasticity.

The second part of my thesis examines how newborn neurons migrate within the adult mouse hippocampus. Adult-born hippocampal neurons are glutamatergic, excitatory dentate granule cells that are thought to abide by migration rules of the developing neocortex to migrate exclusively in a radial direction away from the neurogenic niche.

Using a novel system to visualize clones of neurogenic neural stem cells and their clonal progeny, I quantitatively studied newborn neuron migration. I found that newborn neurons exhibit extensive and almost exclusive tangential migration, which utilizes direct contacts with niche vasculature as a migration substrate. This finding represents a novel form of glutamatergic cell migration.

The third part of my thesis examines how newborn neurons grow their dendrites and axons in the adult mouse hippocampus. To date, studying axon development with single-axon resolution has been impossible due to technological limitations precluding capturing whole, intact, fine axonal processes. In collaboration with Kurt Sailor, I developed a new technology, named SEBI (**s**erial **e**nd-**b**lock **i**maging), to seamlessly reconstruct large volumes of tissue and recover full, native, intact cellular structure with high resolution. Using this technology, I studied the development of newborn hippocampal granule cells and discovered complex axonal projections and ordered lamination patterns. My findings represent the first characterization of the development and structure of the full intact, primary dendrite and axon structure for newborn hippocampal granule cells.

In summary, my thesis work presented here has contributed significant novel discoveries in neurodevelopment in the adult mouse hippocampus. I have found novel mechanisms for regulating neural stem cell fate decisions, a new form of excitatory neuron migration, and complex dendrite and axon development in the mature central nervous system. My findings have great relevance to better understanding brain development, degeneration, and regeneration.

Thesis Readers

Hongjun Song, Ph.D. (Advisor), Professor, Department of Neurology

Angelika Doetzlhofer, Ph.D., Assistant Professor, Department of Neuroscience

Preface

First and foremost, I thank my wonderful parents for bringing me into this world, raising me to be a compassionate, responsible, and knowledgeable adult, and their continuing support for me and everything I do. They are my role models. I also thank my brother, who has always taken great care of me and from whom I've learned so much from. I am grateful to Steve Hsaio, David Ginty, Dwight Bergles, and Rick Huganir for believing in me and giving me the opportunity to come to Hopkins and be a part of the Neuroscience family. I am particularly grateful to Steve, who also believed in and recruited my bride-to-be, Ting Feng, to the Neuroscience program. Ting, throughout my graduate career and the rest of my life is my closest companion and who I love dearly (and who contributed behind the scenes to difficult analysis problems for my thesis work here). I owe a lot to Steve Yantis, and his wonderful lab — Mike Esterman, Yu-chin Chiu, and Ben Tamber-Rosenau — along with Ed Connor and R. Jacob Vogelstein, who all helped foster my love of a quantitative systems-level approach to Neuroscience (often involving Matlab heavy-lifting). I also would like to thank my undergraduate research mentors, Bosco Tjan and Eun-jin Lee, for supporting me and providing invaluable research experiences that enabled me to take part in a PhD program.

I of course, am thankful to my mentor, Hongjun Song, for providing a rich, nurturing environment filled with endless possibilities and scientific ideas during my graduate career. In his lab, I owe so much to the mentorship from Michael Bonaguidi, who took me under his wing during my first year rotation, as well as when I joined the lab, and who contributed significantly to my thesis work here. I also thank Kurt Sailor and Yi Zhou

(Joey) for being my close friends and collaborators and for both of their scientific curiosity, innovation, and contributions to the work we did together. None of my work would have been possible if not for the generous contributions of other lab members, especially during my early graduate career: Cindy Liu, Ju-young Kim, Kim Christian, Juan Song, Dengke Ma, Junjie Guo, Chun Zhong, Miheyon Jiang, and Eunchai Kang. And all my work was ultimately a team effort of many other brilliant minds, first and foremost Shiori Ito, who had spent nearly 3 years as a stellar undergraduate research assistant with me, as well as Qasim Hussaini, Genevieve Stein-O'Brien, Sang Hyuck Yu, Deep Singh, Nikhil Chavali, Qasim Mahmood, Jing Hui Adeline Yong, Nicholas Kawasaki, Nikhil Modak, Jerry Ji, and Alex Phan. I am also grateful to the backbone of our lab, Lihong Liu and Yuan Cai, for all their gracious, reliable support; and to my collaborators outside of Hopkins, Yuan Zhu, Nico Toni, and Jon Moss, for their contributions; to the Children's Tumor Foundation for supporting my research; and to all other Song and Ming lab members whom I've had the privilege of working alongside.

I thank my thesis committee: Angelika Doetzlhofer, Erika Matunis, David Ginty, and Dwight Bergles for providing critical feedback and guidance throughout my graduate career and for always looking out for my best interests. I also am grateful for the support of Rita Ragan and Beth Wood-Roig, who together are the dynamic duo that holds our Neuroscience family together. I would also like to thank my Neuroscience classmates, especially Vijay Mohan—together we have been through a wonderful journey.

Finally and again, I thank my family, Ting, and Hongjun—you have all shaped the scientist and person I am today and I am forever grateful.

Contents

Abstract ii

Preface v

List of Figures xii

Abbreviations xiv

1 — Introduction 1

1.1 Regeneration and homeostasis of the adult body 1

1.2 Adult neurogenesis: an overview 2

1.3 Adult neural stem cells of the hippocampus 3

1.4 Intermediate precursors of adult-born dentate granule neurons 5

1.5 Adult-born dentate granule neuron growth and integration 7

2 — General Methods 9

3 — Regulation of adult neural stem cell fate decisions 14

3.1 Introduction 14

3.2 Methods 15

3.3 Results 18

3.3.1 De novo generation of OPC lineage from adult hippocampal neural progenitors 18

3.3.2 Newly generated OPCs are derived from the NF1-inactivated RGL lineage 22

3.3.3 Individual RGLs are intrinsically tri-potent 25

3.3.4 OPCs are generated at the expense of the neuronal lineage 28

3.3.5 Differentiation capacity of de novo generated OPCs 28

3.4 Discussion 32

3.4.1 Active suppression of OPC fate by NF1 35
3.4.2 Neural stem cell tri-potency with mutually exclusive fate choices 36
3.4.3 Differentiation capacity of newborn OPCs 38
3.4.4 Conclusions 38
4 — Adult-born glutamatergic neuron migration 40
4.1 Introduction 40
4.2 Materials and Methods 41
4.3 Results 48
4.3.1 Spatial distribution of clonally-related neuronal progeny with defined birthdate 48
4.3.2 Developmental stage-specific tangential distribution 53
4.3.3 Patterns and magnitude of tangential distribution 57
4.3.4 Vascular substrate for putative tangential migration 60
4.3.5 Global view of neural precursors and niche-wide vascular-mediated migration 66
4.4.1 Tangential migration of glutamatergic neurons 71
4.4.2 Implications of tangential migration as a dominant form of newborn neuron distribution in adult hippocampus 72
4.4.3 New insight into function of vascular niche: substrate for tangential migration 73
4.4.4 Novel approaches for studying newborn neuron development and adult neurogenesis 74
4.4.5 Conclusion 75

5 — Axon and dendrite development of adult-born neurons 76
5.1 Introduction 76
5.2 Methods 77
5.3 Results 86
5.3.1 SEBI of intact cellular structure: whole hippocampus and axonal trajectory of adult-born dentate granule cells 86
5.3.2 Characteristic axonal targeting and growth of individual newborn granule cells in the adult hippocampus 90
5.3.3 Highly organized axonal projections within cohorts of adult-born granule cells 94
5.3.4 Axon bouton development of adult-born dentate granule cells 95
5.3.5 Complete dendritic structure of adult-born granule cells and relationship to axonal development 98
5.4 Discussion 104
5.4.1 Morphology and patterns of adult-born granule cell axons 108
5.4.2 Distinct phases of axonal and dendritic development by adult-born granule cells 110
5.4.3 Coordination of axonal and dendritic development during adult neurogenesis 111
5.4.4 SEBI methodology and considerations 111
5.4.5 Conclusion 112
6 — General Discussion 113
References 120

Curriculum Vitae 132

List of Figures

Figure 1. Conditional inactivation of NF1 in adult hippocampal neural progenitors using Nestin^{CreERT2}-based cell targeting. 20

Figure 2. Clonal lineage tracing of RGLs upon conditional NF1 inactivation using Nestin^{CreERT2}-based cell targeting. 23

Figure 3. Clonal lineage tracing of RGLs upon conditional NF1 inactivation using Gli1^{CreERT2}-based cell targeting. 26

Figure 4. Differentiation capacity of OPCs generated upon NF1 inactivation under physiological and injury conditions. 30

Figure 5. Summary model of neural stem cell fate choice capacity in the adult hippocampus. 33

Figure 6. Tangential distribution of newborn granule neurons away from their parental radial glia-like cells of origin in the dentate gyrus of the adult mouse hippocampus, which were clonally lineage-traced *in vivo*. 50

Figure 7. Developmental stage-specific tangential distribution of newborn neural progeny. 55

Figure 8. Tangential distribution among newborn neural progeny at 3 dpi, 7 dpi, and 1-2 mpi in the adult dentate gyrus. 58

Figure 9. Close association between tangentially migrating neuroblasts and blood vessels in the adult dentate gyrus. 61

Figure 10. Direct contact between tangentially migrating neuroblasts and blood vessels in the adult dentate gyrus. 64

Figure 11. Neuroblast–vasculature interaction using a partial “whole-mount” dentate gyrus SGZ preparation. 67

Figure 12. A two-step model for neuronal migration during adult hippocampal neurogenesis. 69

Figure 13. SEBI imaging paradigm, image reconstruction technique, and normalization. 84

Figure 14. Complete reconstruction of intact adult mouse hippocampus with SEBI. 88

Figure 15. Axonal development, targeting, and organization of newborn granule cells in the adult mouse hippocampus. 92

Figure 16. Axon bouton development of newborn granule cells in the adult mouse hippocampus. 96

Figure 17. Dendritic development of newborn granule cells in the adult mouse hippocampus. 100

Figure 18. Relationship between axonal and dendritic development of individual newborn granule cells during adult hippocampal neurogenesis. 102

Figure 19. Summary of newborn granule cell axonal and dendritic morphological characteristics and development milestones during young adult mouse hippocampal neurogenesis. 105

Figure 20. Neural development in the adult mouse hippocampus from stem cell to nerve cell. 116

Figure 21. SEBI-reconstructed anterior hippocampus from Thy-1-GFP-M mouse, highlighting the still unknown complexities of neural circuits and their development. . 118

Abbreviations

A: astrocyte or astroglial lineage

BV: blood vessel

D: dorsal

GCL: granule cell layer

IN: immature neuron

IPC: intermediate progenitor cell

L: lateral

M: medial

ML: molecular layer

N: mature neuron or neuronal lineage

NB: neuroblast

NF1: neurofibromin 1

NP: neural progenitor

OPC or O: oligodendrocyte progenitor cell or oligodendroglial lineage

RGL or R: radial glia-like cell

S: septal

SGZ: subgranular zone

SVZ: subventricular zone

T: temporal

V: ventral

1 — Introduction

1.1 Regeneration and homeostasis of the adult body

One remarkable theme in organismal biology is the striking capacity for regeneration and maintenance of nearly every somatic tissue. It has been well known that evolutionarily primitive organisms can regrow significant portions of lost body tissue[1]. However more recently it has been appreciated that even evolutionarily complex, high-order organisms possess, albeit more limited, capacity to help replenish lost tissue, repair wounds, and maintain tissue homeostasis throughout adult life. Such capacity is now known to be conferred by adult stem cells that, in many cases, can give rise to all primary cells of a given tissue they serve[2–4].

Extensive work has been performed to understand the regenerative capacity of adult stem cells across many somatic tissues, with broad applicability to understanding tissue function, development, and disease. Adult stem cells have been most readily appreciated in tissues that undergo constant cellular turnover such as in the intestine and skin[4], or those important for reproduction[5]. Most strikingly, in some cases such as the in hematopoietic system, adult stem cells can fully and functionally reconstitute all cell types for a tissue[6].

The adult central nervous system was thought as one of few areas whereby new growth was impossible and hypothesized to be unnecessary or even detrimental to normal brain function[7]. Indeed, Santiago Ramón y Cajal famously deemed the mature central nervous system as a place where “everything may die, nothing may be regenerated” (1913)[8].

Beginning from the first descriptions of putative proliferating cells in rat hippocampus by Altman and Das[9], it has been increasingly clear in the past two decades that the mammalian adult brain—including human brains[10,11]—also possesses stem cells that generate new, functional cells[12,13]. This raises the tantalizing prospect of utilizing neural stem cells to regenerate and repair brain tissue; the existence of adult neurogenesis implies that the adult brain already contains necessary mechanisms to generate, support, and grow new neurons in the mature, dense, and complex network of existing neurons. In order to realize such therapeutic promise, we must first understand the basic cellular mechanisms used to achieve adult neurogenesis: what cells can be generated? How do they migrate to a proper position? How do they grow and integrate into the mature adult circuit?

1.2 Adult neurogenesis: an overview

It is now firmly established that neurogenesis persists in the adult mammalian brain in at least two specific brain regions: the subventricular zone (SVZ) of the lateral ventricles and the subgranular zone (SGZ) of the hippocampal dentate gyrus[12]. In the SVZ, neural stem cells, or type B cells, generate new inhibitory neurons, astroglia, and oligodendroglia[14–16]. Newborn neurons migrate tangentially to the olfactory bulb and develop into periglomerular and granule neurons to modulate its primary circuitry and lack axons[17,18]. In the SGZ, neural stem cells, or radial glia-like cells (RGLs), generate excitatory neurons and astroglia, but not oligodendroglia[19]. Newborn neurons are thought to migrate radially into the dentate gyrus granule cell layer and become excitatory, glutamatergic, principal granule neurons[12,20]. In contrast to the interneurons generated in

SVZ, newborn granule cells possess axons; these extend into CA3 to take part in the hippocampal processing circuit[20,21].

Adult hippocampal neurogenesis in particular provides an elegant platform for studying basic neural stem cell and neurodevelopmental biology. Hippocampal neurogenesis occurs in the restricted space of dentate gyrus; newborn granule neurons remain comparatively close to their adult germinal zone and project axons only within the hippocampus. Therefore sparse labeling of neural stem cells and newborn granule cells allows for high spatial resolution to resolve individual cells for morphological analyses to assess cell divisions, movement, and growth of neurites and processes all in the same brain structure. Further, unlike in embryonic development, the adult brain is more accessible to experimental manipulation and cell dynamics typically occur over a much longer time scale[22]. This high temporal resolution facilitates powerful retrospective analyses of cell behavior. Together, the study of adult hippocampal neurogenesis has allowed for, in the thesis presented here, the answering of fundamental questions in neural stem cell biology and newborn neuron migration, growth, and development.

1.3 Adult neural stem cells of the hippocampus

Adult neural stem cells of the hippocampal dentate gyrus most closely resemble the radial glia neural stem cells of the embryonic brain[23] and are therefore most logically known as radial glia-like stem cells (RGLs). RGLs are $GFAP^{+}Nestin^{+}Sox2^{+}S100\beta^{-}$ and possess a triangular soma with a distinct primary radial fiber that extends through the granule cell layer and terminates into a dense mesh of astrocyte-like processes in the molecular layer

of the dentate gyrus. Although isolated hippocampal progenitors cultured *in vitro* were known to generate neurons and astrocytes[24,25], controversy existed as to whether or not such multi-potent properties could be present *in vivo*, especially given potential alterations of stem cell properties due to *in vitro* culture conditions[25–27]. The development of retroviruses and transgenic mice with cell type specific expression to label neural progenitors of the adult hippocampus gave first hints that neural stem cells existed in the dentate gyrus; replenishment and recovery of neurogenesis upon ablation of mitotic cells further supported this notion[28–32]. However only recently has inducible Cre-Lox technology with clonal labelling finally enabled *in vivo* analysis of RGLs to determine their properties with high spatio-temporal resolution[19]. We now have strong evidence that RGLs generate neurons, generate astrocytes either directly or through terminal differentiation, and symmetrically self-renew and exhibit long-term maintenance[19,33]. In contrast to neural stem cells of the SVZ, however, RGLs lack ability to generate the oligodendroglial lineage under normal conditions[19].

With powerful tools to study RGLs, we have now begun to address critical unanswered questions of neural stem cell biology. It is becoming increasingly clear that neural stem cells face distinct decision points while performing their functions to maintain tissue homeostasis[34]. Cell cycle entry represents one early decision that must be made. Recent data suggests that cell cycle entry is mediated at least in part by PTEN, a negative regulator of PI3K signaling important for controlling cell proliferation. Conditional ablation of PTEN in clonally lineage traced RGLs led to cell cycle entry and their premature terminal differentiation[19]. Cell extrinsically, RGLs were also found to respond

to tonic GABA signaling from local dentate gyrus interneurons via $GABA_A$ receptors. Decreased GABA signaling from interneurons or conditional removal of the γ-2 subunit of the $GABA_A$ receptor in RGLs caused RGLs to enter cell cycle and undergo symmetric self-renewing divisions, highlighting an important coupling of neural circuit activity and neurogenesis[35].

A similarly important, but less well understood decision point of RGLs is that of choosing the fate of the cell to be generated, or cell fate choice. It is currently unknown when an RGL chooses a cell fate, whether there exists a 'point of no return' for fate determination, and most fundamentally, what cell fates are intrinsically available to the RGL to choose from. Forced overexpression of Ascl1 has been shown to transform retrovirally-labeled proliferating SGZ progenitors from neuronal to oligodendroglial fate commitment[21]. In SVZ, infusion of growth factors can potentially de-differentiate newborn progeny into a neural stem cell state[36], and certain injuries have been shown to redirect fate of SVZ neural progeny from neuronal to oligodendroglial lineages[37]. These results are perhaps unsurprising, especially given the notion that adult stem / progenitor cells inherently possess increased capability for reprogramming, as compared to terminally differentiated somatic cells[38]. Nonetheless, mechanisms of cell fate choice of RGLs remain poorly explored.

1.4 Intermediate precursors of adult-born dentate granule neurons

Despite the generation of both new astrocytes and neurons in the hippocampus, the latter has garnered most attention due in large part to the remarkable plasticity they contribute

to the mature neural circuit. Dentate granule neurons are derived from neural intermediate progenitor cells (IPCs). Recent evidence showed that Nestin^{+}GFAP^{+} RGLs directly generate GFAP^{-} IPCs in an asymmetric division[19]. IPCs have small somas with little cytoplasm, possess multiple short processes, and express early neuronal differentiation markers such as Ascl1 and Tbr2 within the first 0-2 days of birth[12]. IPCs are highly proliferative, as evidenced by their rapid expansion of numbers and expression of cell cycle markers such as PCNA, Mcm2, and Ki67[12,19], their ability to incorporate thymidine analogs[39], and their susceptibility to ablation by anti-mitotic drugs[28–30]. IPCs mature into neuronal fate-committed neuroblasts within 3 days of birth.

Neuroblasts possess an elongated cell soma, typically flanked by single long processes tangential to the plane of the SGZ[40]. Neuroblasts express doublecortin (Dcx), PSA-NCAM, Prox1, and can still remain in cell cycle[12]. Although synaptically silent, neuroblasts express functional GABA and glutamate receptors[41] and respond to tonic GABA[42]. Both IPCs and neuroblasts are susceptible to death during an early critical period of survival[43], which is mediated in part by local interneuron activity[44]. Thus, although many neural precursors of dentate granule cells are typically generated, only a subset survive to mature and integrate into the hippocampal circuit. Importantly, although neuroblasts originating from the SVZ are known to migrate tangentially long distances to the olfactory bulb, analogous tangential migration of SGZ neuroblasts has been poorly explored in the adult brain[40]. Whether migration exists for and if so, what may be the precise migration mode of neural precursors of adult-born dentate granule neurons is an important unanswered question.

1.5 Adult-born dentate granule neuron growth and integration

Beyond 7 days, neuroblasts begin penetrating the granule cell layer and orient perpendicular to the SGZ; the process within the GCL becomes dendrite and a process remaining in the SGZ becomes axon[20]. These now post-mitotic 'immature' neurons still express Dcx, PSA-NCAM, and Prox1, but also begin to upregulate neuron-specific proteins such as NeuN. As they continue growth and maturation, immature neurons are thought to migrate radially into the granule cell layer[29]. Generally, granule cells are known to migrate into the granule cell layer over the course of embryonic, early postnatal, and adult life in a manner whereby the oldest cells populate the most distal layers from the subgranular zone[45]. Important extrinsic molecules such as reelin are known to help prevent granule cells from migrating radially in the wrong direction to the hilus[46]; intrinsic regulators such as DISC1 are known to control the extent to which granule cells migrate into the granule cell layer[47].

By ~14 days, immature neurons develop dendritic spines and first receive GABAergic, and then glutamatergic synaptic inputs, whilst also making functional synapses with CA3 pyramidal neurons; these synaptic developmental processes all strikingly resemble those of embryonic and early postnatal development[20,41,42,48–50]. Dendrite and axon growth persists until at least a month after cell birth[20]. During this time, a second critical period for neuron survival occurs, dependent on recruitment of neurons to specific environmental demands[51]. Interestingly, beyond checkpoints for cell survival, a critical period of enhanced synaptic plasticity exists 1-1.5 months after cell birth[52,53]. This critical

period coincides with preferential recruitment of newborn neurons to supporting spatial memory[54].

All characterizations of adult-born dentate granule neuron growth and integration to date were remarkably achieved by utilizing cut tissue sections with incomplete cell structure. Quantified morphological properties of dendritic arbors, and especially long axons projecting to CA3, were therefore estimations. To date, visualization of the entire axo-dendritic structure of cells has been lacking due in large part to an inability image or reconstruct sufficiently large tissue volumes to fully capture entire cell morphology. We therefore have incomplete knowledge of the full complexity and architecture of newborn neurons, how they grow, and what unique features they may possess that illustrate their remarkable capacity to grow and integrate into a mature central nervous system environment and circuit.

2 — General Methods

Experimental animals and animal procedures

Adult, 8-10 week old mice were used and, where applicable, were backcrossed to the C57BL/6 background for at least six generations. Animals were housed in a 14 hour light/10 hour dark cycle and had free access to food and water. To fluorescently label cells for visualization and analysis, genetic or viral-based approaches were used, and animals were killed at distinct time points after cell labeling to perform retrospective analyses on cell growth, movement, or behavior. For genetic-based approaches, tamoxifen (66.67 mg/ml, Sigma, T5648) was prepared in a 5:1 corn oil (Sigma) to ethanol mixture and injected intraperitoneally. For viral-based approaches, or those requiring direct injection into brain, compounds were stereotaxically injected directly into dentate gyrus of 8-week-old mice using a Nanoject II microinjection glass pipette (Drummond Scientific) with a 5-20 μm tip at 1-2 injection sites per hemisphere. All animal procedures were performed in accordance to institutional guidelines of Johns Hopkins University School of Medicine.

Tissue processing, immunostaining and confocal imaging

Animals were transcardiac perfused with cold 4% paraformaldehyde (wt/vol, in 0.1 M phosphate buffer, PB, pH 7.4), and cryoprotected with 30% sucrose (wt/vol) or simply stored in 0.1 M phosphate buffered saline (PBS). Serial brain sections were cut on either a frozen sliding microtome (Leica Microsystems, SM2010R) or a vibrating microtome (Leica Microsystems, VT1200). For sections requiring immunostaining to reveal various proteins of interest, antibodies (Table 1) were diluted in tris-buffered saline (TBS) with

0.05% Triton X-100 and 3% donkey serum, and incubated overnight at 4°C. Secondary Alexa Fluor antibodies (488, 546, 594, or 647) of the appropriate matching animal species antigen were then incubated at room temperature for 2 hours before sections were taken for mounting and coverslipping on slides for visualization and imaging. A DAPI (4',6-diamidino-2-phenylindole) counterstain was employed to visualize cell nuclei.

Antigen	Manufacturer	Host	Dilution
CD31	BD Biosciences	Rat	1:500
CNPase	Millipore	Mouse	1:500
DCX	Santa Cruz Biotechnology	Goat	1:100
γ-tubulin	BioLegend	Rabbit	1:500
GFAP	Millipore	Mouse	1:1000
GFAP	DAKO	Rabbit	1:1000
GFP	Aves Labs	Chicken	1:500
GFP	Rockland	Goat	1:500
GM130	BD Biosciences	Mouse	1:250
NG2	Millipore	Rabbit	1:200
Nestin	Aves Labs	Chicken	1:500
NeuN	Millipore	Guinea pig	1:500
Prox1	Abcam	Rabbit	1:500
Prox1	Millipore	Mouse	1:500
Tbr2	Abcam	Rabbit	1:250

Table 1. Primary antibodies used.

When needed, antigens were retrieved by incubating brain sections in 1X DAKO target retrieval solution (DAKO) at 68°C for 20 minutes, followed by 10 minutes cooling to room temperature. Confocal imaging was performed at 40X (1.4 numerical aperture) on a Zeiss LSM 710 confocal microscope using multi-track or spectral linear unmixing 'online fingerprinting' configurations (Carl Zeiss). Multi-photon imaging was performed with a 2-photon laser (Coherent, Chameleon) at 20X (1.0 numerical aperture) on a Zeiss LSM 510 microscope using non-descanned detectors.

Image processing and data analyses

All data were analyzed in Imaris software (Bitplane) utilizing various Imaris modules for digital annotations such as cell morphology tracing and marking of cell location in 3D space. When needed, large-volume image reconstructions were executed in Reconstruct (John C. Fiala, NIH) or XuvStitch[55] software. Imaging artifacts precluding accurate data analysis were corrected using 3D deconvolution (Media Cybernetics, Autoquant) or custom written quantile normalization code in Matlab (The Mathworks). Digital annotations were directly imported into Matlab (The Mathworks) via the Imaris Xtension capability for further quantitative analyses.

Statistical analysis

Statistical analysis was performed with one-way ANOVA (with Tukey *post hoc* test), one- or two-tailed unpaired Student's *t* test, or two-sample Kolmogorov-Smirnov test (with Bonferroni correction for multiple comparison, where applicable). When applicable, validation of normality and homogeneity of variance assumptions was

performed using a Shapiro-Wilk test and Monte-Carlo simulation, respectively. All statistical analyses were performed in Origin Software (OriginLab) or Matlab.

3 — Regulation of adult neural stem cell fate decisions

3.1 Introduction

In a classical model of cell differentiation proposed by Waddington (1940)[56], cell fate commitment occurs irreversibly much as a ball rolling down one of many paths into a specific valley; there clearly exists a cellular hierarchy whereby undifferentiated cells with unlimited cell fate potential reside at the top, and whereby reversion up the hierarchy often requires directed artificial reprogramming[57,58]. Between the two extremes of totipotent and fully differentiated cells there exist unique, often multi-potent cells that populate a multitude of niches across the adult mammalian body to contribute new cells for maintaining tissue homeostasis. Emerging evidence suggests that these cells possess a striking capacity for plasticity in cell fate choices beyond their normal repertoire in specific contexts such as injury or disease[59]. How somatic stem cells can have access to some cell fates, but not others, or what regulates their cell fate plasticity is poorly explored.

Stem cells are regulated by a multitude of extrinsic and intrinsic processes that dictate cell development and tissue morphogenesis. Intrinsically, both active and passive transcription control mechanisms help execute differentiation cascades and maintain cellular identity[60]. Extrinsically, secreted morphogens, growth factors, and adhesion molecules direct cell differentiation into complex patterns characteristic of each body tissue and thus impinge on intrinsic cell fate decisions[61]. Thus, transducers of external signals, such as Ras proteins and their regulators, serve as critical points of convergence for affecting cell behavior. One such negative regulator of Ras-mediated signaling,

neurofibromin 1 (NF1), is known to control the balance and abundance of cell types, most markedly in the nervous system, whereby its loss of function leads to rampant tumorigenesis and cognitive impairment[62]. Whether or how NF1 directly regulates stem cell behavior is unclear due in large part to a lack of an appropriately sensitive assay to examine stem cells with single clone resolution, *in vivo*.

The adult mammalian hippocampus contains radial glia-like neural stem cells (RGLs) that possess the capacity for self-renewal and bi-potential fate choice to generate new neurons and astrocytes[12]. We recently developed a method to clonally lineage-trace RGLs and examine their behaviors under normal conditions and upon specific genetic ablation in either quiescent or activating RGLs[19] (Bonaguidi, Stadel et al., unpublished). Utilizing this powerful approach alongside traditional population-based analyses, I studied the effects of conditional NF1 inactivation in RGLs to finely dissect stem cell fate choice behavior. I surprisingly found that upon NF1 inactivation, RGLs generated cells of a new lineage, oligodendrocyte progenitor cells (OPCs). These findings suggest that RGLs may possess intrinsic tri-potency, which is actively suppressed in an NF1-dependent manner. Stem cells may therefore intrinsically possess fate choices that remain hidden under normal circumstances due to active suppression mechanisms that restrict the cells to only a subset of available fate choices.

3.2 Methods

Animals and tamoxifen administration

Nestin^{CreERT2}*;Nf*$^{f/f}$*;Z/EG*$^{f/-}$, Nestin^{CreERT2}; Nf1$^{f/+}$; Z/EG, and *Nestin*^{CreERT2}*;Z/EG*$^{f/-}$ mice were generated by crossing *Nestin*^{CreERT2} [63] with *Z/EG*$^{f/-}$ (Tg(CAG-Bgeo/GFP)21Lbe/J, Jackson Labs) and *Nf1*$^{f/f}$ mice[64], where applicable. *Gli1*^{CreERT2}*;Nf*$^{f/f}$*;Z/EG*$^{f/-}$and *Gli1*^{CreERT2}*;Z/EG*$^{f/-}$ mice were generated in a similar fashion, but with *Gli1*^{CreERT2} mice[30]. All mice in the study were backcrossed to the C57BL/6 background for at least six generations. Animals were housed in a 14 hour light/10 hour dark cycle and had free access to food and water. Tamoxifen (66.67 mg/ml, Sigma, T5648) was prepared in a 5:1 corn oil (Sigma) to ethanol mixture. To achieve sparse labeling for clonal analysis (~8-16 clones per hemisphere), a single 62.5 mg/kg dose of tamoxifen (for *Nestin*^{CreERT2}) or a 125 mg/kg dose every 12 hours for 4 total doses (for *Gli1*^{CreERT2}) was intraperitoneally injected into adult 8-10 week-old male and female mice. For denser, 'population' cell labeling (in *Nestin*^{CreERT2}), a 125 mg/kg dose every 12 hours for 4 total doses was injected. Animals were analyzed at 2 or 14 days post-tamoxifen injection (dpi), or 1-2 months post-tamoxifen injection (mpi). All animal procedures were performed in accordance to institutional guidelines of Johns Hopkins University School of Medicine.

Stereotaxic injection

Lysolecithin (Sigma, L4129) was sonicated into in 0.9% sterile saline and 1 μl of 1% (wt/vol) solution was stereotaxically injected into dentate gyrus of 8-week-old mice using a Nanoject II microinjection glass pipette (Drummond Scientific) with a 20 μm tip at the following coordinates relative to bregma (mm): posterior −2.0, lateral +1.6, ventral −1.6. Wild-type and *Nestin*^{CreERT2}*;Nf*$^{f/f}$*;Z/EG*$^{f/-}$ animals were analyzed at 5 or 30 days post-lysolecithin injection, respectively. For *Nestin*^{CreERT2}*;Nf*$^{f/f}$*;Z/EG*$^{f/-}$ animals, lysolecithin

was injected 3 days after the final of four 125 mg/kg tamoxifen injections given every 12 hours.

Tissue processing, immunostaining and confocal imaging

Animals were transcardiac perfused with cold 4% paraformaldehyde (wt/vol, in 0.1 M phosphate buffer, PB, pH 7.4), and cryoprotected with 30% sucrose (wt/vol). Serial 40 μm-thick coronal brain sections were cut on a frozen sliding microtome (Leica, SM2010R) for immunohistology as previously described (Bonaguidi et al., 2011). Antibodies diluted in TBS with 0.05% Triton X-100 and 3% donkey serum, were used against GFP (Aves Labs, chicken, 1:500; Rockland, goat, 1:500), Tbr2 (Abcam, rabbit, 1:250), GFAP (Millipore, mouse, 1:1000; DAKO, rabbit, 1:1000), Nestin (Aves Labs, chicken, 1:500), Prox1 (Millipore, mouse, 1:500), NG2 (Millipore, rabbit, 1:200), and CNPase (Millipore, mouse, 1:500). Nestin antigen was retrieved by incubating brain sections in 1X DAKO target retrieval solution (DAKO) at 68°C for 20 minutes, followed by 10 minutes cooling to room temperature. Serial sections from the entire dentate gyrus were first immunostained for GFP to allow identification of prospective clone-containing sections on an epifluorescence microscope (Zeiss, Axiovert 200M). Labeled clone-containing sections were taken for further processing and confocal imaging at 40X on a Zeiss LSM 710 confocal microscope using multi-track or spectral linear unmixing 'online fingerprinting' configurations (Carl Zeiss).

Image processing and data analyses

For population cell labeling experiments, cells were counted manually by visualizing the serial dentate gyrus sections on an epifluorescence microscope. For clonal cell labeling experiments, identification of clones amongst GFP-labeled clusters of cells was performed as previously described[19]. Clones that spanned multiple serial sections were reconstructed using Reconstruct software (John C. Fiala, NIH). All aligned images were exported at full resolution for 3D visualization into Imaris (Bitplane) and analyzed. All other confocal images were directly visualized and analyzed in Imaris. Clones were analyzed in a dentate gyrus volume that included the molecular layer, granule cell layer, subgranular zone, and hilus, excluding the polymorphic layer (CA4) protruding into the posterior dentate gyrus. Clone cell fate frequencies were calculated per dentate gyrus and averaged. Statistical analysis was performed with a two-tailed unpaired Student's *t* test. All statistical analyses were performed in Origin Software (OriginLab) or Matlab.

3.3 Results

3.3.1 De novo generation of OPC lineage from adult hippocampal neural progenitors

To target Nf1 inactivation in adult hippocampal neural progenitors, I used a tamoxifen-inducible Nestin^{CreERT2} mouse line that possessed floxed Nf1 exons 31 and 32 and a Z/EG reporter (Nestin^{CreERT2}; Nf1$^{f/f}$; Z/EG[63–65]). Multiple tamoxifen injections were given to experimental animals to ensure complete recombination of alleles; similar paradigms have been previously validated to successfully conditionally inactivate NF1 in the adult hippocampal niche[66]. I observed similar numbers of total neuronal progeny generated 1 month post-tamoxifen injection in Nestin^{CreERT2}; Nf1$^{f/f}$; Z/EG (Nf1^{Nestin}) versus

Nestin^{CreERT2}; Z/EG (control^{Nestin}) animals (mpi; Fig. 1A, B). Surprisingly, in only Nf1^{nestin} animals, I observed a significant presence of GFP-expressing cells with morphology of oligodendrocyte progenitor cells (OPCs). These cells possessed histological features characteristic of OPCs, as they expressed NG2 but not GFAP (Fig. 1C). Consistent with previous characterizations of adult hippocampal neural progenitors[19], OPCs were never observed in control^{Nestin} animals (n = 4897 total cells) or Nestin^{CreERT2}; Nf1$^{f/+}$; Z/EG animals (n = 3204 total cells), suggesting that biallelic NF1 inactivation is required for putative OPC genesis.

Both inactivation of NF1 in OPCs and stress are known to induce OPC proliferation, *in vivo*[67,68]. To rule out the possibility that rare OPCs were labeled initially, I examined cells from 2 days post-tamoxifen injectin (dpi) in Nf1^{Nestin} and control^{Nestin} animals. In both cases, no NG2-expressing cells or cells with OPC morphology were observed in hippocampus (Fig. 1D, E; n = 1876 cells in control^{Nestin}, 670 cells in Nf1^{Nestin}). Therefore together, these data show for the first time *de novo* generation of the OPC lineage from adult neural progenitors of the hippocampus.

Figure 1. Conditional inactivation of NF1 in adult hippocampal neural progenitors using Nestin^{CreERT2}-based cell targeting.

A, Sample projected confocal image of representative coronal section in population-labeling paradigm at 1 mpi in control^{Nestin} (left) and Nf1^{Nestin} (right) animals. **B,** Quantification of total GFP^{+} cell numbers, by lineage, across the dentate gyrus in control^{Nestin} versus Nf1^{Nestin} animals at 1 mpi. Values represent mean ± s.e.m. **C,** High magnification projected confocal image of the boxed region in A. Filled arrowheads denote GFP^{+}NG2^{+}GFAP^{-} OPCs (O). **D,** Representative GFP^{+} cells at 2 dpi include RGLs (R), astrocytes (A), and newborn intermediate neural progenitor cells (N) in Nf1^{Nestin} animals. No NG2-expressing GFP^{+} cells are present. **E,** Quantification of total GFP^{+} cell numbers, by lineage, across the dentate gyrus in control^{Nestin} versus Nf1^{Nestin} animals at 2 dpi. Values represent mean ± s.e.m. Scale = (A) 100 μm, (C-D) 10 μm.

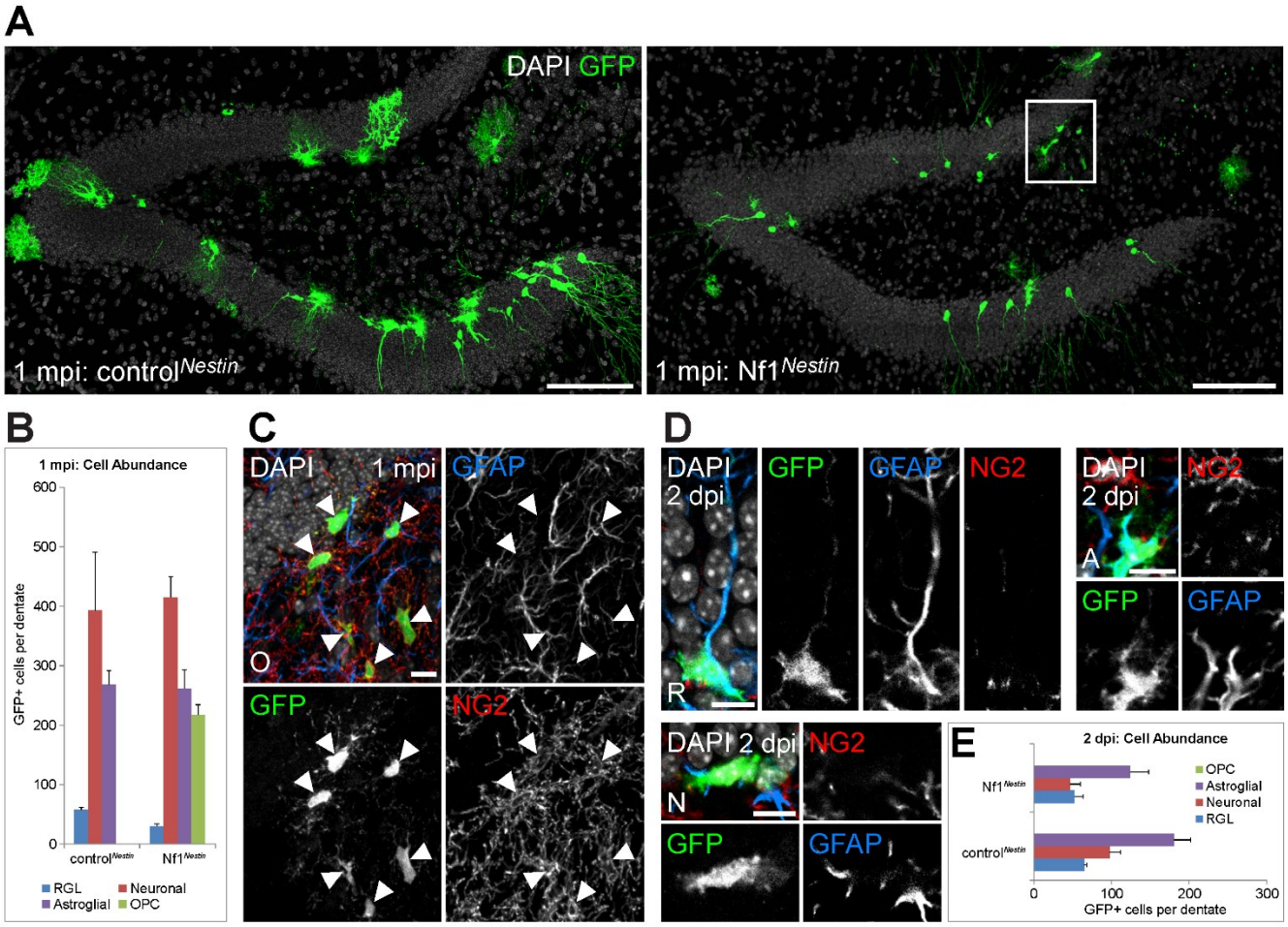
A
DAPI GFP
1 mpi: control Nestin
1 mpi: Nf1 Nestin
B
1 mpi: Cell Abundance
GFP+ cells per dentate
600
500
400
300
200
100
0
control Nestin
Nf1 Nestin
RGL
Neuronal
Astroglial
OPC
C
DAPI
1 mpi
GFAP
O
GFP
NG2
D
DAPI
2 dpi
GFP
GFAP
NG2
R
DAPI
2 dpi
NG2
A
GFP
GFAP
DAPI 2 dpi
NG2
N
GFP
GFAP
E
2 dpi: Cell Abundance
Nf1 Nestin
control Nestin
OPC
Astroglial
Neuronal
RGL
0
100
200
300
GFP+ cells per dentate

3.3.2 Newly generated OPCs are derived from the NF1-inactivated RGL lineage

To investigate the origin of newly generated OPCs upon NF1 inactivation, I performed clonal lineage tracing of radial glia-like adult neural stem cells (RGLs) in the hippocampus. Utilizing a single low-dose tamoxifen injection in $Nf1^{Nestin}$ and $control^{Nestin}$ mice, I sparsely labeled on average 10 ± 1 precursors across the entire dentate gyrus at 2 dpi. Similar to that seen at the population level with multiple tamoxifen injections, no NG2-expressing cells or cells with OPC morphology were observed in any clones at 2 dpi. At 1-2 mpi, I observed rare clones (6/142) that contained NG2-expressing cells with OPC morphology (Fig. 2A, B). Some clones possessed a maintained RGL in close proximity to and at the center of a large clone containing both astrocytes and OPCs but not neurons (Fig. 2A); other clones lacked RGLs, potentially due to differentiation or death (Fig. 2B). Our previous comprehensive characterizations of RGLs demonstrated that RGLs never generate OPCs under normal conditions[19]. In the current study, RGLs undergoing even four rounds of cell cycle entry still failed to generate OPCs in $control^{Nestin}$ animals (Fig. 2C). Most clones (134/142) possessed no overt phenotype, potentially due to incomplete recombination of both the reporter and Nf1 floxed alleles in the same cells (Fig. 2D). However, consistent with a previous study[66], some $Nf1^{Nestin}$ clones at 1-2mpi contained neurons ectopically migrated to the dentate gyrus molecular layer, indicative of successful NF1 inactivation (Fig. 2E). In all, these data provide strong evidence that only upon NF1 inactivation, OPCs are generated and generated from the RGL lineage. These data thus reveal for the first time a new fate capacity of RGLs in the adult hippocampus.

Figure 2. Clonal lineage tracing of RGLs upon conditional NF1 inactivation using Nestin^{CreERT2}-based cell targeting.

A, Clone at 2 mpi in Nf1^{Nestin} animal with maintained RGL (*), OPCs (filled arrowheads), and astrocytes (open arrowheads). Shown also is a proposed lineage tree for the clone. Inset: putative OPCs express NG2, a marker characteristic of only the OPC lineage. Scale = 50 μm, (inset) 10 μm. **B,** Clone at 2 mpi in Nf1^{Nestin} animal with putative differentiated RGL (*), OPCs (filled arrowheads), and astrocytes (open arrowheads). Shown also is a proposed lineage tree for the clone. Inset: putative differentiated RGL still possesses radial morphology but lacks expression of nestin, a marker for RGLs. Scale = 50 μm, (inset) 10 μm. **C,** Clone at 1 mpi in control^{Nestin} animal with maintained RGL (R1, R2) that underwent at least three rounds of division to symmetrically self-renew into two nestin^{+} RGLs (R1, R2), generate two distinct clusters of Tbr2^{+} newborn intermediate neural progenitor cells (N1, N2), and a nestin^{-} astrocyte (A). Shown also is a proposed lineage tree for the clone. Scale = 10 μm. **D,** Quantitative comparison of the frequency of different RGL fate choices observed at 1 mpi in control^{Nestin} versus Nf1^{Nestin} animals. Values represent mean ± s.e.m. R, RGL; A, astroglia; N, neuronal lineage; O, OPC. **E,** Clone at 1 mpi in Nf1^{Nestin} animal with Prox1^{+} newborn dentate granule neurons (N1, N2) ectopically migrated into the molecular layer (ML) of dentate gyrus. ML, molecular layer; GCL, granule cell layer; SGZ, subgranular zone. Scale = 10 μm.

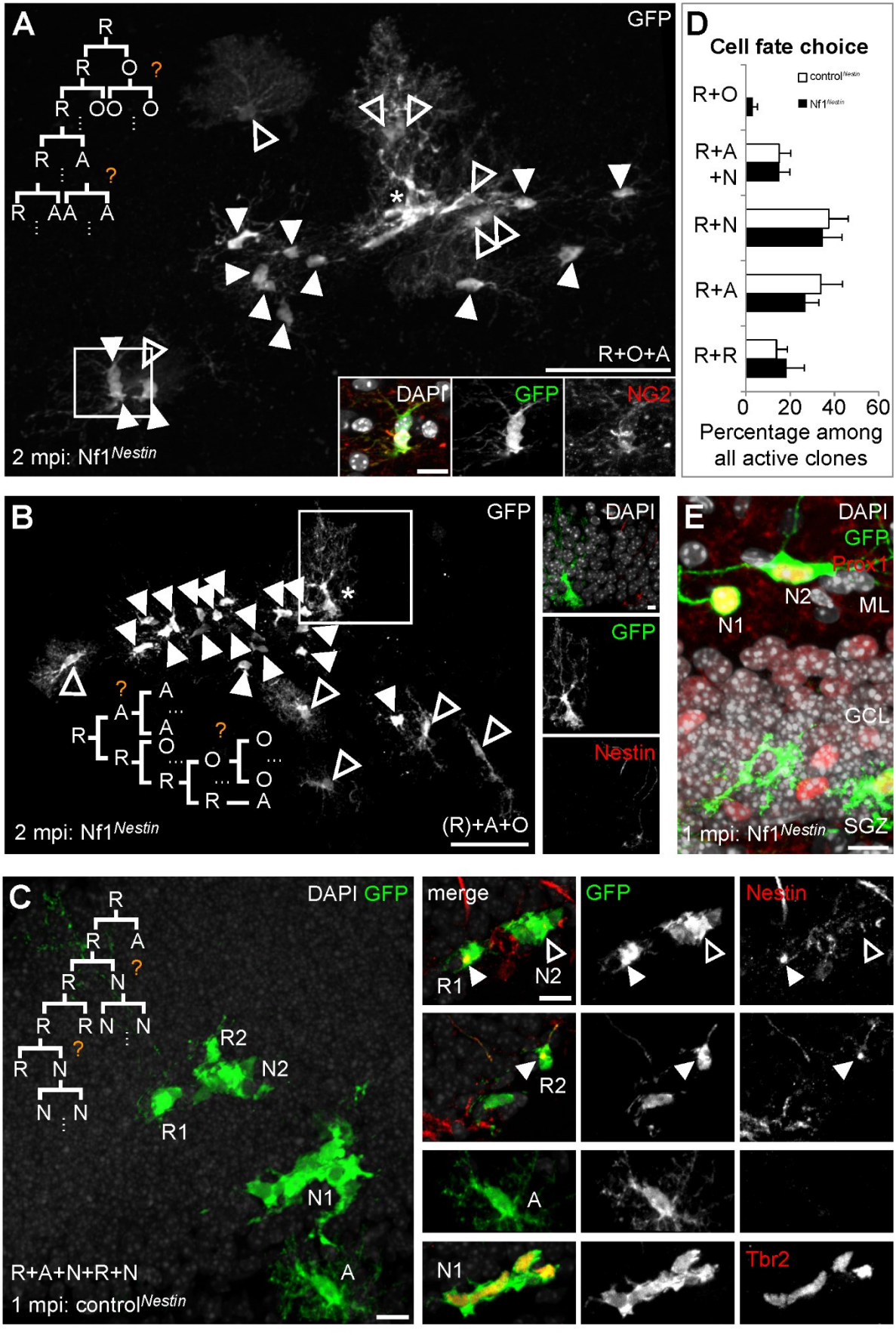
A
GFP
R+O+A
DAPI
GFP
NG2
2 mpi: Nf1Nestin
D
Cell fate choice
controlNestin
Nf1Nestin
R+O
R+A +N
R+N
R+A
R+R
0 20 40 60
Percentage among all active clones
B
GFP
DAPI
GFP
Nestin
2 mpi: Nf1Nestin
(R)+A+O
E
DAPI
GFP
Prox1
N2
ML
N1
GCL
SGZ
1 mpi: Nf1Nestin
C
DAPI GFP
R2
N2
R1
N1
A
R+A+N+R+N
1 mpi: controlNestin
merge
GFP
Nestin
R1
N2
R2
A
N1
Tbr2

3.3.3 Individual RGLs are intrinsically tri-potent

Emerging evidence suggests that RGLs may be a heterogeneous mix of discrete stem cells with unique cell fate potentials (Bonaguidi, Stadel., et al., unpublished). I therefore next asked whether a single RGL possessed the capacity to give rise to all three primary lineages of the nervous system: neuronal, astroglial, and oligodendroglial. The Nestin^{CreERT2} clonal lineage-tracing strategy preferentially enriches for quiescent RGLs[19], precluding high-throughput analysis of RGLs that have undergone multiple rounds of cell cycle and generated OPCs. I thus performed clonal lineage tracing in a tamoxifen-inducible Gli1^{CreERT2} mouse line, which labels the same population of RGLs as in the Nestin^{CreERT2} line, but in an activating state (Fig. 3A; Bonaguidi, Stadel, et al., unpublished). Clonal lineage-tracing was performed in Gli1^{CreERT2}; Nf1$^{f/f}$; Z/EG (Nf1^{Gli1}) and Gli1^{CreERT2}; Nf1$^{f/f}$; Z/EG (control^{Gli1}) animals. Similar to that seen in Nestin^{CreERT2}-based analysis, no NG2-expressing cells or cells with OPC morphology were observed at 2 dpi (0 of 52 clones). At 1 mpi, I observed OPC-containing clones in Nf1^{Gli1} animals (Fig. 3B), but never control^{Gli1} animals (Fig. 3C), independently validating my findings from Nestin^{CreERT2}-based analyses. Strikingly, some clones at 1 mpi in Nf1^{Gli1} animals contained three lineages: mature neurons, astrocytes, and OPCs. RGLs therefore possess the intrinsic ability to generate all three major lineages of the nervous system, and this ability is actively restricted by NF1.

Figure 3. Clonal lineage tracing of RGLs upon conditional NF1 inactivation using Gli1^{CreERT2}-based cell targeting.

A, RGL at 2 dpi in Nf1^{Gli1} animal undergoing neurogenic division. Scale = 10 μm. **B,** Tri-lineage clone at 1 mpi in Nf1^{Gli1} animal with lost or differentiated RGL, astrocytes (open arrowheads), OPCs (closed arrowheads), and mature newborn neurons. Inset: high magnification confocal image of boxed region denoting NG2^{+} OPC. Shown also is a proposed lineage tree for the clone. Scale = 50 μm, (inset) 10 μm. **C,** Clone at 1 mpi in control^{Gli1} animal with maintained RGL (boxed) and mature newborn neurons. Shown also is a proposed lineage tree. Inset: maintained nestin^{+} RGL. Scale = 10 μm. **D,** Quantification of total GFP^{+} cell numbers for only mature neurons and immature neuronal progeny in control^{Nestin} versus Nf1^{Nestin} animals at 1 mpi. *$p < 0.05$, two-sample unpaired Student's t-test.

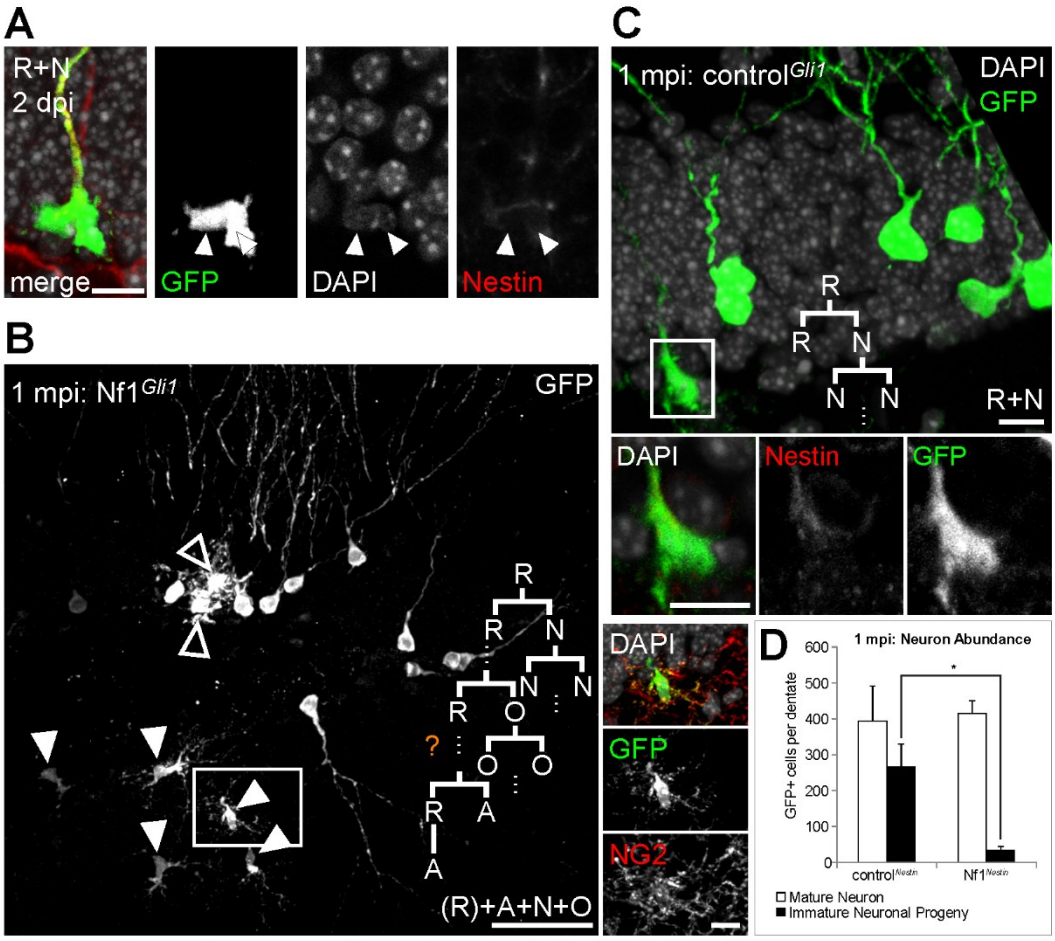
A
R+N
2 dpi
merge
GFP
DAPI
Nestin
B
1 mpi: Nf1Gli1
GFP
R
R N
N N
R O
? O O
R A
A
(R)+A+N+O
C
1 mpi: controlGli1
DAPI
GFP
R
R N
N N
R+N
DAPI
Nestin
GFP
DAPI
GFP
NG2
D
1 mpi: Neuron Abundance
GFP+ cells per dentate
600
500
400
300
200
100
0
*
*
controlNestin
Nf1Nestin
Mature Neuron
Immature Neuronal Progeny

3.3.4 OPCs are generated at the expense of the neuronal lineage

Despite the capacity of RGLs for tri-potential fate choice, the neuronal lineage was strikingly absent in all OPC-containing clones examined in $Nf1^{Nestin}$ animals (6 of 6 clones). Further, only mature neurons and never immature newborn neural progeny were observed in all OPC-containing clones in $Nf1^{Gli1}$ animals (9 of 9 clones). One interpretation of these observations is that neurons could only be generated before NF1 inactivation but not afterwards, and that daughter cell fate was determined by the RGL before the effects of the NF1 inactivation event. To examine this further, clones in $Nf1^{Gli1}$ and $control^{Gli1}$ animals were analyzed at 14 dpi, a time when cells from only the initial round of division had matured. No clones were found to contain OPCs in either $control^{Gli1}$ or $Nf1^{Gli1}$ animals (0 of 95 clones). At the population level in $Nf1^{Nestin}$ animals at 1 mpi, although similar numbers of mature neurons were observed versus in $control^{Nestin}$ animals (Fig. 1B), significantly fewer immature neuronal progeny were observed versus in $control^{Nestin}$ animals (Fig 3D). These data suggest that the first fate of activating RGLs was unaffected by NF1 inactivation, and importantly, that the OPC lineage may be generated at the expense of the neuronal lineage upon NF1 inactivation.

3.3.5 Differentiation capacity of de novo generated OPCs

OPCs serve as a progenitor pool to replenish oligodendrocytes throughout life[69], I therefore examined whether OPCs generated in NF1 inactivation conditions could differentiate into mature oligodendrocytes. Across all clones and cells, I only observed a single clone in an $Nf1^{Nestin}$ animal containing GFP-expressing cells that expressed the oligodendrocyte marker, CNPase, and possessed morphology characteristic of a

myelinating oligodendrocyte (Fig. 4A). To examine this further with conditions more conducive to OPC differentiation, I performed a demyelinating lesion with lysolecithin. At 5 days post-lesion in wild-type animals, considerable loss of myelination and OPCs was observed, in addition to an expected proliferation response of SGZ progenitors in response to the injury[29] (Fig. 4B). I then performed a demyelinating lesion in $Nf1^{Nestin}$ animals given multiple tamoxifen injections, as previously, and 3 days prior to the lesion. At 1 month post-lesion, OPCs were abundant in addition to neurons (Fig. 4C). No GFP-expressing cells expressed molecular markers or morphology of oligodendrocytes, despite a clear qualitative recovery of myelination and OPCs (cf. Fig. 4B, C). In addition, although some cells displayed clear OPC morphology, they lacked both NG2 and CNPase immunoreactivity, suggesting potential, but not complete differentiation (Fig. 4C, open vs. closed arrowheads). OPCs generated upon NF1 inactivation therefore possess the capacity for differentiation into oligodendrocytes, but may not be successfully recruited for myelination repair during severe injury conditions.

Figure 4. Differentiation capacity of OPCs generated upon NF1 inactivation under physiological and injury conditions.

A, Clone at 1 mpi in $NF1^{Nestin}$ animal with astrocyte (open arrowheads), OPCs (closed arrowheads), and $CNPase^{+}GFAP^{-}NG2^{-}$ putative oligodendrocytes (*).Scale = 10 μm. **B,** Proliferating ($PCNA^{+}$), oligodendrocyte ($CNPase^{+}$), and OPC ($NG2^{+}$) cells in control (top row) versus in animal 5 days after single 1 μl 1% wt/vol lysolecithin injection into dentate gyrus (bottom row). Significant loss of both CNPase and NG2 immunoreactivity and marked increase in $PCNA^{+}$ cells reflect the tissue injury and response, respectively. Scale = 20 μm. **C,** Sample projected confocal image of representative coronal section in population-labeling paradigm at 1 month post-lysolecithin injection in $Nf1^{Nestin}$ animal. Inset: high magnification confocal slice of boxed region displaying cells with OPC morphology, all of which are $CNPase^{-}$; only some are $NG2^{+}$ (close arrowheads), while others $NG2^{-}$ (open arrowheads). Scale = 20 μm, (inset) 10 μm.

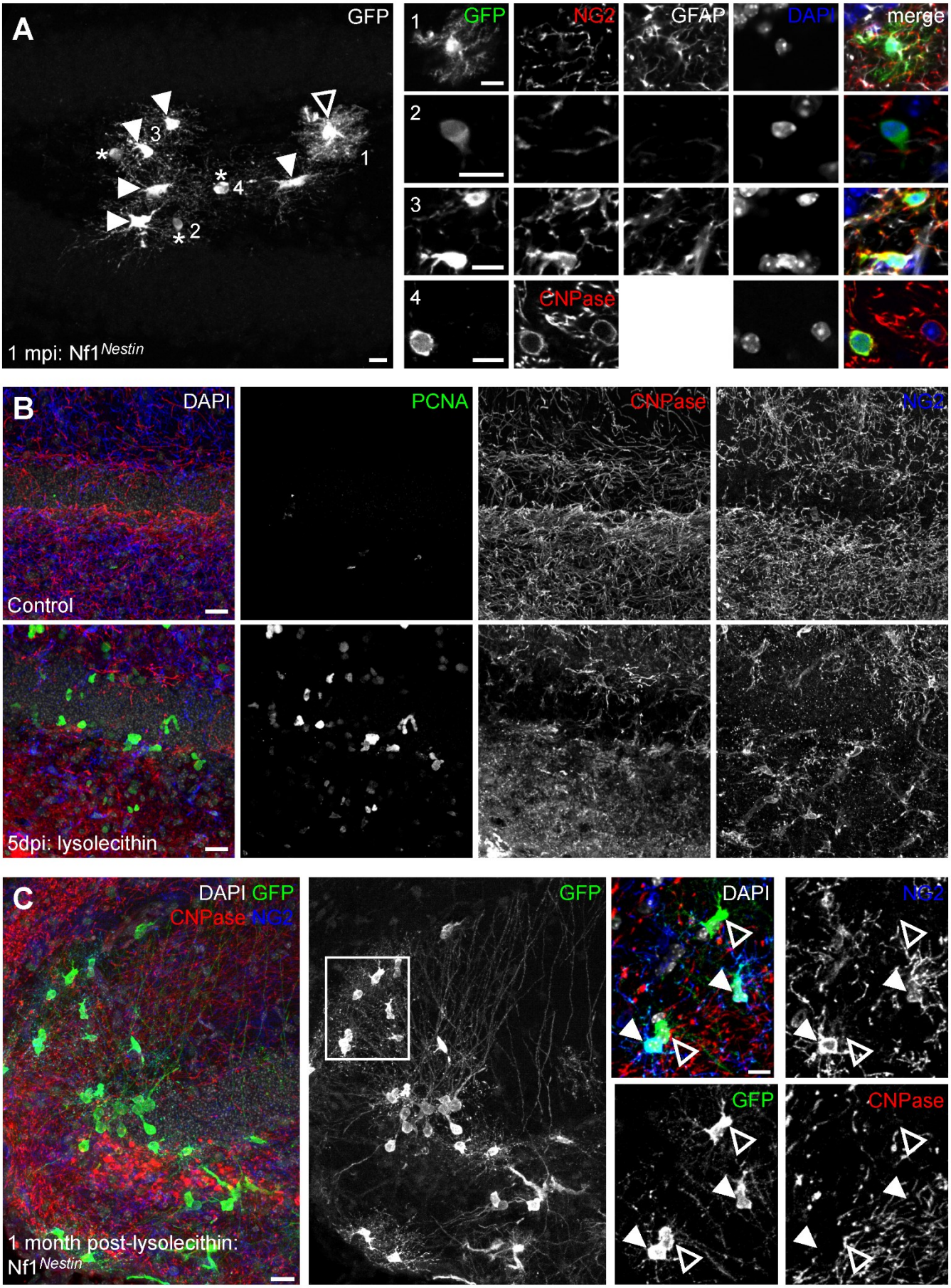
A
GFP
1 mpi: Nf1Nestin
1
2
3
4
GFP
NG2
GFAP
DAPI
merge
CNPase
B
DAPI
PCNA
CNPase
NG2
Control
5dpi: lysolecithin
C
DAPI GFP
CNPase NG2
1 month post-lysolecithin:
Nf1Nestin
GFP
DAPI
NG2
GFP
CNPase

3.4 Discussion

Utilizing multiple independent genetic approaches at the population and clonal levels, I reveal for the first time a new paradigm of stem cell regulation whereby multi-lineage cell generation capacity is actively restricted such that only a subset of available fate choices can manifest. Specifically, removal of a negative regulator of Ras signaling, NF1, allows bi-potent RGLs of the adult hippocampus to reveal their true underlying tri-potentiality and generate the oligodendroglial lineage in addition to that of astrocytes and neurons (Fig. 5). New OPCs appeared to be generated at the expense of neurons and possessed capacity, albeit limited, to differentiate into mature oligodendrocytes. This new paradigm deepens our understanding of fundamental stem cell biology.

Figure 5. Summary model of neural stem cell fate choice capacity in the adult hippocampus.

Under normal conditions, neural stem cells exclusively generate astrocytes and neurons. Upon removal of NF1, neural stem cells can then generate cells of the oligodendroglial lineage.

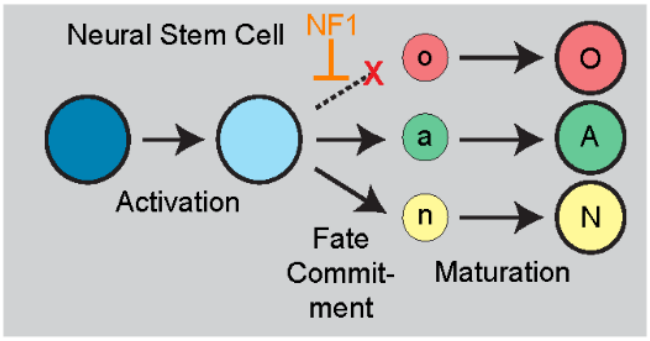
Neural Stem Cell
NF1
X
o
O
a
A
n
N
Activation
Fate
Commit-
ment
Maturation

3.4.1 Active suppression of OPC fate by NF1

Although the role of NF1 in modulating stem/progenitors has been studied extensively both *in vivo* and *in vitro*, the specific properties of neural stem cells regulated by NF1, *in vivo*, were still unknown. For instance, cultured neural stem cells isolated from NF1-inactivated mouse embryo exhibit enhanced proliferation and self-renewal[70,71]. *In vivo* inactivation of NF1 in neural stem cells of the developing cortex has been shown to increase neural stem cell numbers and proliferation[70,72–74]. NF1-inactivation in neural stem cells, but not differentiated neurons or glia, is required for tumor formation[64,75] and leads to OPC over-proliferation, *in vivo*[67]. However all these studies lacked clonal resolution to determine whether NF1 simply regulated proliferation, or could instead affect the balance of daughter cell fates generated from mother stem cells. Here I have provided the first evidence that NF1 may inhibit generation of the oligodendroglial lineage from neural stem cells.

NF1 and Ras signaling it regulates, may generally play a critical role in regulating oligodendrogliogenesis from neural stem cells. The highest levels of neurogenesis occur during embryonic development, which coincides well with ubiquitous high expression of NF1[76]. Oligodendrogliogenesis primarily occurs during early post-natal development, which likewise mirrors marked downregulation of NF1 expression and almost exclusive NF1 expression in neuronal and myelinating cell lineages in the central nervous system[77]. In the adult brain, although RGLs of the hippocampus normally produce only neurons and astrocytes *in vivo*, cultured adult hippocampal progenitors—often with *in vitro* growth factor supplementation—have the capacity to generate neurons, astrocytes, and

oligodendrocytes[24]. Indeed, although neural stem cells of the adult subventricular zone (SVZ) neurogenic niche can already produce all three lineages *in vivo*, SVZ infusion of growth factors, such as EGF or FGF that signal through Ras-regulated receptor tyrosine kinases, promotes oligodendroglial differentiation of progenitors and can improve recovery from demyelinating lesions[78]. Regulation of cellular response to growth factor signaling may therefore be crucial for modulating cell fate choices of progenitors. Cells may possess augmented cell fate potential *in vitro* because high levels of growth factors in culture conditions may saturate the ability of signaling dampers, such as NF1, to maintain control. One potential avenue for future investigation would be to determine the extent to which NF1 expression levels dictate permissiveness to generating the oligodendroglial lineage in neural stem cells of any context.

3.4.2 Neural stem cell tri-potency with mutually exclusive fate choices

My data that OPCs are generated upon NF1 inactivation at the expense of the neuronal lineage interestingly suggest that NF1 may control a switch between two mutually exclusive fates. Recent clonal analysis of cultured SVZ neural stem cell behavior in conditions lacking growth factors support this notion, as no clones containing both neuronal and oligodendroglial lineages were ever observed[79]. These results emphasize that although SVZ neural stem cells as a population exhibit tri-potential fate choice, they are likely a heterogeneous population, with each cell possessing at most bi-potential fate capability. Previous work specifically examining conditional inactivation of NF1 in SVZ progenitors further demonstrated that a critical fate choice point occurs in neuronal intermediate progenitor cells; removal of NF1 in these cells switches their fate to the

oligodendroglial lineage[80]. In contrast to the SVZ, however, my clonal analyses in adult hippocampus strongly suggest that a single RGL can give rise to both neural and oligodendroglial lineages, in addition to the astroglial lineage, and thus possess true tri-potency. Despite this, across all clones, neural fate choices occurred exclusively before OPC-genesis, potentially before NF1-inactivation could affect the cell fate decision, and never occurred thereafter. This was unlikely due to an alteration in neuron survival upon NF1 deletion, as NF1-null cultured neural stem cells still produce surviving neurons[70,73]. Thus, although RGLs possess intrinsic tri-potency, they may only have access to either the neuronal or oligodendroglial lineage in an NF1-dependent manner, but never both simultaneously. NF1 may therefore switch RGLs between two distinct bi-potent states.

The precise molecular mechanism governing NF1-mediated OPC fate choice is unclear and a subject of future investigation. In Gli1^{CreERT2}-based lineage tracing of the current study, OPCs were only generated following the initial fate choice of the activating RGL. This time lag suggests that either NF1 exerts its regulatory role in a critical window of RGL cell fate decision, or gene expression changes induced by NF1 inactivation occurred on a longer time scale than the RGL cell fate decision and subsequent division. These results also suggest that unlike for those of adult SVZ, adult-born neural progeny in hippocampus remain neuronal fate-committed upon NF1 inactivation. Nonetheless, two potential mechanisms could underlie NF1-mediated OPC fate choice. In the first, RGLs may already possess the necessary chromatin structure and RNA molecules to rapidly execute an OPC fate decision in response to NF1 protein loss, and therefore NF1 was not inactivated in time to affect the fate choice. In the second, chromatin remodelers help

switch the potency state of RGLs after NF1 inactivation. In support of this latter hypothesis, one recent study showed that alterations in expression of a histone modifier, SIRT1, modifies production of OPCs from neural stem cells of adult SVZ[81]. Future studies investigating transcriptomes and chromatin states of single neural stem cells could help address this important unanswered question.

3.4.3 Differentiation capacity of newborn OPCs

Although OPCs were robustly generated from the RGL lineage upon NF1 inactivation, they possessed potentially limited capacity for differentiation into mature myelinating oligodendrocytes. These results were particularly surprising, especially my observations that a demyelinating lesion in the adult hippocampal dentate gyrus did not recruit newly born OPCs to replenish lost oligodendrocytes. In contrast, OPCs derived from SVZ neural stem cells possess robust capacity to remyelinate damaged axon tracts upon similar lesions to the corpus callosum in adult animals[37,78]. Given that NF1-inactivated OPCs are highly proliferative, their impaired differentiation capability may contribute to tumor formation in mouse models of glioma[67]. NF1, in addition to gating OPC fate in neural stem cells, may therefore still be required in newborn OPCs to regulate their proliferation and differentiation.

3.4.4 Conclusions

My novel findings show that stem cells may possess intrinsic abilities that are restricted by active mechanisms. My data propose a modified version of Waddington's (1940)[56] classical model: somatic stem cells have many paths available to traverse downwards, but

at critical points of convergence, some are blocked by proteins such as NF1. Given the many challenges in cell therapy to efficiently reprogram somatic cells into undifferentiated states or other lineages, my new model suggests that one potential promising avenue would be to identify and target barriers of a cell's intrinsic differentiation ability. In sum, I highlight yet another layer of complexity for understanding cell fate choice and commitment, with broad implications for the field of stem cell biology.

4 — Adult-born glutamatergic neuron migration

4.1 Introduction

The classical radial unit hypothesis of mammalian brain development postulates that in the developing neocortex, glutamatergic, excitatory, principal neurons migrate radially to form discrete information processing columns of ontogenetic origin[82], whereas GABAergic, inhibitory, modulatory interneurons migrate tangentially across columns[83]. Despite receiving extensive experimental support[82,83], this provocative model has nonetheless been challenged[84–90]. Given that this model has significant implications for brain development, function, and evolution, it is fundamentally important to understand the cellular characteristics and mechanisms of neuronal migration.

Neurogenesis persists in the adult mammalian brain in two specific brain regions whereby the classical migration model is believed to be faithfully recapitulated[91]. In the subventricular zone (SVZ) of the lateral ventricles, new neurons generated from neural stem cells (type B cells) migrate tangentially to the olfactory bulb to become interneurons[17,18,28]. In contrast, in the subgranular zone (SGZ) of the hippocampal dentate gyrus, new neurons generated from radial glia-like neural stem cells (RGLs) migrate radially into the granule cell layer to become glutamatergic granule cells[12,49,92]. However due to technical limitations, migratory patterns have been only examined at a cell population level, and thus we still lack detailed spatial relationship information between individual mother cells and their daughters.

Both adult neurogenic niches are highly vascularized and vasculature is hypothesized to play a critical role in adult neurogenesis[91]. In the adult SVZ, neural precursors directly contact blood vessels[93–95]. In the adult SGZ, proliferating progenitor cells have been shown to contact vasculature and form an angiogenic niche[96]. Despite these observations, the functional role of niche vascularization remains to be fully explored.

Unexpectedly, and contrary to the classical model, my recent clonal lineage-tracing of individual quiescent RGLs showed a previously unknown tangential distribution of glutamatergic dentate granule neurons with respect to their parental RGL[19]. I therefore systematically investigated the migration mode of adult-born cells in the dentate gyrus. Using a novel clonal lineage-tracing approach that preferentially targets activating RGLs, thus birth-dating newborn progeny of RGLs, *in vivo*, I found significant tangential distribution of newborn neuroblasts from their mother cell of origin. Further, I found a direct association of putative migratory neuroblasts with the SGZ vascular network, revealing an important function of vascular as a migration substrate. Together, my results identified a new mode of glutamatergic neuron distribution under physiological conditions.

4.2 Materials and Methods

Animals and tamoxifen administration

Ascl1^{CreERT2}*;Rosa-YFP*$^{f/-}$and *Ascl1*^{CreERT2}*;Confetti*$^{f/-}$ mice were generated by crossing *Ascl1*^{CreERT2} (*Ascl1*$^{tm1.1(Cre/ERT2)Jejo}$/J, knock-in line, Jackson Labs)[97] with *Rosa-YFP*$^{f/-}$ (B6.129X1-*Gt(ROSA)26Sor*$^{tm1(EYFP)Cos}$/J, Jackson Labs) and *Confetti*$^{f/-}$ (B6.129P2-

Gt(ROSA)26Sor$^{tm1(CAG-Brainbow2.1)Cle}$/J, Jackson Labs) mice, respectively. I used two different reporters in the present study to validate reporter independence of migration phenomena. *Nestin-GFP* transgenic mice were from Dr. Grigori N. Enikolopov[98]. All mice in the study were backcrossed to the C57BL/6 background for at least six generations. Animals were housed in a 14 hour light/10 hour dark cycle and had free access to food and water. Tamoxifen (66.67 mg/ml, Sigma, T5648) was prepared in a 5:1 corn oil (Sigma) to ethanol mixture. To achieve sparse labeling for clonal analysis (~8-16 clones per hemisphere), a single dose of tamoxifen (77.5 mg/kg for the *RosaYFP*$^{f/-}$ reporter, 250 mg/kg for the *Confetti*$^{f/-}$ reporter) was intraperitoneally injected into adult 8-10 week-old male and female mice. Animals were analyzed at 1, 3, or 7 days post-tamoxifen injection (dpi), or 1-2 months post-tamoxifen injection (mpi). All animal procedures were performed in accordance to institutional guidelines of Johns Hopkins University School of Medicine.

Tissue processing, immunostaining and confocal imaging

Animals were transcardiac perfused with cold 4% paraformaldehyde (wt/vol, in 0.1 M phosphate buffer, PB, pH 7.4), and cryoprotected with 30% sucrose (wt/vol). Serial 40 μm-thick coronal brain sections were cut on a frozen sliding microtome (Leica, SM2010R) for immunohistology as previously described[19]. For partial "whole-mount" dentate gyrus SGZ preparations, the whole hippocampus was dissected from cortex, mounted dentate-side-up on a frozen sliding microtome, and serial 50 μm horizontal sections were collected. Antibodies diluted in TBS with 0.05% Triton X-100 and 3% donkey serum, were used against GFP (Aves Labs, chicken, 1:500; Rockland, goat,

1:500), Tbr2 (Abcam, rabbit, 1:250), CD31 (BD Biosciences, rat, 1:500), DCX (Santa Cruz, goat, 1:100), GFAP (Millipore, mouse, 1:1000; DAKO, rabbit, 1:1000), GM130 (BD Biosciences, mouse, 1:250), Nestin (Aves Labs, chicken, 1:500), γ-tubulin (BioLegend, rabbit, 1:500), Prox1 (Abcam, rabbit, 1:500), and NeuN (Millipore, guinea pig, 1:500). Nestin and NeuN antigens were retrieved by incubating brain sections in 1X DAKO target retrieval solution (DAKO) at 68°C for 20 minutes, followed by 10 minutes cooling to room temperature. Serial sections from the entire dentate gyrus were first immunostained for GFP to allow identification of prospective clone-containing sections on an epifluorescence microscope (Zeiss, Axiovert 200M). Labeled clone-containing sections were taken for further processing and confocal imaging at 40X on a Zeiss LSM 710 confocal microscope using multi-track or spectral linear unmixing 'online fingerprinting' configurations (Carl Zeiss).

Image processing and data analyses

Simulations to estimate the probability of two cells belonging to a clone, based upon numbers of initially labeled cells per hemisphere, were run from 3D-reconstructed dentate gyri as previously described[19]. For data acquisition, clones that spanned multiple serial sections were reconstructed using Reconstruct software (John C. Fiala, NIH). All aligned images were exported at full resolution for 3D visualization into Imaris (Bitplane) and analyzed. For illustrative purposes, some cells and features were volume-rendered using the Surface module in Imaris. Distance measurements were collected from 7 hemispheres (5 animals) at 3 dpi, 9 hemispheres (6 animals) at 7 dpi, and 12 hemispheres (7 animals) at 1-2 mpi. The Spots module in Imaris was used to digitize cell nucleus

locations in the 3D space and to code cell type classifications, according to distinct morphological and molecular markers (Fig. 7A and Table 2). The Clipping Plane module in Imaris was used to estimate the local SGZ plane for 2D clone projections. Spots and clipping planes were exported to Matlab (The MathWorks) for further distance measurements, calculations, and analyses. The distance between an RGL and a given newborn progeny in the local SGZ plane was calculated for tangential distance measurements (Figs. 6 and 7). The shortest distance between a given labeled newborn cell and the SGZ most proximal to the hilus was calculated for radial distance measurements (Fig. 6C, E). Cells at the dentate gyrus genu were excluded from analysis due to the potential ambiguity of tangential versus radial migration. Clones with multiple RGLs were also excluded due to ambiguity in distinguishing the cell of origin.

Cell type	Molecular Markers	Morphology
Radial glia-like cell (RGL) with neurogenic division	Nestin, GFAP	RGL has its soma in SGZ, radial process in GCL and ML, nuclear cleavage with only one GFAP+ nucleus
Intermediate progenitor cell (IPC)	Tbr2, Nestin$^{\pm}$, (GFAP^{-})	IPC is spherical with short, multipolar processes in the SGZ
Neuroblast (NB)	Tbr2$^{\pm}$, Dcx, Prox1	NB has elongated soma, bipolar processes
Immature neuron (IN)	Dcx, Prox1, NeuN	IN has soma in the apical GCL, thin dendrite through the GCL
Mature neuron (N)	Prox1, NeuN, (Dcx^{-})	N has multi-branched spiny dendrites in the ML and axon to CA3

Table 2. Summary of morphological markers used in the current study for identification of each cell type during adult hippocampal neurogenesis.

For vasculature association analysis at the clonal level, cells were classified into one of three groups: (1) those with no $CD31^+$ vasculature contact, (2) those with their soma directly contacting a $CD31^+$ blood vessel, and (3) those which contacted $CD31^+$ vasculature only through one or more processes. All labeled clones and the percentage of their vasculature association were quantified and averaged across 10 hemispheres (5 animals). For vasculature association analysis at the population level, all cells in a horizontal section from 3 *Nestin-GFP* animals were quantified and results were averaged across animals. Locations of cell nuclei were digitized according to GFP, Tbr2, and DCX expression using Spots. Blood vessels were digitized using the Filament Tracer module in Imaris. 3D coordinates were exported to Matlab and distance between cells and vasculature was measured. Cells with nuclei within 7 μm of a blood vessel centerline were considered to be in contact with the blood vessel. Simulated vasculature associations (Fig. 11D) were performed by randomly placing cells in the same 2D SGZ space, as estimated by a third-degree polynomial plane fit. One-hundred iterations of the simulation were performed for each cell type.

Electron microscopy analysis

Adult C57BL/6 female mice were stereotaxically injected with engineered murine oncoretrovirus expressing GFP as previously described[35]. Mice were processed 2 days after injection and transcardiac-perfused with 4% paraformaldehyde (wt/vol) with 0.1% glutaraldehyde (vol/vol; Sigma) in 0.1 M PB, pH 7.4. Coronal sections (50 μm thick) were sectioned on a vibrating microtome (VT1200S, Leica Biosystems). Sections were immunostained in phosphate-buffered saline (PBS) for CD31 and examined using an

epifluorescence microscope to identify GFP^+ retrovirally-labeled newborn cells. Sections containing clearly labeled newborn progeny in close association with the $CD31^+$ vasculature were placed in cryoprotectant (25% sucrose wt/vol, 10% glycerol vol/vol, in 0.05 M PB) for 2 hours and freeze-thawed three times in liquid nitrogen. After three washes in PBS and then 0.5% bovine serum albumin in 0.1 M PB (vol/vol, BSA-C, Aurion) to block the tissue, sections were incubated overnight in the primary antibody (biotinylated rabbit anti-GFP, Vector Laboratories, 1:1000; BA-0702) in 0.1% BSA-C in 0.1 M PB, shaking at room temperature). Sections were washed out of the primary antibody with one wash in 0.1% BSA-C in 0.1 M PB and three washes in PBS, before incubation for 90 minutes in avidin biotin peroxidase complex (ABC Elite, Vector Laboratories). After three washes in PBS and then Tris buffer, a 3,3-diaminobenzidine (DAB) peroxidase reaction was performed (Vector Laboratories Kit, 4 minutes). The sections were then washed three times in Tris buffer, three times in PBS and left overnight at 4°C. The next day, sections were washed in 0.1M PB in glass vials and post-fixed in 1% osmium tetroxide in 0.1M PB for 30 minutes. They were then dehydrated in ascending concentrations of ethanol (two 50% ethanol washes, one 70% wash with 1% uranyl acetate, one 95% wash and two 100% washes) and three washes in acetone, before being lifted into resin (Durcupan ACM, Fluka) and left overnight at room temperature. The resin was then warmed to decrease its viscosity and sections were placed onto microscope slides with coverslips, before the resin was cured at 65°C over three days. Locations of clearly labeled newborn progeny in close association with $CD31^+$ blood vessels were identified at the light microscopic level and followed through to the electron microscopic level. Serial sections (70 nm thick) were collected onto Formvar-coated,

single-slot copper grids and contrasted with a lead stain (15 minutes). Sections were then examined using a Philips CM10 transmission electron microscope and serial images of the labeled structures were captured using a digital camera (Morada SIS, Olympus). These images were used to create 3D reconstructions with Fiji Image J software and individual images were processed using Adobe Creative Suite software.

Statistical analysis

Statistical analysis was performed with one-way ANOVA (with Tukey *post hoc* test), one-tailed unpaired Student's *t* test, or two-sample Kolmogorov-Smirnov test (with Bonferroni correction for multiple comparison, where applicable), as indicated in the text and figures. When applicable, validation of normality and homogeneity of variance assumptions was performed for all compared data groups using a Shapiro-Wilk test and Monte-Carlo simulation, respectively. All statistical analyses were performed in Origin Software (OriginLab) or Matlab.

4.3 Results

4.3.1 Spatial distribution of clonally-related neuronal progeny with defined birthdate

I utilized a tamoxifen inducible *Ascl1*^{CreERT2} knock-in mouse[97] to sparsely label (~8-16 cells per dentate gyrus) and lineage-trace clones of adult neural precursors (Fig. 6A). Consistent with previous fate-mapping at the population level using this mouse model[97], cells labeled at one day post-tamoxifen injection (1 dpi) in the adult SGZ consisted of 92 ± 2% RGLs and few early intermediate progenitor cells (IPCs; n = 10 dentate gyri), as

assessed by morphology and molecular marker expression (Table 2). Computational simulations[19] estimated that given 16 initially labeled cells, any two labeled cells within 150 μm of each other had a 99% probability of belonging to the same clone (Fig. 6B). Importantly, at 1 dpi, the majority of RGLs (96 ± 2%, n = 10 dentate gyri) had just divided (with one adjacent progeny) or were in the process of cell division (Fig. 6A). Therefore, in contrast to previous *Nestin*^{CreERT2}-based clonal lineage-tracing of quiescent RGLs that exhibited stochastic activation over time[19], my current approach enriches for activating RGLs, allowing for the first time birth-dating of RGL progeny to track their development with high temporal precision. At 1-month post-tamoxifen injection (mpi), I observed clones in which Prox-1^{+}NeuN^{+} mature dentate granule cells were distributed at a significant distance (~100 μm) away from their mother RGL along the SGZ (Fig. 6C). Contrary to the classic model, these results suggest significant tangential migration of neuroblasts for a glutamatergic neuronal subtype in the adult mammalian brain under physiological conditions.

Figure 6. Tangential distribution of newborn granule neurons away from their parental radial glia-like cells of origin in the dentate gyrus of the adult mouse hippocampus, which were clonally lineage-traced *in vivo*.

A, Sample projected confocal image of an active *Ascl1*^{CreERT2}; *Rosa-YFP*$^{f/-}$-labeled RGL in the dentate gyrus at 1 dpi. A high magnification image of the labeled RGL is shown in the bottom panels. This GFAP^{+} RGL (filled arrowhead) underwent an asymmetric division to produce a GFAP^{-} neuronal progeny (open arrowhead). Scale bar: (top panel) 100 μm, (bottom panels) 10 μm. **B,** Computational simulations of nearest distances between two cells in the 3D dentate gyrus space. Each colored line represents the reverse cumulative distribution of nearest cell distances from a simulation with a given number of total cells. With 16 total initially labeled cells, the probability of cells within 150 μm of each other as being from the same clone is 99%. **C,** Sample projection confocal image of a labeled clone in *Ascl1*^{CreERT2}; *Rosa-YFP*$^{f/-}$ mice at 1 mpi, showing significant tangential distribution of Prox1^{+}NeuN^{+} mature glutamatergic granule neurons (right bottom panel) and their parental GFAP^{+} RGL (left bottom panel). Inset: 2D SGZ plane projection of all clonally related cell locations. Shown on the right top panel is a schematic diagram for measurements of tangential and radial distance of neuronal progeny from the parental RGL. Scale bar: 10 μm. GCL: granule cell layer; SGZ: subgranular zone. **D,** Distribution plot of tangential distance between labeled RGL and its progeny within each clone at 3 dpi, 7 dpi, and 1-2 mpi (**$P < 0.05$; *$P < 0.1$; two-sample Kolmogorov-Smirnov test statistic = 0.85, 0.66, and 0.23 for 3, 7, and 1-2 mpi, respectively). Raw distributions are shown as bar graphs; curved lines correspond to

smoothed distributions. **E,** Dot plot of tangential versus radial distance from the parental RGL for each neural progeny in all labeled RGL-containing clones at 3 dpi, 7 dpi, and 1-2 mpi. Inset: tangential distance of each neural progeny to its parental RGL.

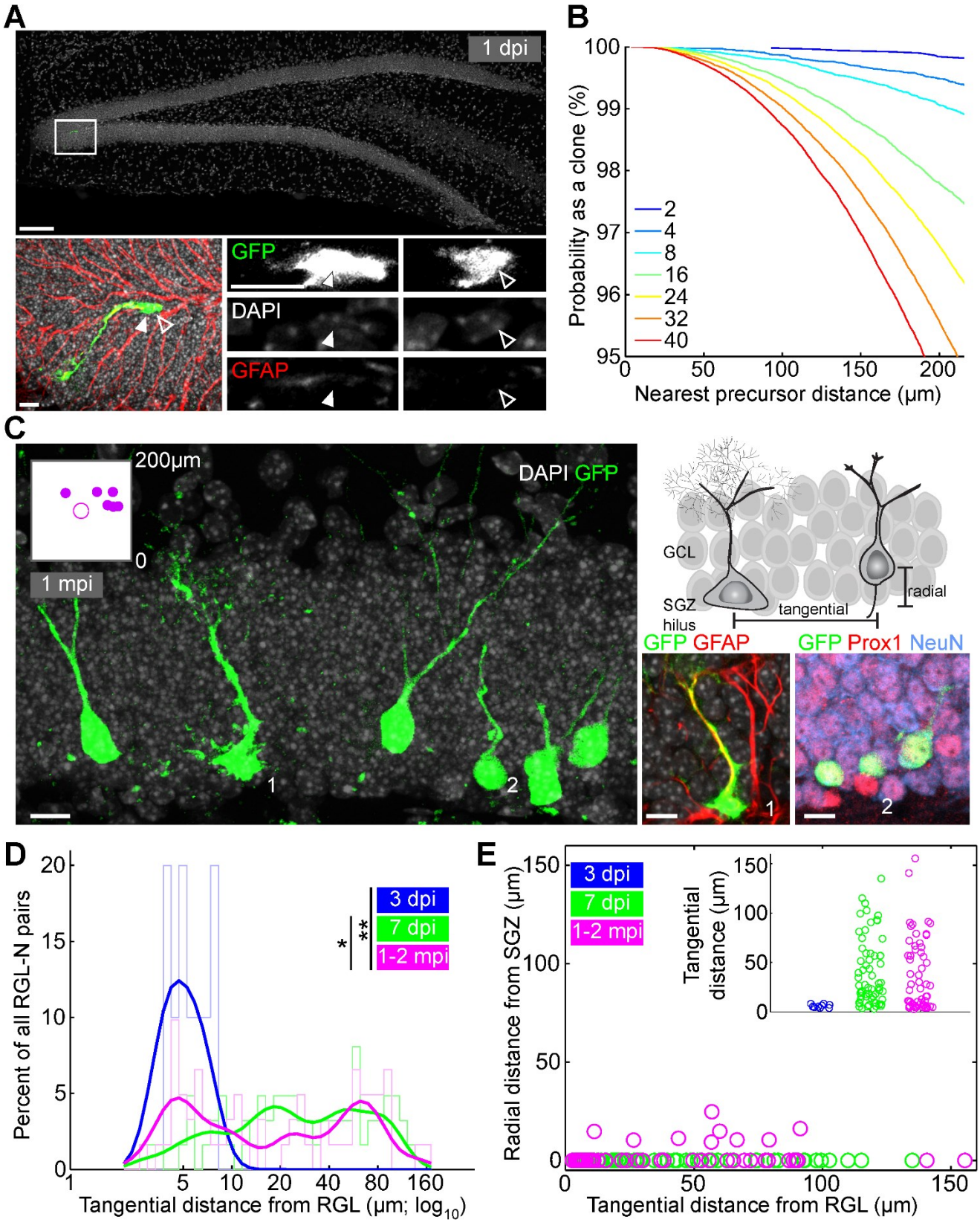
A
1 dpi
GFP
DAPI
GFAP
B
Probability as a clone (%)
100
99
98
97
96
95
2
4
8
16
24
32
40
0
50
100
150
200
Nearest precursor distance (μm)
C
200μm
0
1 mpi
DAPI GFP
1
2
GCL
SGZ
hilus
tangential
radial
GFP GFAP
GFP Prox1 NeuN
D
Percent of all RGL-N pairs
20
15
10
5
0
3 dpi
7 dpi
1-2 mpi
*
**
1
5
10
20
40
80
160
Tangential distance from RGL (μm; log10)
E
Radial distance from SGZ (μm)
150
100
50
0
3 dpi
7 dpi
1-2 mpi
Tangential distance (μm)
Tangential distance from RGL (μm)

4.3.2 Developmental stage-specific tangential distribution

To explore the temporal dynamics of putative neuronal migration, I examined labeled clones at different time points after tamoxifen injection. At 3 dpi, labeled cells exhibited little displacement from each other (Fig. 6D; blue curve). In contrast, at 7 dpi there was already significant tangential distance along the SGZ between labeled newborn neural progenitors and their parental RGLs, the distribution of which was very similar to that at 1-2 mpi (Fig. 6D; green and magenta curves). Notably, while only ~15% of labeled newborn neurons exhibited measurable radial displacement away from the SGZ into the granule cell layer even at 1 or 2 mpi (all < 25 μm), ~47% of them were more than 25 μm tangentially away from their parental RGL (Fig. 1E). The average tangential distance also exceeded that of radial distance by almost 18-fold. Time-course analysis further suggested that tangential distribution preceded any radial migration, and no correlation between tangential and radial migration was observed among individual cells that possessed both ($R = 0.08$, $p = 0.85$). Taken together, these results establish that tangential distribution of newborn neural progeny from their RGL within 3-7 days after birth represents the dominant mode of migration in the adult dentate gyrus.

I next asked whether tangential migration occurred during a specific developmental stage or stages. Adult hippocampal neurogenesis proceeds in a stereotypic sequence – dividing RGLs give rise to intermediate progenitor cells (IPCs), which in turn develop through neuroblast (NB) and immature neuron (IN) stages before becoming glutamatergic excitatory mature granule neurons[12,20,29]. Utilizing distinct morphological and molecular markers to distinguish labeled cells at different developmental stages (Fig. 7A and Table

2), I found that neuroblasts, corresponding to 3-7 day-old DCX^+ cells with a bipolar, elongated morphology, were the earliest cells in the developmental lineage that showed significant tangential distribution away from their parental RGL (Fig. 7B; $p = 5.4\times10^{-7}$; Kolmogorov-Smirnov test). On average, neuroblasts, immature neurons, and mature neurons exhibited similar tangential distances away from their parental RGLs (Fig. 7B). These results suggest that the majority of tangential migration occurs at the neuroblast stage of adult hippocampal neurogenesis.

Figure 7. Developmental stage-specific tangential distribution of newborn neural progeny.

A, Summary of molecular markers used in the current study for identification of each cell type during adult hippocampal neurogenesis. Newborn cells are generated from $GFAP^{+}Nestin^{+}$ radial glia-like cells that undergo asymmetric neuronal divisions. Newborn cells develop into $Tbr2^{+}$ intermediate progenitor cells (IPC) with short, multipolar processes within three days of birth. Within 3-7 days, newborn cells possess long, bipolar processes and elongated somas in a $Tbr2^{+/-}Dcx^{+}$ neuroblast stage (NB) before penetrating the granule cell layer and becoming a polarized $Prox1^{+}Dcx^{+}$ immature neuron (IN) with axon and dendrite. Over the next month, newborn cells mature into $Prox1^{+}NeuN^{+}$ neurons (N) with spiny dendrites and long axons that project to CA3. See also Table 1. **B,** Summary of tangential distance of each neural progeny from its parental RGL for progeny at each developmental stage. IPC: intermediate progenitor cell; NB: neuroblast; IN: immature neuron; N: mature granule neuron. Values represent mean ± s.e.m. ($^{*}P < 0.05$; $^{\#}P > 0.1$; two-sample Kolmogorov-Smirnov test with Bonferroni correction for multiple comparisons; test statistic = 0.80 and 0.47, respectively).

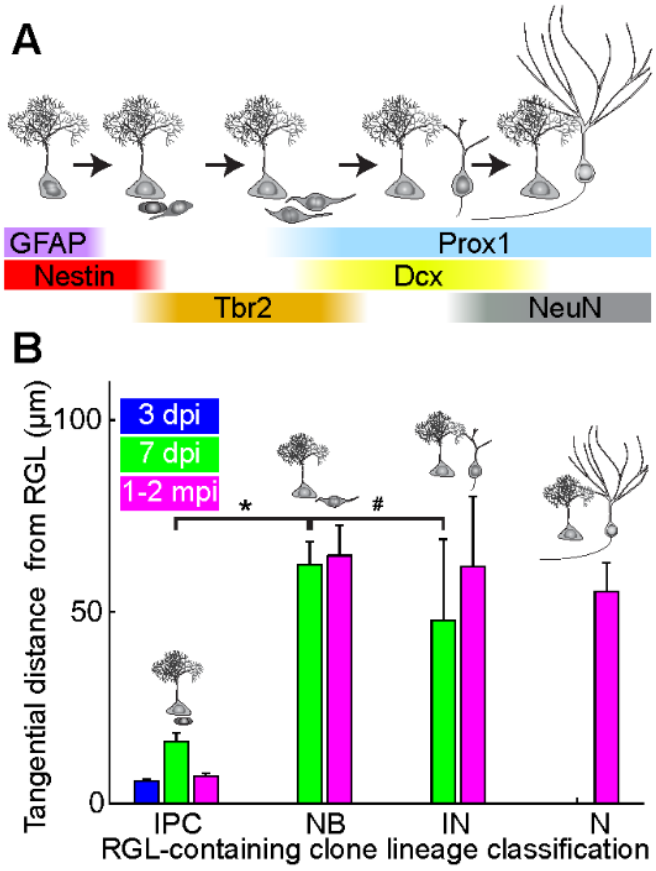
A
GFAP
Prox1
Nestin
Dcx
Tbr2
NeuN
B
Tangential distance from RGL (μm)
100
50
0
3 dpi
7 dpi
1-2 mpi
*
#
IPC
NB
IN
N
RGL-containing clone lineage classification

4.3.3 Patterns and magnitude of tangential distribution

A consequence of tangential migration of neuronal progeny is that individual clones disperse over areas beyond that of a radial unit, potentially allowing individual RGLs to modify a large domain of the hippocampal circuitry via neurogenesis. I therefore visualized 2D SGZ projections of clones over time in 300 μm square windows (Fig. 8A-C; excluding clones with single RGLs that had not completed division). Consistent with previous reports of age-related decline of RGLs[19,33], some clones at 1-2 mpi lacked RGLs, despite my enrichment of RGL-containing clones at 1 dpi. I therefore included RGL non-containing clones only for 1-2 mpi. Qualitatively, clones dispersed over large areas, strongly suggestive of widespread tangential migration (Fig. 8A-C).

To quantitatively determine the extent of tangential distribution of neuronal progeny in each 2D SGZ projected clone, I measured the maximum distance amongst all newborn neural progeny within each clone in the projected dentate space. The mean values were ~43 ± 16 μm and ~69 ± 19 μm at 7 dpi and 1-2 mpi, respectively. This considerable spacing between neural progeny supports my model of neuronal migration as opposed to only RGL motility. The distribution of maximum distances was slightly increased from 7 dpi to 1-2 mpi (Fig. 7C; $p = 0.06$; Kolmogorov-Smirnov test), which may reflect the contribution of additional cohorts of newborn neural progeny from re-activation of RGLs.

Figure 8. Tangential distribution among newborn neural progeny at 3 dpi, 7 dpi, and 1-2 mpi in the adult dentate gyrus.

A-C, 2-dimensional SGZ plane projection of all RGL-containing clones containing at least IPCs at **(A)** 3 dpi, **(B)** 7 dpi, and **(C)** 1-2 mpi, plotted in a 300 μm square window. RGLs are represented as open circles; neural progeny are represented as closed circles. Different time points or developmental stages are encoded with color. Clones that lack RGLs at 1-2 mpi were also plotted in gray boxes and included in histogram in **(D)**. **D,** Histogram (left panel) and cumulative distribution plot (right panel) of the maximum distance between clonally related neural progeny for all labeled clones (*$P < 0.1$; two-sample Kolmogorov-Smirnov test statistic = 0.38).

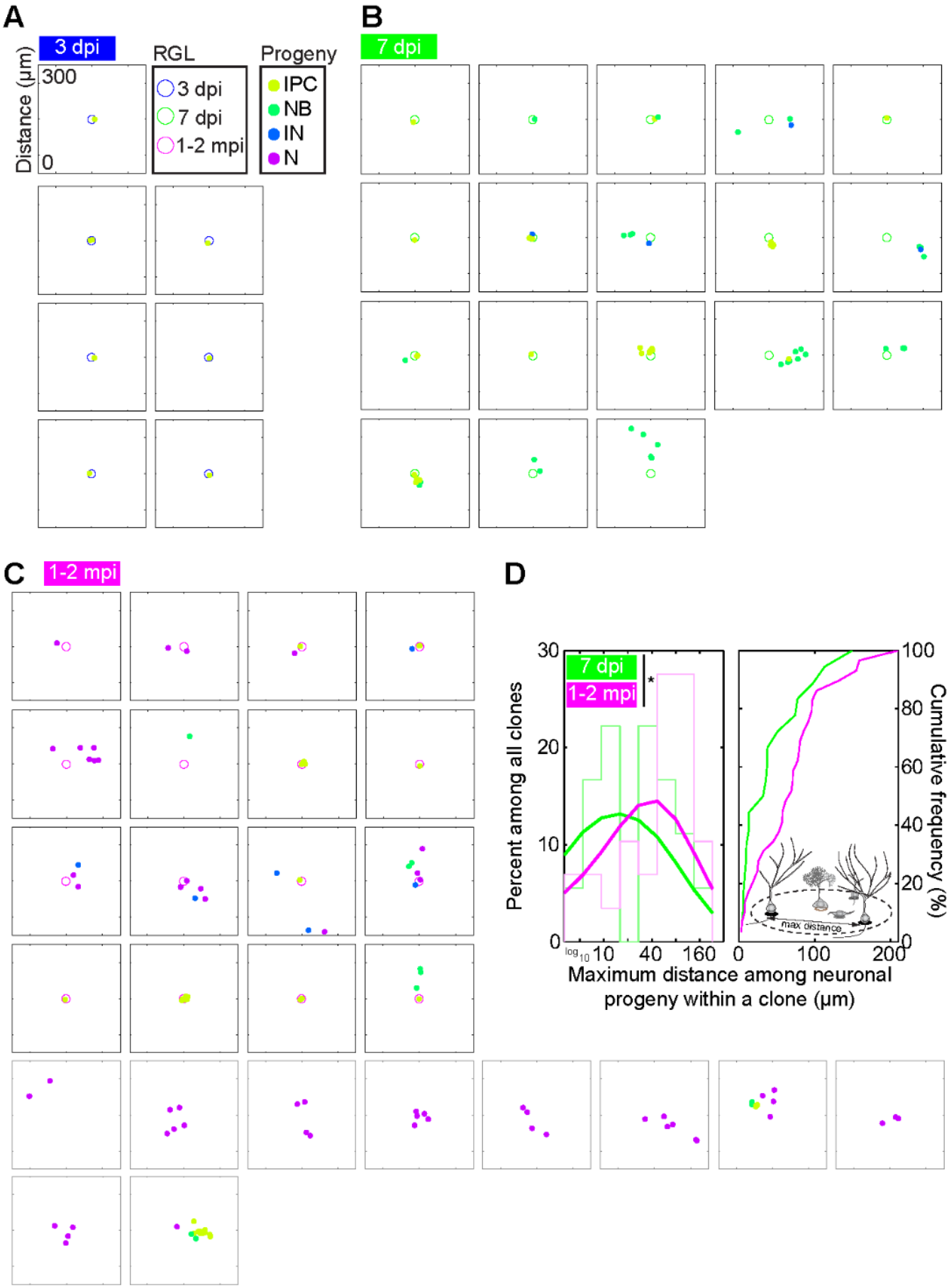
A
3 dpi
Distance (µm)
300
0
RGL
3 dpi
7 dpi
1-2 mpi
Progeny
IPC
NB
IN
N
B
7 dpi
C
1-2 mpi
D
7 dpi
1-2 mpi
*
Percent among all clones
30
20
10
0
log10 10
40
160
Cumulative frequency (%)
100
80
60
40
20
0
0
100
200
max distance
Maximum distance among neuronal progeny within a clone (µm)

4.3.4 Vascular substrate for putative tangential migration

I next investigated the potential cellular mechanism underlying tangential migration of neuronal precursors in the adult hippocampus. Tangential migration of GABAergic interneurons has been shown to be facilitated by a combination of homotypic and heterotypic cellular interactions, such as migration in chains and along existing axonal processes, respectively[99]. I therefore searched for potential substrates that could support tangential migration during adult hippocampal neurogenesis. In the adult dentate gyrus, BrdU-incorporating cells are known to be in close association with the vasculature[96]. Indeed, I found that labeled neuroblasts were mostly in very close contact with $CD31^+$ vasculature (Fig. 9A, B). Notably, these neuroblasts exhibited polarized organelles, such as $GM130^+$ Golgi apparatus (Fig. 9C) and γ-$tubulin^+$ centrosomes (Fig. 9D), characteristic of migrating, locomoting cells[99].

Figure 9. Close association between tangentially migrating neuroblasts and blood vessels in the adult dentate gyrus.

A, Sample confocal image (right panels) and 3D rendering (left panel) of a CFP^+ clone at 7 dpi with a neuroblast whose soma and tangential process closely associated with $CD31^+$ blood vessel. **B,** Sample confocal image (bottom panels) and 3D rendering (top panel) of a GFP^+ clone at 7 dpi containing a parental RGL and dispersed $Tbr2^+DCX^+$ neuroblast (NB) progeny in close association with $CD31^+$ blood vessels. Note that CD31 and Tbr2 shared the same channel due to limited availability of channels, but could be distinguished by different morphology (Tbr2, nuclear staining; CD31, tubular staining). **C,** Sample confocal image (bottom panels) and 3D rendering (top panel) of a GFP^+ clone at 7 dpi with a neuroblast whose tangential process extended along a blood vessel and contained polarized $GM130^+$ Golgi apparatus at its base, proximal to the cell soma. **D,** Sample confocal image (bottom panels) and 3D rendering (top panel) of GFP^+ neuroblasts at 7 dpi with polarized γ-$tubulin^+$ centrosomes and $GM130^+$ Golgi apparatus, and in close association with $CD31^+$ blood vessels. All scale bars: 10 μm.

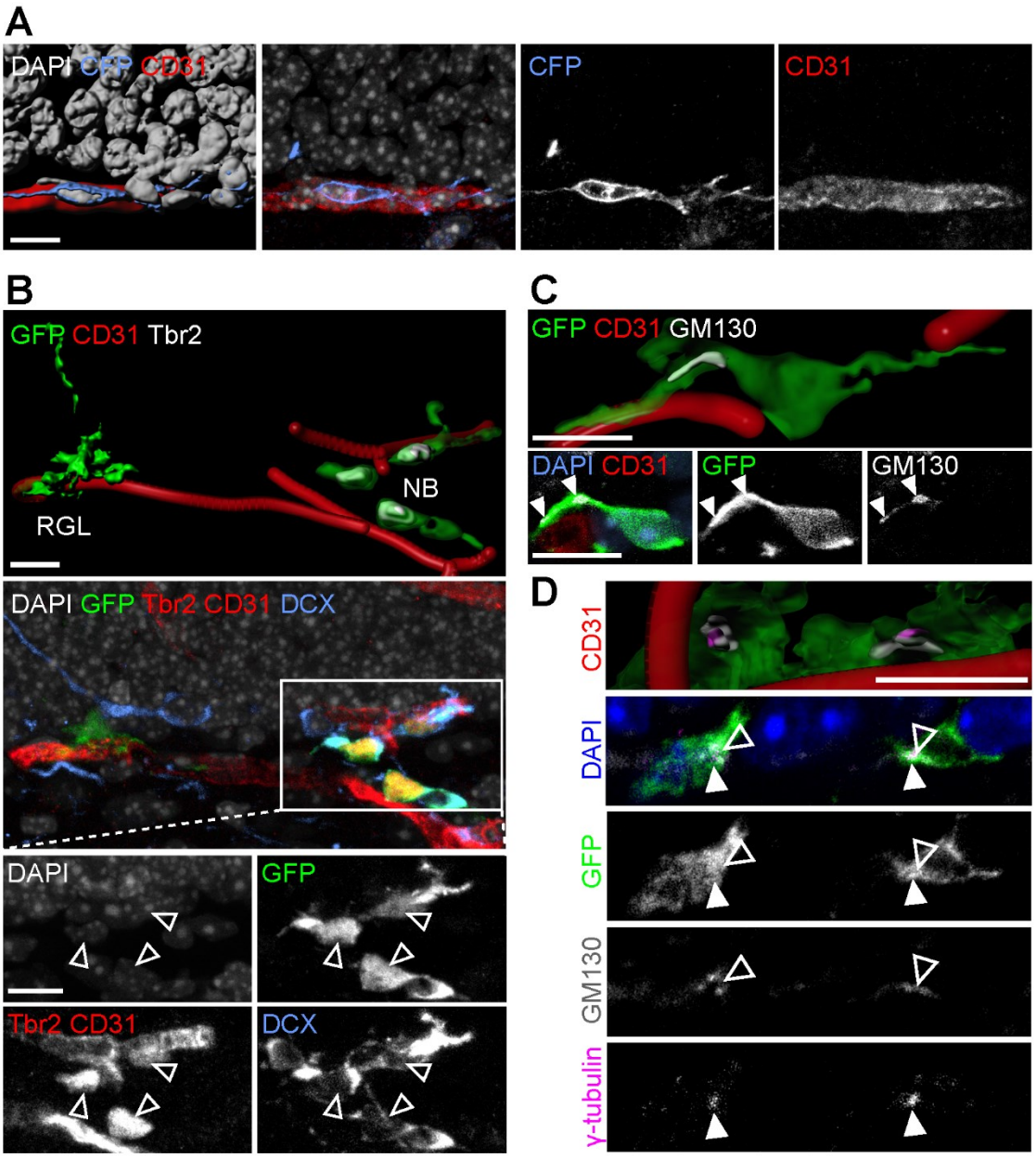
A
DAPI CFP CD31
CFP
CD31
B
GFP CD31 Tbr2
NB
RGL
DAPI GFP Tbr2 CD31 DCX
DAPI
GFP
Tbr2 CD31
DCX
C
GFP CD31 GM130
DAPI CD31
GFP
GM130
D
CD31
DAPI
GFP
GM130
γ-tubulin

Quantitative analysis further showed that, among all clonally labeled cells, $Tbr2^{+}DCX^{+}$ and $Tbr2^{-}DCX^{+}$neuroblasts were the two major cell types in direct contact with the vasculature, either via the cell soma or processes (Fig. 10A; left graph). Within each cell subtype of a specific developmental stage, 88% and 80% of $Tbr2^{+}DCX^{+}$ and $Tbr2^{-}DCX^{+}$ cells with tangential processes were associated with the vasculature, respectively (Fig. 10A; right column). In contrast, $Tbr2^{+}DCX^{-}$ IPCs or $Tbr2^{-}DCX^{+}$ immature neurons with radial processes mostly lacked the vascular contact (Fig. 10A). I further examined the interaction between labeled newborn neural progeny and endothelial cells at the ultrastructural level using electron microscopy. Remarkably, the process and soma of some neuroblasts were in direct contact with the blood vessel (Fig. 10B). These data support the notion that neuroblasts represent the dominant cell stage actively migrating and utilizing a vascular migration substrate.

Figure 10. Direct contact between tangentially migrating neuroblasts and blood vessels in the adult dentate gyrus.

A, Quantification of distribution of various labeled precursors in close association with the vasculature at 7 dpi. Values represent mean ± s.e.m. Also shown are summaries of precursor cell molecular marker expression and the percentage of a given cell subtype in close association with vasculature (right panels). **B,** 3D reconstruction, from serial electron microscopic sections, of a GFP^+ SGZ neuronal precursor (NP1) extending a tangential process along a blood vessel (BV). The immunofluorescence-identified, immunoperoxidase-labeled cell (top panels) sits alongside another neuronal precursor (NP2) and apposes the blood vessel with both its tangential process (mid-left panel) and its cell body (top right panel, arrowhead). SGZ: subgranular zone; GCL: granule cell layer; BV: blood vessel. Scale bars: 5 μm.

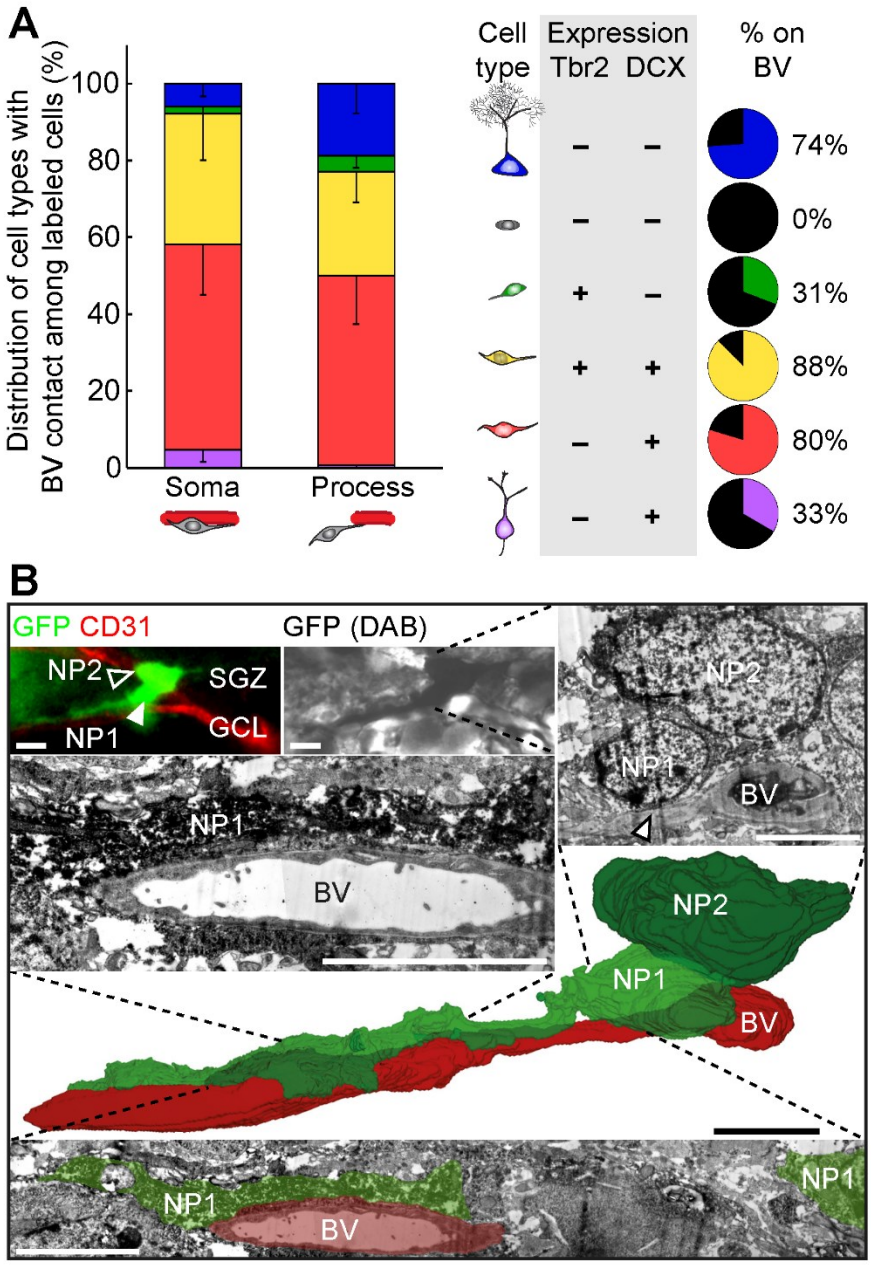
A
Distribution of cell types with BV contact among labeled cells (%)
100
80
60
40
20
0
Soma
Process
Cell type
Expression Tbr2 DCX
% on BV
74%
0%
31%
88%
80%
33%
B
GFP CD31
GFP (DAB)
NP2
SGZ
NP1
GCL
NP1
BV
NP2
NP1
BV
NP2
NP1
BV
NP1
NP1
BV

4.3.5 Global view of neural precursors and niche-wide vascular-mediated migration

To determine whether the general population of neural precursors exhibited properties similar to those clonally labeled in *Ascl1*^{CreERT2} mice, I developed a partial "whole-mount" preparation by sectioning the hippocampus parallel to the SGZ (Fig. 11A). This preparation enabled large sheets of SGZ to be visualized in a single section. I first visualized CD31^{+} vasculature and found a rich, dense bed of blood vessels within the SGZ, in contrast to a sparse, columnar architecture of vessels within the granule cell layer (Fig. 11B). The SGZ vascular architecture may therefore be uniquely suited to support tangential distribution of newborn neural progeny within the SGZ in the adult dentate gyrus.

Using *Nestin-GFP* reporter mice[98] in combination with the same immunohistological and morphological markers as for clonal analysis (Fig. 7A and Table 2), I examined the association of SGZ progenitors with vasculature (Fig. 11C). A fraction of all cell types was in close proximity to blood vessels. I therefore simulated vascular association of the same number of each cell type randomly placed in the same SGZ space and found that DCX^{+} neuroblasts were most significantly associated with CD31^{+} blood vessels above chance (Fig. 11D). These neuroblasts on blood vessels also contained polarized GM130^{+} Golgi apparatus characteristic of migrating cells (Fig. 11E). Together with findings from clonal analysis (Fig. 9 and 10), these results support a model whereby vasculature serves as a substrate for tangential migration of newborn neural progeny during adult hippocampal neurogenesis.

Figure 11. Neuroblast–vasculature interaction using a partial "whole-mount" dentate gyrus SGZ preparation.

A, Schematic illustration of the partial "whole-mount" dentate gyrus SGZ preparation. **B,** $CD31^+$ blood vessels using "whole-mount" preparation visualized in SGZ (left panel) and GCL (right panel). Scale bar: 100 μm. **C,** Sample projected confocal image of *Nestin-GFP* tissue from "whole-mount" preparation immunostained for Tbr2, CD31 and DCX. Scale bar: 100 μm. **D,** Quantification of vascular association of different cell types expressing various combinations of Nestin-GFP, Tbr2, and DCX, utilizing the "whole-mount" preparation to view the population of progenitors in the SGZ. Association was defined as having cell soma on a blood vessel and compared with simulated random distributions of the same numbers of cells in the same space. Values represent means ± s.e.m. (n = 3 animals; *P < 0.05; **P < 0.01; one-tailed unpaired Student's t-test; $Tbr2^+$: $t(4) = 2.20$; $Tbr2^+Dcx^+$: $t(4) = 2.44$; Dcx^+(neuroblast): $t(4) = 3.76$).**E,** Sample confocal image and 3D rendering of $Tbr2^+Dcx^+$ neuroblast migrating on $CD31^+$ blood vessel with polarized $GM130^+$ Golgi apparatus from "whole-mount" preparation in *Nestin-GFP* mouse. Scale bar: 10 μm.

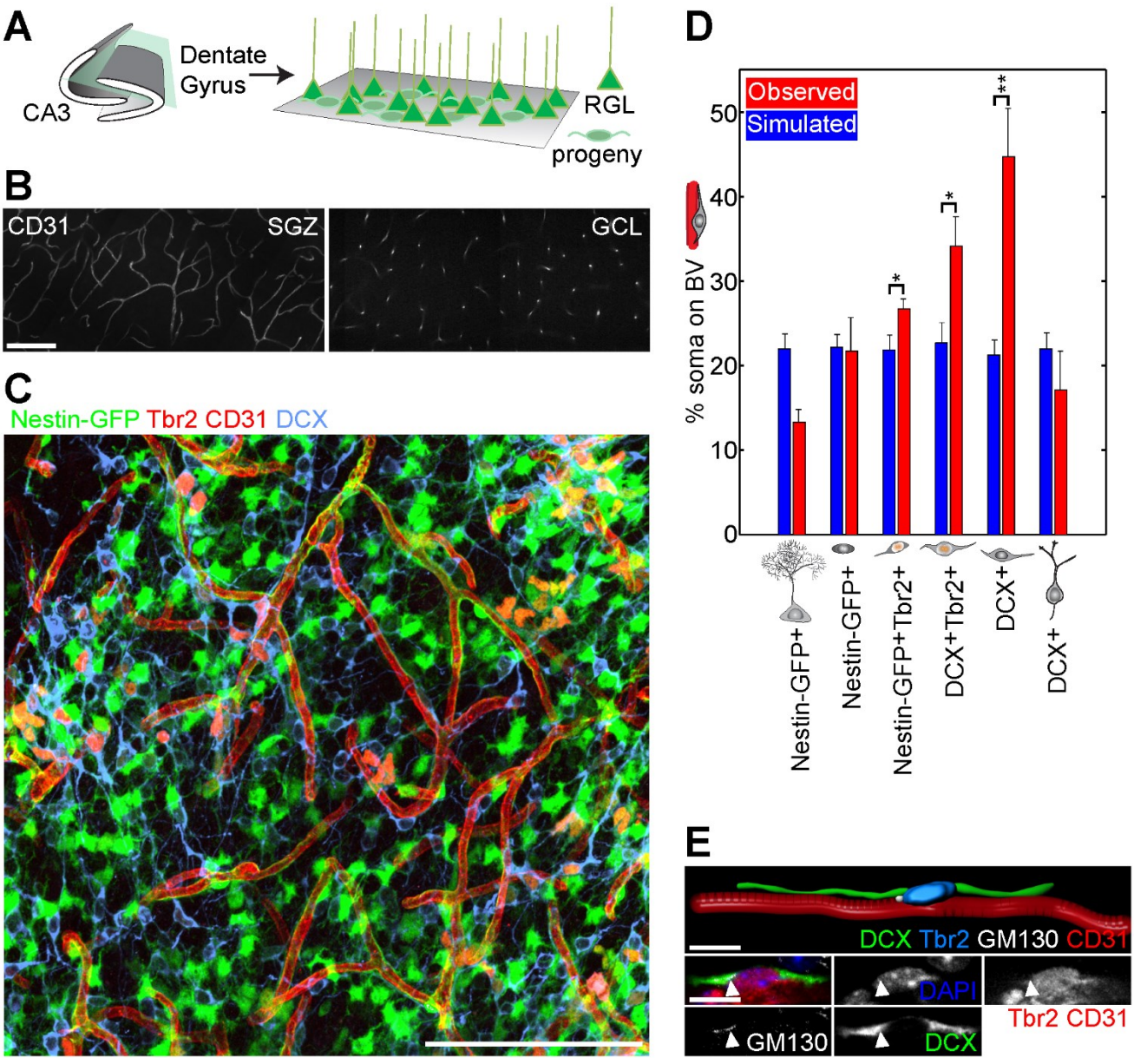
A
Dentate
Gyrus
CA3
RGL
progeny
B
CD31
SGZ
GCL
C
Nestin-GFP Tbr2 CD31 DCX
D
Observed
Simulated
% soma on BV
50
40
30
20
10
0
*
*
**
Nestin-GFP+
Nestin-GFP+
Nestin-GFP+Tbr2+
DCX+Tbr2+
DCX+
DCX+
E
DCX Tbr2 GM130 CD31
DAPI
Tbr2 CD31
GM130
DCX

Figure 12. A two-step model for neuronal migration during adult hippocampal neurogenesis.

A, During adult hippocampal neurogenesis, radial glia-like cells (RGLs) can undergo neurogenic divisions and give rise to $Tbr2^+$ intermediate progenitor cells (IPCs) within 3 days. In the next 4 days, the cells become DCX^+ proliferating neuroblasts (NBs) that extend long processes tangential to the SGZ, and contact blood vessels directly. During this phase, neuroblasts utilize blood vessels as a substrate to migrate tangentially away from their parental RGL. After 7 days, newborn neural progeny extend radial dendritic processes and develop into mature, $NeuN^+Prox1^+$ dentate granule neurons and exhibit limited radial migration through the granule cell layer. **B,** Global-view illustration of RGLs, neural progeny, and vasculature in SGZ across the adult hippocampus. The SGZ contains a dense bed of capillaries on which neuroblasts with tangential morphology migrate.

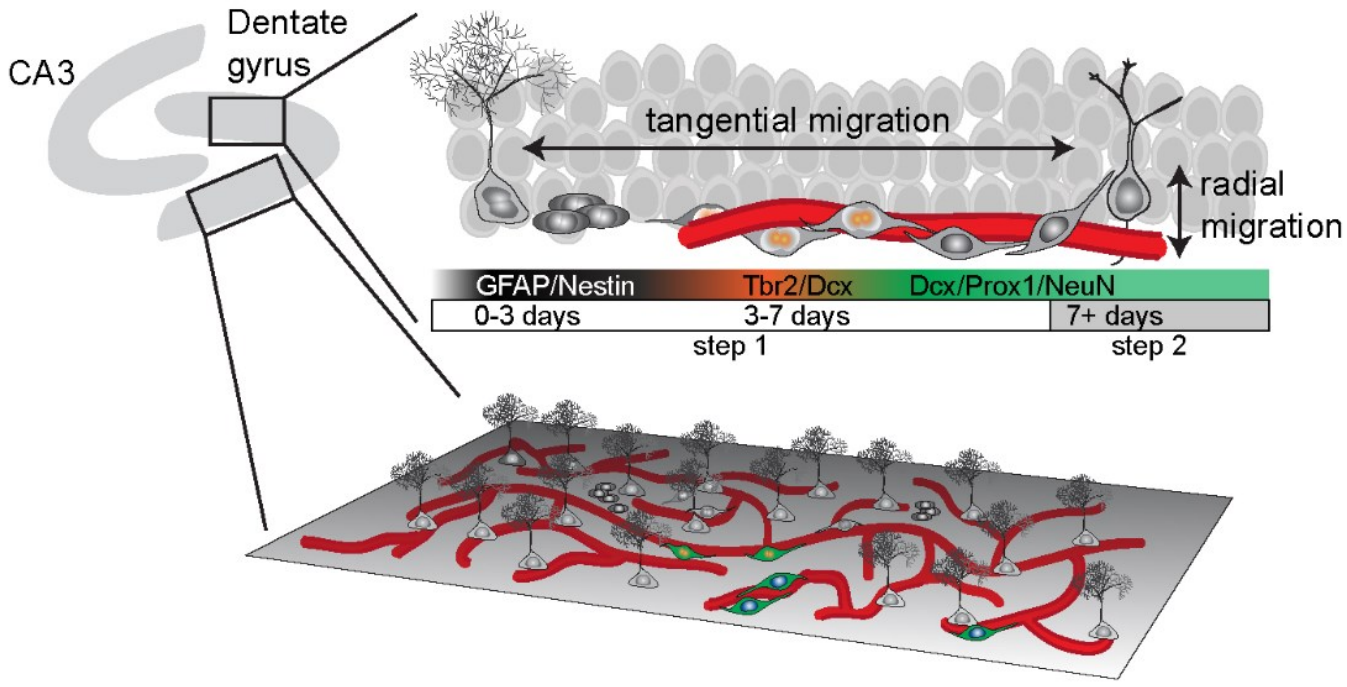
CA3
Dentate
gyrus
tangential migration
radial
migration
GFAP/Nestin
Tbr2/Dcx
Dcx/Prox1/NeuN
0-3 days
3-7 days
7+ days
step 1
step 2

4.4.1 Tangential migration of glutamatergic neurons

My data showing dominant tangential migration of neural precursors of glutamatergic dentate granule cells in the adult brain tempers the classical radial unit hypothesis of early cortical development[82]. Interestingly, several recent studies support the notion that at least some rare[89], although usually transient[88,90], populations of excitatory cortical neurons may migrate tangentially. Furthermore, earlier studies describing tangential neuronal migration in embryonic cortex[84–87] may have actually described the later discovered tangentially migrating inhibitory neurons[100,101]. Radial and tangential migration modes may not be specific to any given neuronal type and may depend on both intrinsic and extrinsic mechanisms. Indeed, in cerebellum, inhibitory principal purkinje neurons exhibit radial migration, whereas excitatory modulatory granule neurons migrate tangentially as well as radially[102]. Motor neurons in the spinal cord possess both radial and tangential migration[103]. Additionally, neurons originating from the diencephalon can migrate tangentially to populate a telencephalic nucleus, the amygdala[104].

Here, I have described an example of tangential migration of neural precursors of excitatory principal neurons within the neocortex and, for the first time, in the adult mammalian brain. The migration magnitude observed, although significant, is much less than that of migrating SVZ neuroblasts or even radially migrating neocortical neurons. This may be due to differences in tissue architecture. Neuroblasts in SVZ are born far from their target brain structure; neocortex is a thick, 6-layered volume, whereas dentate gyrus is a comparatively thin single-layer sheet. In addition, my retrospective analyses in this study captured only static, net cell movements. Future long-term *in vivo* time lapse

microscopy of newborn neural progeny would provide richer, detailed kinetics of newborn progeny dispersion. Nonetheless, the existence of tangential in addition to radial migration capacity of adult-born, excitatory dentate granule cells represents an important conceptual advance.

4.4.2 Implications of tangential migration as a dominant form of newborn neuron distribution in adult hippocampus

I provided the first quantitative evidence of neuronal precursor tangential distribution, as well as morphological evidence of migratory cells in the adult mouse hippocampus. Given my data that newborn granule cells along the hippocampal axis possess different, ordered mossy fiber axonal projections to and through CA3 (see Chapter 5), tangential migration may allow individual neural precursor cells to induce plasticity over a much larger post-synaptic circuit than if otherwise restricted to a radial column. Moreover, tangential migration allows for a larger area of structural plasticity induction in pre-synaptic perforant path axons. Together with recent evidence that neuronal circuit activity regulates neural stem cell activation[35], my results highlight the rich capability for widespread structural plasticity across the network of adult hippocampus interfaced by the dentate gyrus.

Evidence suggests that in many contexts including the adult neurogenic niches[105–108], migrating newborn progeny provide feedback signaling onto their mother cell of origin or other niche progenitors to control important processes such as proliferation and fate commitment[109]. Recent studies have also shown that neuroblasts are subject to neuronal

circuit activity-dependent regulation of survival[44] and therefore represent a highly dynamic and mobile population that has the potential to interact with and affect the dentate gyrus network and stem cell niche. Thus, in addition to supporting tissue development or growth, newborn cells may play a critical role as second messengers for cell-cell communication and contribute to niche homeostasis.

4.4.3 New insight into function of vascular niche: substrate for tangential migration

Vasculature has been previously proposed as a crucial niche component for adult neurogenesis in both SGZ and SVZ[93–96], however, its functional role is not well-understood. My results that neuroblasts exhibit several features of migrating cells, such as polarized organelle distribution, and that there exists tight, direct association between neuroblasts and vasculature at cellular and ultrastructural levels suggest that one function of this niche component is to support migration of neuronal progeny away from their parental origin. Interestingly, GABAergic neurons generated in the adult SVZ have also been shown to migrate along blood vessels in the rostral migratory stream[110,111] and towards injury sites following stroke[112]. Thus, in the adult brain, vasculature may serve as a common substrate for migration of different neuronal subtypes. The postulated recruitment of angiogenesis by clusters of proliferating newborn neural progeny in adult SGZ[96] also suggests a tantalizing mechanism by which cells utilize vascular "on-ramps" to access the highway of blood vessels for migration. Such mechanisms to support cell migration may exist during early development, as vascular outgrowth often precedes neural outgrowth, and migrating cells can be found in regions lacking classical migration substrates such as glial fibers[113,114].

4.4.4 Novel approaches for studying newborn neuron development and adult neurogenesis

We and others have previously only been able to document radial migration during adult hippocampal neurogenesis[29,47], due to population level analyses that lacked lineage-relationship information of individual stem cells and their progeny. Our new approach for clonal analysis of activating RGLs in the adult dentate gyrus using the *Ascl1*^{CreERT2} knock-in mouse line[97] enables examination of cell dispersion of individual newborn neural progeny with respect to their parental RGL. With the high temporal and spatial resolution our approach afforded, I for the first time directly compared tangential and radial migration for single cells. Interestingly, the two forms of migration appeared to be uncorrelated and tangential preceded and exceeded radial migration; together these data suggest independent mechanisms may regulate the two migration modes. Combined with conditional gene inactivation, our new clonal analysis approach could directly address this problem in a future study to elucidate the mutual or exclusive underlying molecular mechanisms governing different forms of migration.

I also developed a new partial "whole-mount" preparation to maximally visualize the SGZ niche and showed that the general population of neuroblasts is in close contact with the blood vessel network and exhibits polarized Golgi, characteristic of migrating cells. This enabling technique will allow for future systematic characterization of the complete global architecture of the hippocampal niche. Such characterization could potentially reveal important motifs and structure to provide context for my observed network of

vasculature and migrating cells. Ultimately, my technique can help broaden our knowledge of the general principles of neurogenic niches, especially in combination with that learned from similar approaches in the adult SVZ[93–95].

4.4.5 Conclusion

My clonal analyses of activating radial glia-like neural stem cells revealed a new migration mode of neuroblast precursors of glutamatergic neurons in the mature mammalian nervous system. Given that adult neural stem cells are dynamically regulated by their local environment, including neuronal activity[35], my findings have significant implications for understanding how individual neural stem cells could impact the function of the existing microcircuit via delivery of newborn neurons with enhanced plasticity[52,115]. My findings also provide a new direction to understand aberrant migration of newborn granule cells under pathological conditions, such as epilepsy[116,117]. In addition, the identification of a novel mode of glutamatergic cell tangential migration along the vasculature suggests a new strategy to overcome current challenges in targeting glutamatergic neurons to injured or degenerating regions for successful cell transplantation therapy in the adult mammalian brain[118]. Together, my results open the possibility that diverse modes of migration may be ubiquitous among different neuron classes in the adult mammalian brain, providing important conceptual groundwork for future studies of neural development, regeneration, repair and brain disorders.

5 — Axon and dendrite development of adult-born neurons

5.1 Introduction

The adult mammalian hippocampus undergoes remarkable structural plasticity whereby new dentate granule cells are continuously generated and integrated into the existing circuitry[12]. Cumulative evidence suggests contributions of newborn neurons to specific hippocampal functions, attributed partly to special properties that arise transiently during their development and maturation[50,52,53,119,120]. How new neurons directly impact hippocampal function is not well understood, in part because there is little knowledge about the spatial extent and development of their efferent projections. Understanding basic features of adult-born granule cell development may not only provide novel insight into fundamental principles of neuronal development and function of adult neurogenesis, but also strategies for cell replacement therapy in the mature nervous system.

Proper guidance of a developing axon to its target is an essential step of circuit formation. Significant progress has been made in the last two decades in deciphering axon guidance processes, including growth, targeting, and fasciculation in the developing nervous system[121]. In the adult rodent hippocampus, studies using nucleotide analog or onco-retrovirus labeling have demonstrated that newborn granule neurons rapidly extend their axons to the CA3 region and form morphologically and functionally characteristic mossy fiber bouton synapses[20,48–50,122,123]. In these early studies, however, complex axonal processes became fragmented in histological slices; and tissue loss and distortion from sectioning prevented faithful serial reconstruction of individual thin, long axons[124]. As a result, we know very little about axonal guidance and development of newborn neurons

in the adult brain. The relationship of axonal to dendritic development of individual newborn neurons and among different newborn neurons is also unknown. Knowledge of full neuronal structure and development will provide a better understanding of new neuron function in the adult brain. Such information would be also invaluable for understanding neurological disorders, such as epilepsy and schizophrenia, in which adult-born granule axonal development is thought to be greatly altered[48,125,126].

To elucidate the structure and development of intact adult-born granule cells in vivo, I developed a novel method of serial sectioning and imaging, termed serial end-block imaging (SEBI), for seamless reconstruction of unlimited tissue volume. I characterized axonal and dendritic development of newborn neurons in the adult mouse hippocampus between 10 and 77 d after retroviral labeling. I found that axons of newborn neurons follow a highly stereotyped, tortuous path from the dentate gyrus through the CA3 subfields and exhibit regular laminar organization along the hippocampal septo-temporal axis. Furthermore, rapid primary axonal process and dendritic development occurs within the first 21 d. My study provides novel insights into adult neurogenesis and demonstrates a striking capacity of the mature brain environment to support long-distance growth and guidance of neuronal axons.

5.2 Methods

Stereotaxic virus injection and tissue processing

Engineered murine onco-retrovirus containing green fluorescent protein (GFP) or GFP-tagged Channelrhodopsin 2 cDNA and Woodchuck hepatitis post-transcriptional

regulatory element, both driven by the Ubiquitin-C promoter, were generated as previously described[42,47,127]. High titers of retrovirus were stereotaxically injected into the dentate gyrus of 8-week-old C57BL/6 female mice (Charles River) using a Nanoject II microinjection glass pipette (Drummond Scientific) at four sites (0.5 μl per site) with a 5–10 μm tip using the following coordinates from bregma (mm): anterior—posterior (AP) −2.0, lateral ± 1.6, ventral −1.6; AP −3.0, lateral ± 2.5, ventral −1.8. All animal procedures followed approved institutional protocols.

At 10, 17, 21, 35, 56, and 77 d post-injection (dpi) of retrovirus, mice (n = 2, 1, 2, 2, 1, 2, respectively) were perfused with 4% paraformaldehyde (PFA) and brains were postfixed in PFA overnight. Brains were then transferred to PBS with 0.02% sodium azide and stored at 4°C. One to 2 mm of tissue was removed from the lateral portion of the posterior cerebral cortex and cerebellum at ∼15° angle to provide a flat surface for mounting. The brain was then separated at the midline into hemispheres and cyanoacrylate glued to a 2 mm agarose disc on the posterior 15° mounting surface of the brain, which translates into a 15° cut angle off the sagittal plane for serial imaging/sectioning. The sample was then placed in a 6-well culture dish and covered with 2% agarose (Sigma-Aldrich) in saline. The tissue-containing gel cube was glued to the base of a vibrating microtome chamber. The chamber was rinsed and filled with normal saline for the imaging procedure.

Serial imaging and vibrating microtome sectioning

The tissue block was imaged using an upright confocal microscope (LSM 510; Carl Zeiss) with a two-photon laser (Chameleon; Coherent) tuned to 910 nm and a 20× 1.0 NA water-dipping objective (Carl Zeiss) using a tile scan (8-bit, 0.88 μm × 0.88 μm × 2 μm) with a 10% overlap. Once imaged at a z-depth of 120 μm, the tissue block was sectioned with a sapphire blade (121–18; Ted Pella) at a depth of 60 μm using a vibrating microtome with digital z-indexing (VT1200; Leica Microsystems). The sections were collected and stored in PBS with 0.02% sodium azide. The procedure was repeated until the tissue was sectioned and imaged in its entirety (see Fig. 13A, B). Images were acquired with sufficient overlap in all three dimensions (50% in z-axis, 10% in x, y-axis) for computer-guided tissue volume reconstruction.

The chamber was reproducibly positioned on the microscope and vibrating microtome stages using modified hardware, consisting of an aluminum plate with three conical holes and two linear slots that were machined and mated with the chamber (Fig. 13C). A microscope stage adapter was also manufactured with three 3/8-inch tooling balls (McMaster-Carr) that matched the conical hole dimensions of the chamber to provide accurate, reproducible chamber positioning on the microscope stage. Metal rails were attached to the vibrating microtome stage; these mated with the linear slots of the chamber for accurate positioning and reproducible sectioning on the vibrating microtome.

Volume reconstruction of hippocampus via rigid-body transformation

Acquired images were aligned for volume reconstruction in XuvStitch software[55]. XuvStitch calculates and uses only rigid-body transformations; the software outputs

aligned image volumes and the associated x, y, z coordinates used for alignment. Blind or guided alignment algorithms can be used by the software, with increased memory usage and ability to robustly align arbitrary images for the blind algorithm.

Each imaged tissue section, or "slab," consisted of tiled cubes with 10% x, y-overlap between adjacent within-slab cubes and 50% overlap between those of previous or successive slabs. Image slabs were first split into their constitutive tiled cubes. One cube from each imaged slab was paired with its z-overlapping counterpart from a successive slab, loaded into XuvStitch, and x, y, z alignment coordinates were collected from blind, "exhaustive search" stitching (Fig. 13D). These coordinates were propagated to all cubes within a respective slab to yield a theoretical alignment of all cubes from all slabs. The propagated coordinates were then loaded, along with their associated cubes, into XuvStitch for final alignment using the memory-efficient guided, "current coordinate" alignment algorithm (Fig. 13D).

Image deconvolution and normalization

To correct for imaging artifacts (e.g., z-spreading) inherent to laser-scanning microscopy, 3D deconvolution was performed on the reconstructed hippocampus volumes (Autoquant; MediaCybernetics). Inherent to imaging through opaque tissue, there was a significant decay of signal intensity with increasing imaging depth. In addition, acquisition parameters varied depending on strength of fluorescent signal and alignment and power output of the multiphoton imaging laser throughout the multiday SEBI acquisition process. Z-slices within a given reconstructed hippocampus volume were

therefore quantile normalized. Originally used to normalize identical features across replicates of microarray chips[128], quantile normalization preserves relative intensity values within an image, while normalizing intensities between images. Quantile normalization produced both qualitatively (Fig. 13E) and quantitatively (Fig. 13F) uniform intensity across the z-axis in the volume of tissue.

Neuronal structure tracing and quantification

The complete granule cell structure was traced using the FilamentTracer module in Imaris (Bitplane) software on a computer containing a Quadro 5000 (Nvidia) video card with 3D Vision (Nvidia) stereoscopic visualization. Three-dimensional glasses were used to visualize the large datasets and the autodepth and/or autopath tracing modes were used for tracing. In addition, the orthoslicer feature was used to visualize the 2D data to discriminate difficult-to-resolve structures. The complete dendritic structure and primary branch of axons of individual GFP^+ granule cells were traced. Given a previous report of differential developmental rates of newborn neurons in the septal and temporal hippocampus[129], only traced cells in the septal half of the hippocampus were used for quantitative analysis of primary axonal length and total dendritic length (3, 8 cells at 10 dpi; 10 cells at 17 dpi; 11, 3 cells at 21 dpi; 10, 3 cells at 35 dpi; 15 cells at 56 dpi; and 6, 7 cells at 77 dpi; cell numbers are listed per mouse) and these cells were combined with additional cells traced from the temporal half for analysis of organization of axonal projections within cohorts of adult-born granule cells along the septo-temporal axis (n = 5 cells at 77 dpi; see Fig. 15D). Axon collaterals were excluded from analyses due to their thin (<0.2 μm)[130] and highly convoluted, overlapping structure that precluded reliable

tracing with our imaging resolution and GFP brightness. In accordance with previous anatomical characterizations, axon boutons were defined as puncta directly connected to the axonal structure with a diameter >3 μm[131]. Similar to axon collaterals, axon boutons <3 μm in diameter, although numerous and important[130], were excluded from analyses due to their small size, which precluded reliable identification with our imaging resolution and GFP brightness.

Sholl analysis (in 3D) for assessing dendritic complexity was performed in Imaris and neuronal structure parameters were exported to an Excel spreadsheet. Total dendrite length was reported as the sum of all dendrite branches; axon length was reported as the length of only the single primary axon branch. Statistical analyses were performed using one-way ANOVA with a Tukey *post hoc* test in OriginPro Software (OriginLab) and the two-sample Kolmogorov–Smirnov test in MATLAB (MathWorks). Correlation was calculated in MATLAB and reported as a Pearson's correlation coefficient, R^2, with an associated p value calculated using Student's t test. Ordinary least-squares linear regressions and associated SEM, 95% confidence intervals, and p values were calculated using multiple linear regression analysis and a bootstrapping procedure in MATLAB. For data where x values were not experimentally fixed, ordinary least products regression was used.

Axon stacking was defined as the instance when an axon from a more septal granule cell projected dorsally over a neighboring axon from a more temporal granule cell (Fig. 15D). Axon staggering was defined as the instance when an axon from a more septal GFP^+

granule cell terminated before that of a more temporal GFP^+ granule cell along the septo-temporal axis. Both axon traits were quantified on a per cell basis across cells from adjacent transverse planes. Cells that violated either pattern were quantified only once to prevent spurious classifications upon comparison with other cells.

Figure 13. SEBI imaging paradigm, image reconstruction technique, and normalization.

A, SEBI imaging paradigm to obtain optimal image quality of intact tissue: tissue of interest (depicted by a brown cube) is end-block imaged, sectioned, and serially reconstructed by overlaying high-quality signal within the superficial layers on top of the lower quality signal within deep regions. **B,** A schematic diagram of SEBI procedure. **C,** Tissue chamber with conical holes (filled arrows) and slots (open arrows) that mates with imaging and sectioning stages for reproducible positioning. **D,** Image reconstruction technique (from left to right): end-block imaging yields an imaged tissue slab array of 10%-overlapping tiled cubes. Cubes in adjacent slabs are used to determine x, y, z-offset values. Offsets are then propagated to all cubes within the dataset to allow for complete volume stitching and seamless reconstruction. **E,** Sample X-Z projection image of unprocessed reconstructed adult hippocampus with high signal intensity variation (red circle, left image), and subsequent uniform signal intensity after quantile normalization (red circle, right image). Scale bar, 300 μm. **F,** Plot of intensity change versus z-depth of reconstructed hippocampus subregion in E before (black line) and after (red line) normalization. Note that before normalization, intensity variability existed within a tissue slab (a) and between imaging sessions (b).

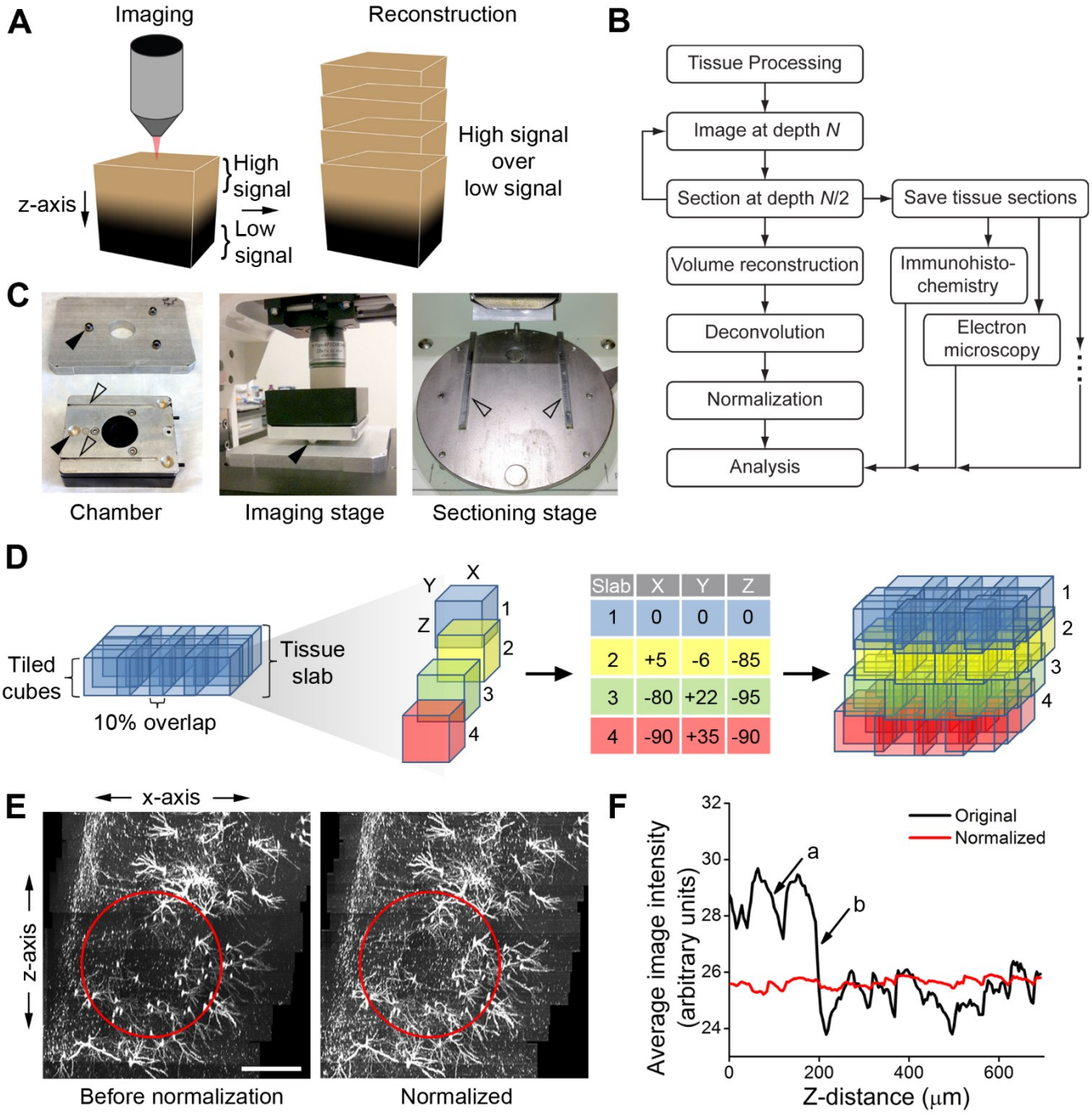
A
Imaging
Reconstruction
High signal over low signal
z-axis
High signal
Low signal
B
Tissue Processing
Image at depth N
Section at depth N/2
Save tissue sections
Volume reconstruction
Immunohisto-chemistry
Deconvolution
Electron microscopy
Normalization
Analysis
C
Chamber
Imaging stage
Sectioning stage
D
Tiled cubes
Tissue slab
10% overlap
Slab X Y Z
1 0 0 0
2 +5 -6 -85
3 -80 +22 -95
4 -90 +35 -90
E
x-axis
z-axis
Before normalization
Normalized
F
Original
Normalized
Average image intensity (arbitrary units)
Z-distance (μm)
a
b

5.3 Results

5.3.1 SEBI of intact cellular structure: whole hippocampus and axonal trajectory of adult-born dentate granule cells

To reconstruct the complete, fine primary axonal processes of adult-born dentate granule cells in the intact hippocampus, I developed a serial imaging and sectioning method, named SEBI. The fundamental principle underlying SEBI is to oversample imaging of intact tissue along the z-axis and reconstruct complete tissue volumes by overlaying high-quality signal from superficial layers onto lower quality signal from deep layers of successively imaged tissue (Fig. 13A). SEBI is achieved by serially imaging and then sectioning of a tissue block end-face (Fig. 13B). Block end-face imaging ensures that fully intact cellular structures are acquired in their native conformation. Utilizing a simple tissue chamber alignment apparatus (Fig. 13C), serial sectioning was highly reproducible. Because tissue slices are collected throughout the SEBI procedure, SEBI enables potential *post hoc* analysis with immunohistochemistry, electron microscopy, or other techniques (Fig. 13B). Importantly, I have also incorporated existing software and established a simple, effective means for rapid large volume reconstruction and image normalization to correct for significant decay of signal intensity with increasing imaging depth (Fig. 13E, F). Together, my SEBI technology provides a robust, flexible, and easily implemented method of imaging complete, intact cellular structure in essentially unlimited tissue volume.

I first applied the SEBI approach to examine the complete structure of GFP-labeled mature adult-born hippocampal dentate granule cells at 56–77 dpi. I successfully

reconstructed the entire mouse hippocampus and could, for the first time, visualize and trace the intact axonal primary projection to CA3 and complete dendritic processes of individual newborn neurons across the hippocampal septo-temporal axis (Fig. 14A). When annotating axon projection patterns, the CA3 region was subdivided into three subdomains (CA3a, CA3b, CA3c; Fig. 14B) in accordance with characterization by Lorente de Nó (1934)[132]. While projecting through the dentate gyrus hilar region toward CA3c, GFP^+ axons turned at an angle whose magnitude varied depending on the axon's parent soma location (range = 0–180°; Fig. 14B, #1). After projecting through the hilus and CA3c region, all axons analyzed exhibited a second, 90° turn from ventral to dorsal, as they traversed the CA3b subregion (Fig. 14B, #2). Turns #1 and #2 occurred precisely in the transverse hippocampal plane. Finally, upon entering CA3a, all axons analyzed exhibited a third, 90° turn, projecting toward the temporal pole of the hippocampus (Fig. 14B, #3). This complex axonal projection trajectory was highly stereotyped across all mature adult-born granule cells examined (n = 33) and may be present in all mature adult-born granule cells along the septo-temporal hippocampal axis. These results suggest a highly regulated axon-targeting process in the adult CNS.

Figure 14. Complete reconstruction of intact adult mouse hippocampus with SEBI.

A, Complete reconstruction of retrovirally labeled GFP+ newborn granule neurons (at 77 dpi) in the adult mouse hippocampus projected onto horizontal (A1), coronal (A2), and sagittal (A3) planes, with respect to the hippocampal axis as indicated. DG, dentate gyrus. Scale bar, 500 μm. **B,** Sample tracing of a single adult-born granule cell at 56 dpi shown in the same orientations as in A, with CA3 subregions color-coded for CA3c (orange), CA3b (green), and CA3a (purple), as defined by Lorente de Nó (1934)[132]. Primary axon projections of adult-born granule cells make as many as three distinct turns: (#1) up to 180° within the hilus, (#2) a ventral to dorsal turn within CA3b, and (#3) a longitudinal turn toward the temporal pole within CA3a. T, temporal; S, septal; L, lateral; M, medial; D, dorsal; V, ventral. Scale bar, 150 μm.

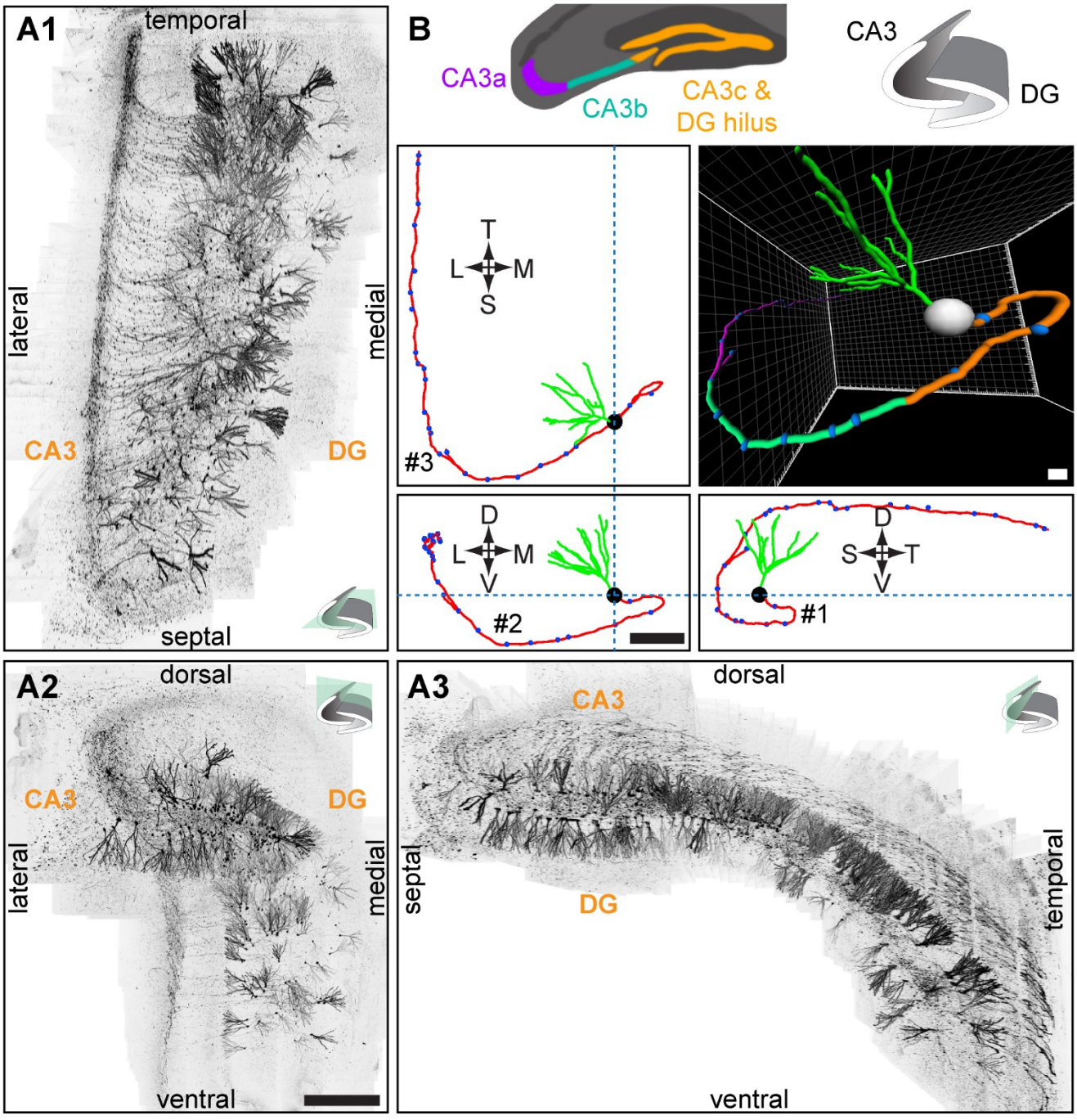
A1
temporal
lateral
medial
CA3
DG
septal
B
CA3a
CA3b
CA3c &
DG hilus
CA3
DG
T
L
M
S
#3
D
L
M
V
#2
D
S
T
V
#1
A2
dorsal
CA3
DG
lateral
medial
ventral
A3
dorsal
CA3
septal
DG
temporal
ventral

5.3.2 Characteristic axonal targeting and growth of individual newborn granule cells in the adult hippocampus

Having observed a stereotyped axon trajectory of mature adult-born granule cells, I next examined whether axons of newborn neurons follow such a tortuous path and target CA3 precisely throughout the course of their development. Two-month-old mice were injected with GFP-expressing retrovirus and examined at 10, 17, 21, 35, 56, and 77 dpi. All GFP^+ neurons exhibited a single axon from the cell body. Across all developmental time points examined, axons followed a very stereotypical path through the hilus and into CA3 (Fig. 15A). At 10 dpi, axons exhibited only the initial turn in the hilar region and projected as far as CA3b. No evidence of multiple growth cones was observed, suggesting that axons are precisely targeted. By 17 dpi, most axons made both hilar and CA3b turns, and by 21 dpi, axons had made all three stereotypical turns and projected into CA3a. Beyond 21 dpi, the primary axon projection patterns remained unchanged. These results suggest that developing axons of newborn granule cells follow their final projection path in the adult hippocampus.

Quantification of primary axon length of adult-born granule cells revealed two distinct developmental phases. During the initial phase from 10–21 dpi, axons rapidly increased their length (Fig. 15B). This first growth phase exactly matched the developmental window in which axons targeted and traversed through all CA3 subregions. Primary axonal length appeared to exhibit minimal change during a second phase from 21 to 77 dpi, a time when adult-born granule cells can evoke stable synaptic responses in CA3[50]. At 77 dpi, primary axons of adult-born dentate granule neurons exhibited an average

length of ~1.9 mm with the longest traced axon observed at 2.3 mm (Fig. 15B). Notably, my measurement represents an underestimation of total axonal length of adult-born neurons, as my analyses omitted their numerous, fine axon collaterals. Together, these results demonstrate that newborn neurons can extend very long axonal projections in an otherwise highly inhibitory adult CNS environment for regenerating axons of mature neurons.

Figure 15. Axonal development, targeting, and organization of newborn granule cells in the adult mouse hippocampus.

A, Horizontal view of sample traced axons from 10, 17, 21, 35, 56, and 77 dpi. Scale bar, 100 μm. **B**, Primary axon length of newborn granule neurons at different times after labeling. Open orange circles represent data from individual GFP^+ neurons examined. Numbers associated with open circles indicate total number of GFP^+ neurons examined for each condition. Values representing mean ± SEM are also shown (●; *$p < 0.01$; #$p = 0.12$; one-way ANOVA, $F_{(5,70)} = 61.92$, $p \approx 0$). **C**, Representative tracings of three adult-born granule cells with temporal (a), center (b), and septal (c) relative positions. Arrows highlight sharp turn of more laterally positioned granule cells. **D**, Coronal view and illustration of axon organization among adult-born granule cells in C along the septo-temporal axis: (i) horizontal view illustrating axon stacking and staggering of termination points; (ii) coronal view illustrating graded axon hilar turns. T, temporal; S, septal; D, dorsal; V, ventral.

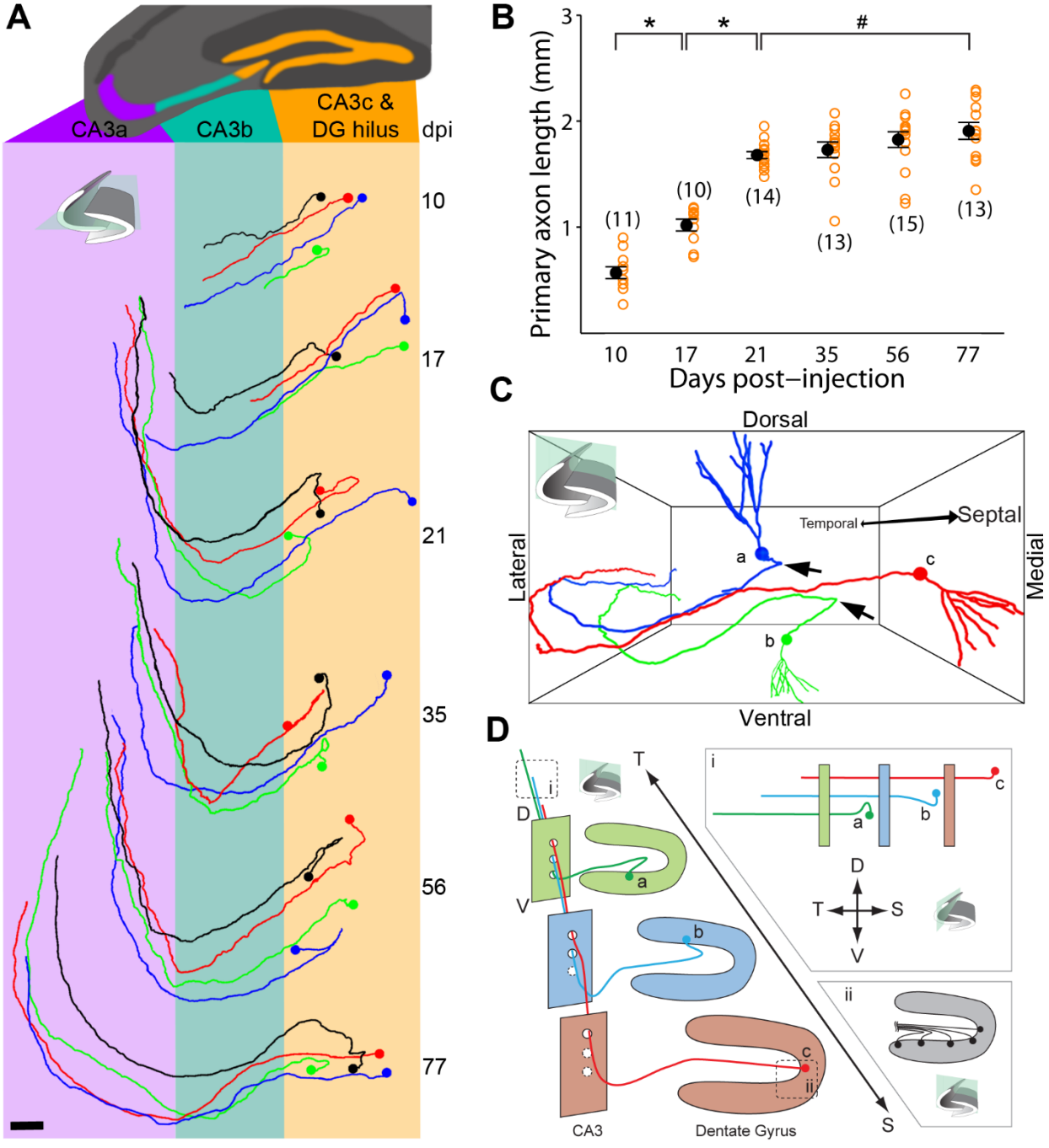
A
CA3a
CA3b
CA3c &
DG hilus
dpi
10
17
21
35
56
77
B
Primary axon length (mm)
Days post−injection
(11)
(10)
(14)
(13)
(15)
(13)
C
Dorsal
Ventral
Lateral
Medial
Temporal
Septal
a
b
c
D
CA3
Dentate Gyrus
T
S
D
V
i
ii

5.3.3 Highly organized axonal projections within cohorts of adult-born granule cells

After characterizing axon growth and targeting of individual neurons, I next addressed whether any organizational patterns or lamination existed among cohorts of developing adult-born granule cells. During adult hippocampal neurogenesis, newborn neurons arise from adult neural stem cells via transient cell amplification stages, thus my GFP^+ cells represented cohorts of sister new neurons born around the same time[34]. When comparing neighboring GFP^+ neurons at a given time point (between 21 and 77 dpi), I observed a highly regular lamination pattern in the CA3a region (Fig. 15D). Approximately 90% (45/50) of traced axons originating from more septal neurons (Fig. 15C, D, c) stacked dorsally on top of those from more temporally positioned neurons (Fig. 15C, D, b). I also observed staggering of axon termination points in the CA3 region, whereby 84% (42/50) of traced axons from more septal neurons terminated sooner than those from more temporal neurons (Fig. 15D, i). This organization was present throughout the septo-temporal axis and independent of total axonal length of adult-born neurons. Finally, hilar axon segments differed in curvature depending on the granule cell soma location across the dentate gyrus granule cell layer. The initial hilar turn (Fig. 14B, #1) was present in ever-increasing curvature from 0° at the genu to 180° at tips of the granule cell layer (Fig. 15D, ii). Thus, axons originating from more lateral granule cells would first grow medially toward the genu before making an about-face turn toward CA3c. Together, these studies reveal a stereotypic organization between axons of adult-born neurons born around the same time and suggest an intricate axon guidance behavior during adult neurogenesis.

5.3.4 Axon bouton development of adult-born dentate granule cells

Dentate granule cell axons are also known as mossy fibers because they make morphologically distinct, large (>3 μm diameter) *en passant* synapses or boutons with targets in the hilus and CA3 regions[131]. I focused my study on the development of these large mossy fiber boutons in the same previously analyzed (Fig. 15) set of GFP^+ neurons between 10 and 77 dpi (Fig. 16A). Similar to axonal development, I observed two phases of bouton development. At the population level, average bouton density increased dramatically from 10 to 21 dpi and remained constant thereafter (21–77 dpi; Fig. 16B). To examine whether granule cell axons developed a constant number of boutons, or whether bouton numbers scaled directly with primary axon length, I quantified total bouton number and axon length at an individual cell level (Fig. 16C). At 10 dpi, boutons were mostly absent (Fig. 16B) and therefore uncorrelated with axon length ($R^2 = 0.02$, $p = 0.71$). Primary axon length correlated strongly with bouton number from 17 through 35 dpi ($R^2 = 0.79$, $p < 0.0001$). From 56 to 77 dpi, bouton numbers were weakly correlated with primary axon length ($R^2 = 0.19$, $p = 0.02$). Heterogeneity in both primary axon length and bouton numbers was most marked at 56 and 77 dpi (Fig. 16C). Such heterogeneity may have implications for how newborn granule cells choose and maintain synaptic partners in CA3 of the adult dentate gyrus.

Figure 16. Axon bouton development of newborn granule cells in the adult mouse hippocampus.

A, Sample confocal images of axon segments within the CA3b (2 μm depth). Arrows denote axon boutons. Scale bar, 10 μm. **B**, Axonal mossy fiber bouton density of newborn granule neurons at different times after labeling. Open orange circles represent data from individual GFP^+ neurons examined (the same set of neurons as in Fig. 15). Values representing mean ± SEM are also shown (●; *$p < 0.01$; #$p = 0.98$; one-way ANOVA, $F_{(5,70)} = 44.01$, $p \approx 0$). **C**, Relationship between total number of axon boutons and primary axon length for individual adult-born granule cells at different developmental stages. Top graph, Scatter plot of data from individual neurons (same set as in B). Bottom graphs, Individual plots for 10, 17–35, and 56–77 dpi with linear fit and Pearson's correlation R^2 (p value from Student's t test).

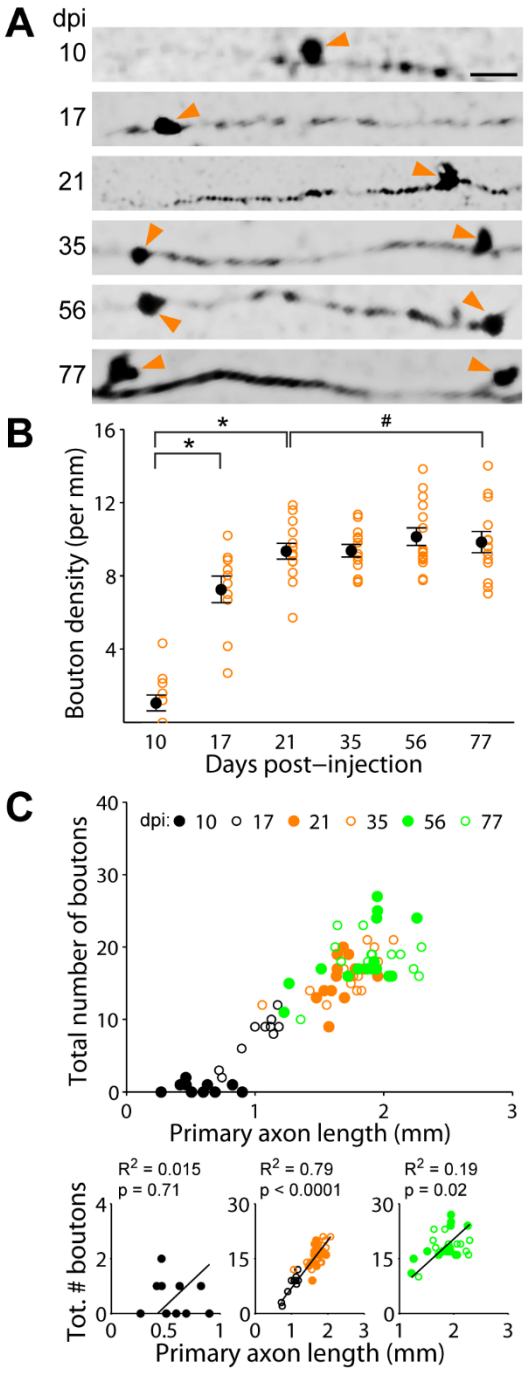
A
dpi
10
17
21
35
56
77
B
Bouton density (per mm)
Days post–injection
C
dpi: 10 17 21 35 56 77
Total number of boutons
Primary axon length (mm)
R2 = 0.015
p = 0.71
R2 = 0.79
p < 0.0001
R2 = 0.19
p = 0.02
Tot. # boutons
Primary axon length (mm)

5.3.5 Complete dendritic structure of adult-born granule cells and relationship to axonal development

SEBI also enables reconstruction of complete dendritic arbors without sectioning artifact; this allowed for the first full-structure characterization of intact newborn granule cell dendritic development in the adult mouse hippocampus (Fig. 17A). Interestingly, and similar to axonal development, dendrites of newborn neurons exhibited a defined window of rapid growth. Consistent with previous characterizations of dendritic arbors from histological slices[20,42], dendritic growth was most rapid and average total dendritic length more than doubled during an initial phase from 10 to 21 dpi (Fig. 17B). The total number of dendritic branches peaked by 17 dpi (Fig. 17C). Sholl analysis revealed that dendritic complexity stabilized by the end of the first growth phase at 21 dpi (Fig. 17D). Similar to that seen in axonal development, there appeared to be minimal growth of dendrites during the phase from 21 to 77 dpi (Fig. 17B). By 77 dpi, the average total dendritic length was ~1.5 mm.

My fully reconstructed axons and dendrites were from discrete cells during different developmental stages, thus my approach enabled investigation of potential correlations between axonal and dendritic development (Fig. 18A). As observed individually, both primary axons and total dendrites exhibited a rapid growth phase (10–21 dpi) followed by a phase of minimal growth (21–77 dpi). Interestingly, axon to dendrite length ratio of individual neurons fluctuated from high to low from 10 to 17 dpi before stabilizing at a constant ~6:5 ratio between 17 and 77 dpi (Fig. 18A, B). I also calculated the growth rates of axons and dendrites for their two developmental phases (Fig. 18C). From 10 to

21 dpi, axon primary projections grew at a rate of 97 ± 5.7 μm per day (mean ± SEM) and exhibited strong linear correlation with time ($R^2 = 0.931$, $p = 0.17$). The same analysis of dendrite growth from 10 to 21 dpi also yielded strong correlation ($R^2 = 0.98$, $p = 0.10$), with a growth rate of 111 ± 5 μm per day. From these linear fits, axon growth would therefore begin ~4.7 d (x-intercept) after new neurons were born, and dendrites would commence growth ~8 d after their birth. Interestingly, although from 21 to 77 dpi newborn neurons appeared to show minimal change in their primary axon and total dendritic length, there were statistically significant and measureable growth rates for both primary axons (4.1 ± 1.5 μm) and dendrites (3.2 ± 1.3 μm per day; Fig. 18C). Together, my individual cell analyses reveal for the first time how primary axon and whole dendrite outgrowth is coordinated at different developmental phases during adult hippocampal neurogenesis in vivo.

Figure 17. Dendritic development of newborn granule cells in the adult mouse hippocampus.

A, Sample 2D-projection tracings of complete dendritic processes of adult-born granule cells at different times after labeling. Scale, 30 μm. **B**, **C**, Total dendritic length (B) and branch number (C) of newborn granule neurons at different stages during adult hippocampal neurogenesis (same set of GFP^+ neurons as in Figs. 15, 16). Open orange circles represent data from individual GFP^+ neurons examined. Values representing mean ± SEM are also shown (●; *$p < 0.01$; **$p < 0.05$; #$p = 0.76$; ##$p \approx 1$; one-way ANOVA, (***B***) $F_{(5,70)} = 62.60$, $p \approx 0$, (***C***) $F_{(5,70)} = 39.29$, $p \approx 0$). **D**, Sholl analysis of dendritic complexity (the same set of neurons as in B and C). Values represent mean ± SEM (*$p < 0.05$; #$p = 0.68$; two-sample Kolmogorov–Smirnov test).

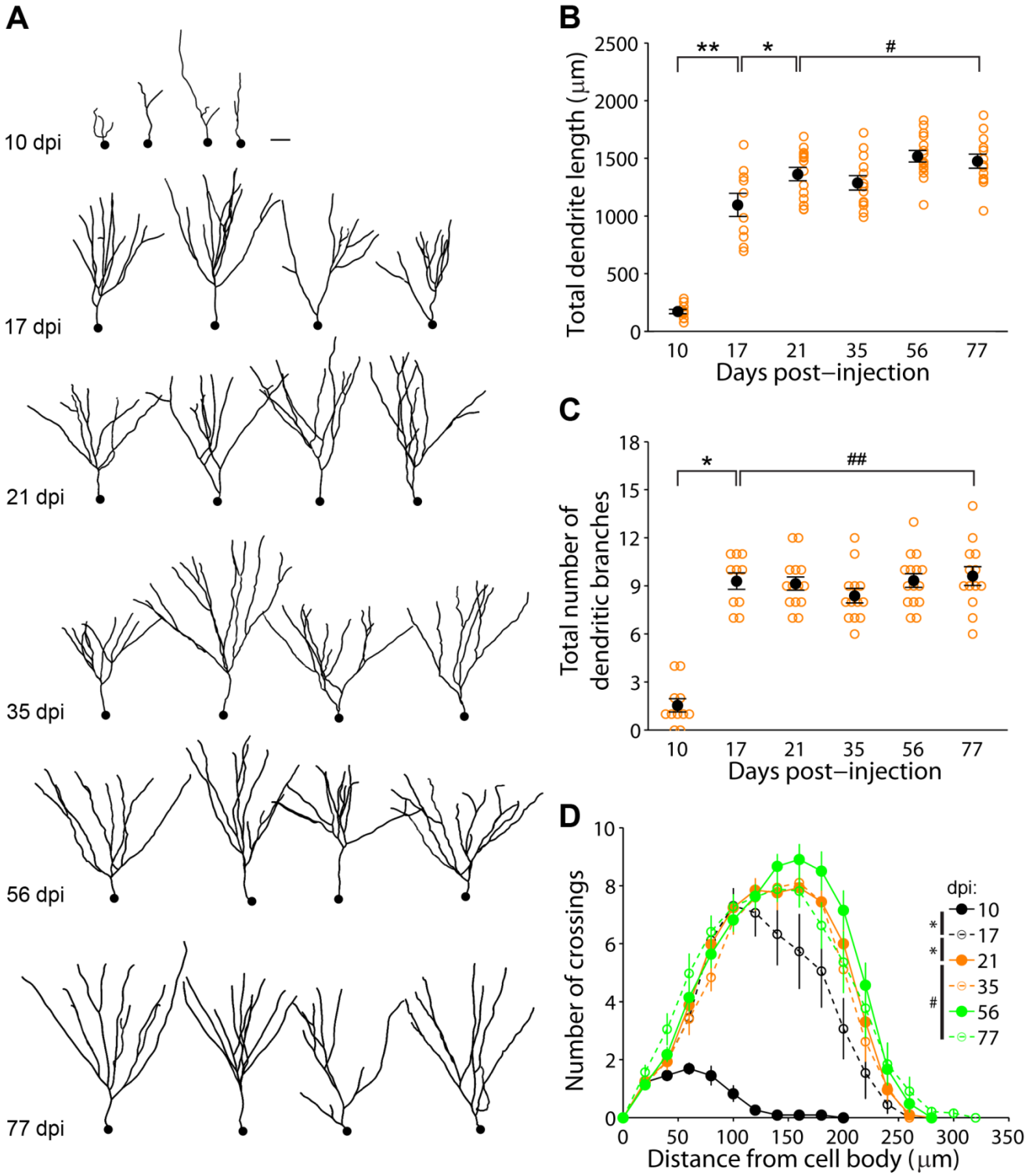
A
10 dpi
17 dpi
21 dpi
35 dpi
56 dpi
77 dpi
B
Total dendrite length (μm)
2500
2000
1500
1000
500
0
**
*
#
10
17
21
35
56
77
Days post−injection
C
Total number of dendritic branches
18
15
12
9
6
3
0
*
##
10
17
21
35
56
77
Days post−injection
D
Number of crossings
10
8
6
4
2
0
0
50
100
150
200
250
300
350
Distance from cell body (μm)
dpi:
10
17
21
35
56
77
*
*
#

Figure 18. Relationship between axonal and dendritic development of individual newborn granule cells during adult hippocampal neurogenesis.

A, Scatter plot of primary axon and total dendritic length of individual adult-born granule cells examined for all time points (the same set of GFP^+ neurons as in Fig. 15). Also shown is a linear fit of data from 10 to 77 dpi ($y = 1068x + 235.7$) with Pearson's correlation R^2 (p value from Student's t test). **B**, Ratio of primary axonal and total dendritic length of individual adult-born granule cells at different developmental stages (same set of neurons as in A). Open orange circles represent data from individual GFP^+ neurons examined. Values representing mean ± SD are also shown (●; *p < 0.01; #p = 0.98; one-way ANOVA, $F_{(5,70)} = 12.47$, $p = 1.16 \times 10^{-8}$). **C**, Mean neurite length (primary axon or total dendrite length) of adult-born granule cells at different times after labeling. The same data from Figs. 15B and 17B were replotted in the same graph for direct comparison of growth rates. Values represent mean ± SEM, a_1, First phase axon growth rate linear fit (10–21 dpi): $y = 96.8x - 458$ ($p = 3.5 \times 10^{-15}$; 95% confidence interval: 84.1 to 113.5 and −728 to −228 for slope and y-intercept, respectively). a_2, Second phase axon growth rate linear fit: $y = 4.1x + 1591$ ($p = 0.01$; 95% confidence interval: 0.99 to 7.29 and 1428 to 1753 for slope and y-intercept, respectively). d_1, First phase dendrite growth rate linear fit (10–21 dpi): $y = 111x - 896$, ($p = 1.6 \times 10^{-14}$; 95% confidence interval: 92.4 to 126.8 and −1177 to −592 for slope and y-intercept, respectively). d_2, Second phase dendrite growth rate linear fit: $y = 3.2x + 1262$ (p = 0.03; 95% confidence interval: 0.32 to 5.98 and 1120 to 1412 for slope and y-intercept, respectively).

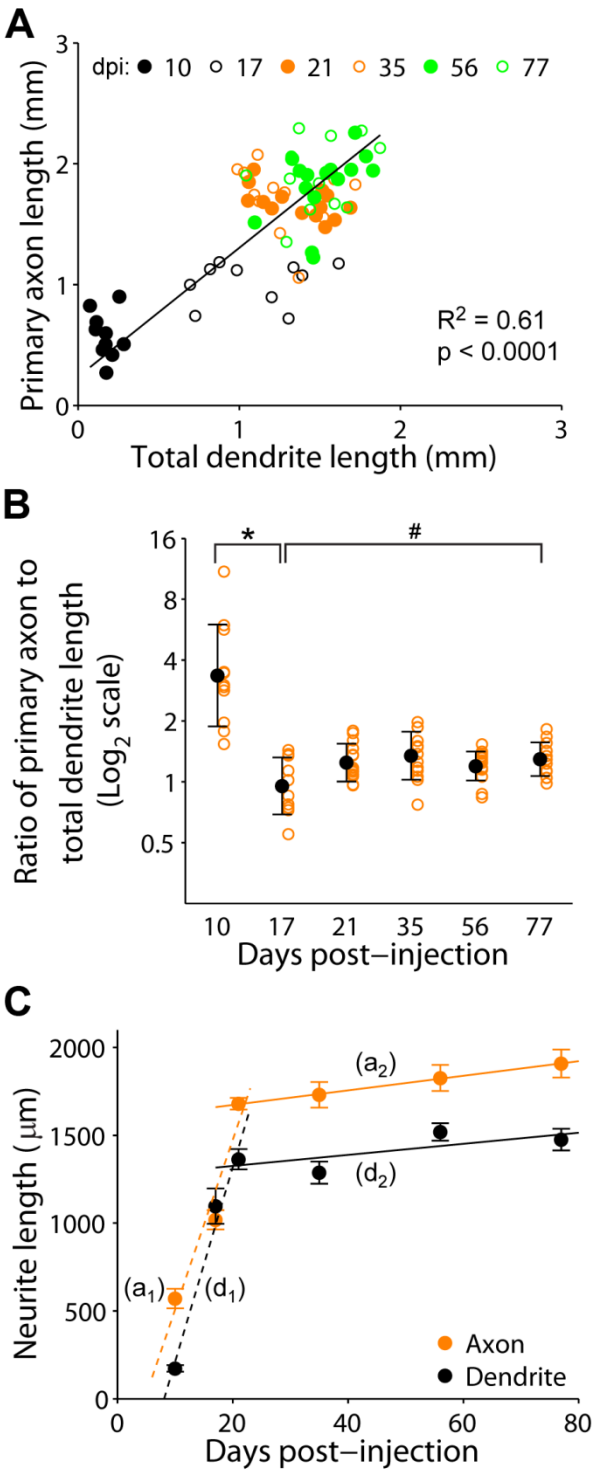
A
dpi: 10 17 21 35 56 77
Primary axon length (mm)
Total dendrite length (mm)
R2 = 0.61
p < 0.0001
B
Ratio of primary axon to total dendrite length (Log2 scale)
*
#
Days post−injection
C
Neurite length (μm)
(a2)
(d2)
(a1)
(d1)
Axon
Dendrite
Days post−injection

5.4 Discussion

I have for the first time reconstructed the complete axonal primary projection and total dendritic structure of intact adult-born hippocampal dentate granule cells, and have identified their morphological characteristics and developmental milestones (Fig. 19). My detailed morphological studies revealed that axons follow a stereotyped trajectory to their targets and exhibit a unique laminar architecture (Fig. 19A, 1–4), suggesting the existence of highly complex mechanisms of axon targeting within the adult brain. My quantitative analysis at the individual cell level also revealed coordinated axonal and dendritic development of adult-born neurons during distinct developmental phases (Fig. 19B, C). My findings are particularly relevant for understanding the potential of this newborn population to influence downstream information processing in the CA3 region, an important parameter given many studies suggesting that newborn neurons make unique contributions to hippocampal function during a critical period of development[50,52,53,119,120]. My findings also establish the basis for future studies of underlying molecular mechanisms and aberrant granule cell morphology in pathological conditions.

Figure 19. Summary of newborn granule cell axonal and dendritic morphological characteristics and development milestones during young adult mouse hippocampal neurogenesis.

A, Overview of adult dentate gyrus and CA3 regions (subregions CAa–c colored in purple, green, and orange, respectively) of the hippocampus with representative axon primary projection patterns overlaid. Boxed regions highlight important axon trajectory features and patterns: (1) characteristic 0–180° hilar axon turn, as viewed in the transverse plane; (2) characteristic 90° ventral to dorsal CA3 turn, as viewed in the transverse plane; (3) characteristic 90° septal to temporal CA3 turn, as viewed in the horizontal (longitudinal) plane; (4) characteristic dorsal stacking of axons originating from more septal dentate gyrus and staggering of axon termination points, as viewed in a sagittal plane with respect to the hippocampal axis. **B**, Schematic depiction of axon and dendrite development of adult-born granule neurons. Representative granule cells are color-coded according to their phase of structural development. Development is divided into two phases. Phase 1 is further subdivided on the basis of key morphological changes: 1a corresponds to rapid axon, but limited dendrite growth; 1b corresponds to rapid dendrite growth and axon targeting through all CA3 subregions; and 1c corresponds to complete axo-dendritic targeting. Phase 2 is characterized by minimal growth of existing axonal and dendritic structures. **C**, Time course of axonal and dendritic development of adult-born granule neurons. Most growth and changes occur during phase 1 when axon and dendrite growth is maximal; axon to dendrite length ratio starts high and then rapidly decreases and stabilizes; and dendrite branching and axon bouton density rapidly

increase. Very modest growth of axon primary projections and dendrites occurs during phase 2.

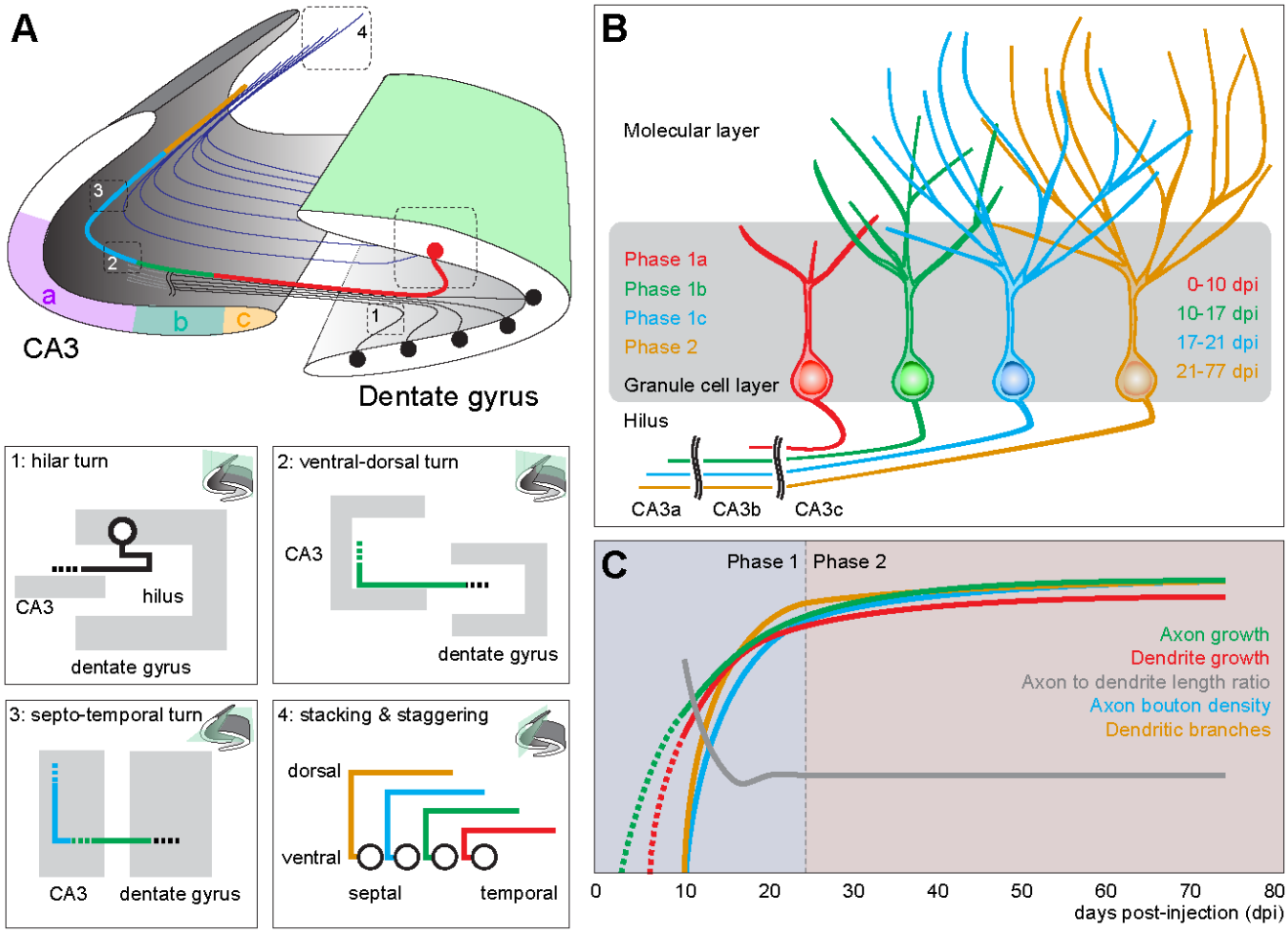
A
4
3
2
a
b
c
1
CA3
Dentate gyrus
1: hilar turn
CA3
hilus
dentate gyrus
2: ventral-dorsal turn
CA3
dentate gyrus
3: septo-temporal turn
CA3
dentate gyrus
4: stacking & staggering
dorsal
ventral
septal
temporal
B
Molecular layer
Phase 1a
Phase 1b
Phase 1c
Phase 2
Granule cell layer
Hilus
CA3a
CA3b
CA3c
0-10 dpi
10-17 dpi
17-21 dpi
21-77 dpi
C
Phase 1
Phase 2
Axon growth
Dendrite growth
Axon to dendrite length ratio
Axon bouton density
Dendritic branches
0
10
20
30
40
50
60
70
80
days post-injection (dpi)

5.4.1 Morphology and patterns of adult-born granule cell axons

Individual adult-born neurons achieve stereotyped and highly complex axonal projections in the adult hippocampus via three distinct choice points (Fig. 19A, 1–3). First, axons turn various degrees in the dentate gyrus hilus depending on their parent soma location and converge in the stratum lucidum to join the mossy fiber pathway into CA3c (Fig. 19A, 1). The finding that axons of newborn neurons at the lateral-most granule cell layer can initiate outgrowth in a direction opposite to their ultimate trajectory suggests precisely positioned, finely tuned guidance cues in the hilus and CA3c region to fasciculate these axons. Second, axons project from ventral to dorsal in the transverse plane of CA3b (Fig. 19A, 2). Previous studies of adult-born granule cell axonal development predominantly reported this segment[20,48–50,133], which represents only ~25% of the entire axonal CA3 projection length of mature adult-born granule cells. Last, axons turn to project longitudinally in CA3a toward the temporal hippocampal pole (Fig. 19A, 3). This longitudinal projection accounts for ~50% of primary axon length (~950 μm) and has historically been disputed. Work by Blackstad et al. (1970)[134] proposed that only the transverse CA3 projection exists, whereas Ramón y Cajal (1893)[135], Lorente de Nó (1934)[132], and later McLardy (1963, 1970)[136,137] suggested an additional longitudinal projection. My results support more recent evidence of a longitudinal projection in dentate granule cells[122,138–140].

My study revealed, for the first time, that cohorts of adult-born granule cells born around the same time organized their axons into highly stereotypic lamination patterns along the septo-temporal axis (Fig. 19A, 4). More septal granule cells terminate their longitudinal

projections earlier and more dorsal than those from more temporal regions, resulting in a precise stacking and staggering of axons within CA3a. Such exquisitely regular architecture exists, at least in adult-born neurons, throughout the septo-temporal extent of the hippocampus, in contrast to a previous study that suggested longitudinally projecting granule cell axons primarily existed in the septal, but not temporal hippocampal region[141].

Functionally, since multiple longitudinally projecting granule cell axons are coincident in the same CA3a transverse plane, it is likely that CA3a pyramidal cells receive inputs from multiple dentate granule cells originating from different septo-temporal regions. In contrast, CA3b and CA3c pyramidal cells may receive inputs from multiple dentate granule cells of the same transverse plane. This organizational structure suggests that CA3 has at least two distinct domains, in which neurons may perform different computations based upon mossy fiber input. Furthermore, axon stacking implies that, for a given CA3a pyramidal cell, axons from more septal granule cells are more proximal to CA3a neuron somas, potentially wielding more control than their temporal counterparts during integration of synaptic inputs. In all, my findings illustrate the previously underappreciated complexity of adult-born granule cell connections to CA3. This may inform our understanding of the role newborn neurons play in the hippocampal circuit and further suggest a new framework to explore the anatomical and functional relationship between the dentate gyrus and CA3.

5.4.2 Distinct phases of axonal and dendritic development by adult-born granule cells

I identified two phases of axonal and dendritic development within which key developmental milestones occur. Phase 1 is characterized by rapid neurite outgrowth (0–21 dpi), which decelerates drastically in phase 2. As dendritic growth has been characterized previously[20], my current study focused on axon developmental milestones.

Phase 1a, corresponding to 0–10 dpi, is marked by rapid axon penetration through CA3c into CA3b (Fig. 19B). Mossy fiber boutons are mostly absent at this stage. My result is consistent with the finding that newborn neurons are unable to elicit CA3 pyramidal cell responses at this stage[50], despite the presence of functional synaptic inputs[41,42]. In phase 1b (10–17 dpi), axons penetrate CA3a and start to form mossy fiber boutons, which is consistent with previous electron microscopic results[48] and recent electrophysiological findings[50]. Interestingly, phase 1b axons project minimally along the longitudinal axis of CA3a. Pyramidal cells from the same transverse plane are thus the predominant recipients of initial synaptic input, which limits the impact of adult-born granule cells on existing circuitry at this stage. In phase 1c (17–21 dpi), axon outgrowth continues and axons possess all morphological hallmarks of mossy fibers (Fig. 19A, 1–3) and reach maximum bouton density by 21 dpi.

Phase 2 (21–77 dpi) represents a very modest, but continued growth phase for both primary axons and whole dendrites of adult-born neurons. My results underestimate the total amount of axonal growth due to my exclusion of axon collaterals. It is possible that

axon collaterals exhibit different growth properties than the primary axon. Given the numerous collaterals and synaptic contacts of granule cells in the hilar region[130], future studies of newborn granule cell axon collateral development and growth dynamics using a sparse labeling approach would be fruitful and may reveal additional intricacies of axon targeting, maturation, and synaptic development.

5.4.3 Coordination of axonal and dendritic development during adult neurogenesis

My reconstruction of neuronal processes of intact individual neurons revealed how axons and dendrites coordinate their development, which has been rarely examined in vivo. Quantitative analysis revealed that axon growth most likely preceded that of dendrites by ~3.3 d (phase 1a; Figs. 18B, C, 19C). At the onset of concurrent, rapid axonal and dendritic outgrowth (phase 1b), the numbers of mossy fiber boutons and dendritic branch points increase ~4-fold. Dendritic spines have been previously shown to appear rapidly during the same period[20]. Both afferent perforant path and efferent CA3 responses can be elicited during phase 1b[42,50]. Axonal and dendritic development coupling may therefore allow for coincident onset of presynaptic and postsynaptic responses that aid functional integration of newborn neurons into the existing hippocampal circuit.

5.4.4 SEBI methodology and considerations

My development and application of the novel SEBI technique for seamless, complete hippocampal volume reconstruction was essential for detailed morphological and developmental characterization of adult-born granule cells. In contrast to a similar technique[142], SEBI uses hardware and software readily available in most lab settings and

thus can be widely applied. More recently, novel tissue-clearing techniques have been developed[143–145], which allow for limitless imaging through tissue. Given working distance limitations of most microscope objectives, SEBI may still be required in conjunction and is fully compatible with tissue clearing. In addition, SEBI yields serial brain sections amenable for further post hoc analyses, including immunohistology and electron microscopy.

5.4.5 Conclusion

Using the SEBI methodology, I have revealed the complete axonal primary projection and total dendritic structure of intact adult-born hippocampal dentate granule cells in vivo. I identified highly stereotyped patterns of axonal development at the individual cell level and among neurons born around the same time. These findings, coupled with new insights into dendritic development, suggest a tightly regulated growth and targeting process during adult neurogenesis. My comprehensive data provide the foundation for future studies to determine how this complicated process is regulated at the molecular level, whether anatomical or morphological disruptions occur in neurological disorders, and whether embryonic versus adult granule cell development may differ. Importantly, my studies have demonstrated that an adult brain region, the hippocampus, can support intricate guidance of long axonal projections. Accurate axonal targeting in the adult brain is a critical challenge for cell transplantation therapy to treat neurological disease and injury and the adult hippocampus could thus serve as a model system to explore the necessary and sufficient factors.

6 — General Discussion

In this thesis, I have conducted a comprehensive study of adult hippocampal neurogenesis from stem cell to nerve cell. My work has significantly advanced our understanding of how, at a cellular level, adult neural stem cells have the capacity for multi-lineage differentiation, inclusive of generating new glutamatergic neurons that successfully target and integrate into the existing mature adult circuit (Fig. 20). I have specifically made the following novel discoveries:

1) A negative regulator of growth factor signaling, neurofibromin 1, can inhibit certain neural stem cell fate choices,
2) Contrary to the classical radial unit hypothesis, principal, glutamatergic, excitatory neurons can exhibit extensive tangential migration in the adult brain under physiological conditions, and
3) Adult-born dentate granule neurons exhibit sophisticated primary axon projections and lamination patterns.

In addition, I have developed, or contributed significantly to the development of new, powerful techniques to study neurogenesis with single-cell and high spatiotemporal resolution, such as:

1) Clonal lineage tracing of adult hippocampal neural stem cells, allowing for the first time the characterization of single stem cell properties,
2) Pseudo whole-mount dentate gyrus preparation, allowing for visualization of stem cell niche-wide architecture, organization, and patterns of neural stem/progenitor cells,

3) Serial end-block imaging technology for seamless large-volume imaging and reconstruction, allowing for characterization of complete, complex cell morphology and structures, and
4) Computational, automation, image processing, and optimized imaging techniques that serve as a backbone for experimental pipelines of the above techniques.

Together, my thesis work provides strong foundations for future work examining plasticity in the adult central nervous system, as well as my personal interest in developing neuro-regenerative therapies. One significant limitation of my thesis work is its descriptive nature; although it provides elegant, comprehensive descriptions of cell genesis, migration, and growth capacity in the mature nervous system, future work will have to examine the precise molecular mechanisms governing the processes described. In addition, the generalizability of my findings to other brain regions, especially for neuroregeneration applications, must be validated; and whether there exists unique molecular or structural features of the adult hippocampal microenvironment that somehow provide permissiveness to neurogenesis, migration, and long-distance axon growth remains unclear and should be studied. Further, the entire field would benefit from more studies employing comparative neuroanatomical approaches that integrate insights and principles from organisms with very limited neuroregenerative capacity, such as us humans, to those with robust capability for neuro-regeneration. Finally, although embryonic and adult neurogenesis share many features, they differ greatly with respect to the convolution of tempo, stem cell fate capacity and choice, and complexity or size of space in which neurogenesis occurs. Adult neurogenesis may therefore possess its

own distinct mechanisms for cell genesis, governed by principles similar to that of the developing embryo, but wholly evolutionarily optimized for the unique challenges of a mature brain environment.

Amongst all regenerating somatic tissues, the nervous system perhaps represents the most significantly difficult to repair. Notwithstanding the highly growth-inhibitory central nervous system environment, this difficulty is due in large part because in the brain specifically, the complex structure and connections between cells are critical for and define tissue function (Fig. 21). Mere transplantation or grafting of nervous tissue is insufficient for repair, unlike that for skin, blood, or other somatic tissues. Instead, repairing the nervous system will require a designed, systematic approach that draws upon fundamental cellular and molecular principles of cell genesis in the adult—and not embryonic—brain. My thesis work here and the proposed future directions combined with the advent of synthetic biology[146], large-scale initiatives to characterize all cell types[147], synapses[148], and connectivity[149], and additive manufacturing of biological tissue[150], together form a tractable means of addressing the urgent, unmet therapeutic need for brain regeneration and repair.

Figure 20. Neural development in the adult mouse hippocampus from stem cell to nerve cell.

Neural stem cells of the adult mouse hippocampus, RGLs, generate new glutamatergic granule neurons and astrocytes, as well as new OPCs, but in an NF1-regulated manner. 3-7 day-old neuroblast precursors of new granule cells tangentially migrate along subgranular zone niche vasculature to reach their final destination in dentate gyrus. Upon penetrating the granule cell layer, new granule cells begin growing their axons followed by growth of their dendrites. Over the next weeks, new granule cells complete growth of their complex axon into CA3, and over the next months, have continued, albeit small amounts of axo-dendritic growth.

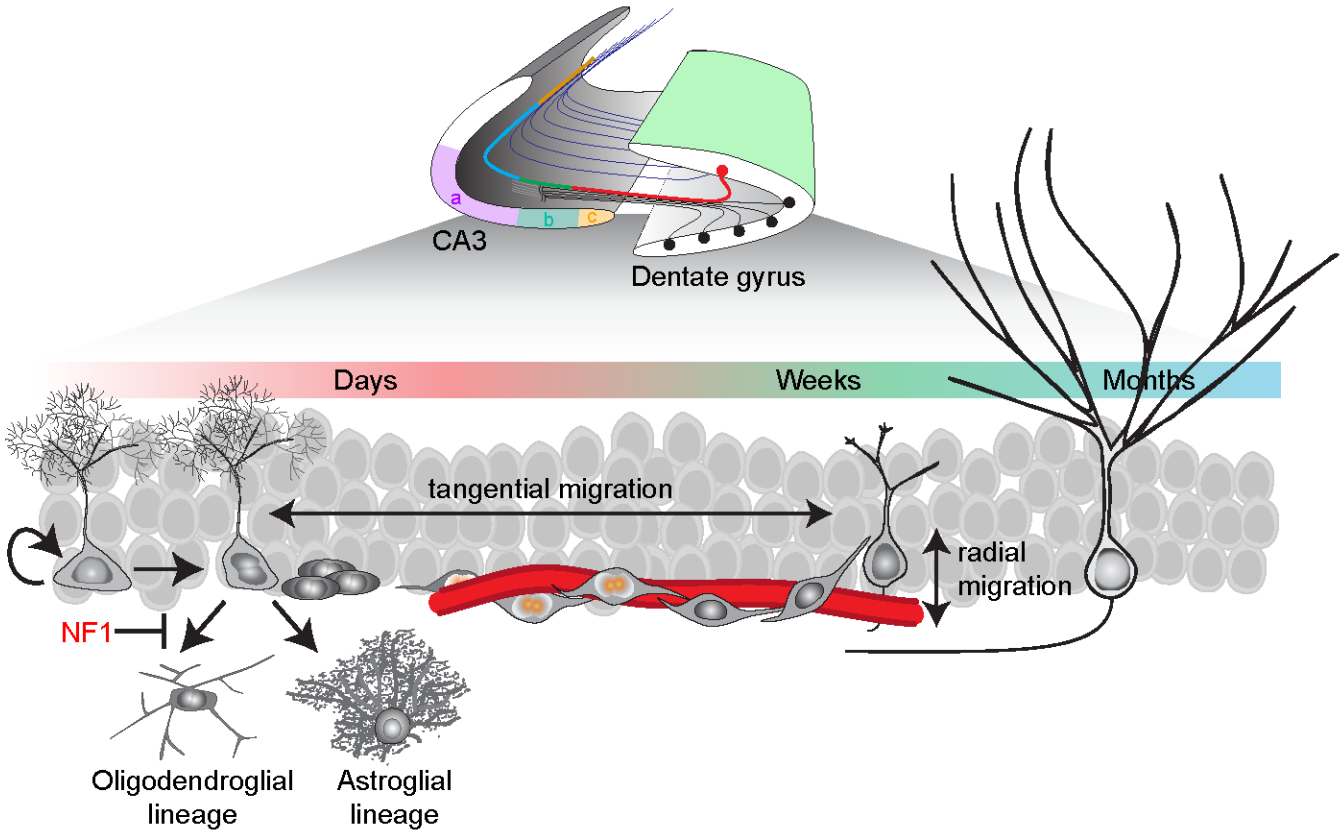
a
b
c
CA3
Dentate gyrus
Days
Weeks
Months
tangential migration
radial
migration
NF1
Oligodendroglial
lineage
Astroglial
lineage

Figure 21. SEBI-reconstructed anterior hippocampus from Thy-1-GFP-M mouse, highlighting the still unknown complexities of neural circuits and their development.

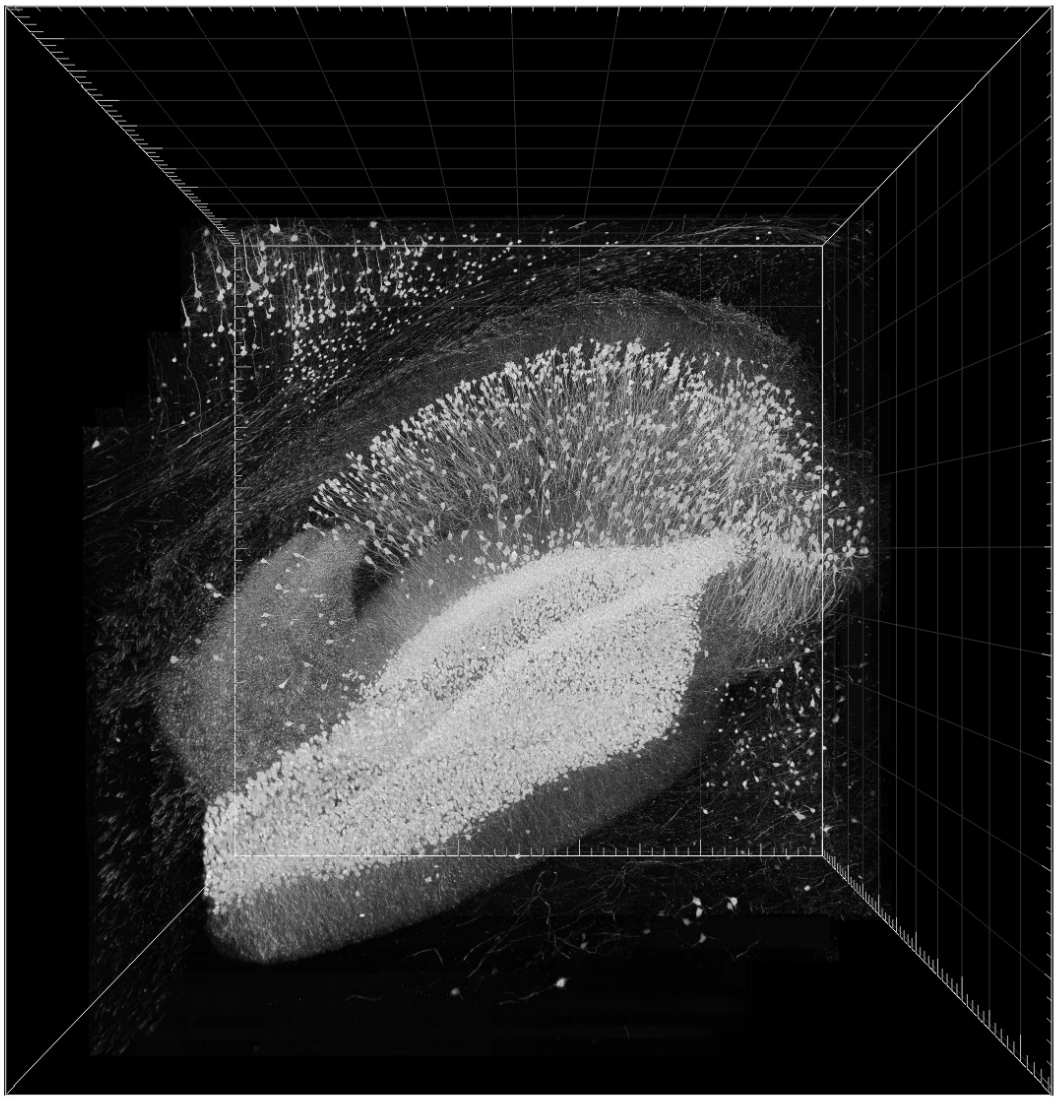

References

1. Fuchs, E. & Segre, J. a. Stem cells: a new lease on life. *Cell* **100,** 143–55 (2000).

2. Nystul, T. G. & Spradling, A. C. Breaking out of the mold : diversity within adult stem cells and their niches. *Curr. Opin. Genet. Dev.* 463–468 (2006). doi:10.1016/j.gde.2006.08.003

3. Morrison, S. J. & Spradling, A. C. Stem cells and niches: mechanisms that promote stem cell maintenance throughout life. *Cell* **132,** 598–611 (2008).

4. Barker, N., Bartfeld, S. & Clevers, H. Tissue-resident adult stem cell populations of rapidly self-renewing organs. *Cell Stem Cell* **7,** 656–70 (2010).

5. Fuller, M. T. & Spradling, A. C. Male and female Drosophila germline stem cells: two versions of immortality. *Science* **316,** 402–4 (2007).

6. Spangrude, G., Heimfeld, S. & Weissman, I. Purification and characterization of mouse hematopoietic stem cells. *Science (80-.).* **241,** 58–62 (1988).

7. Rakic, P. Limits of neurogenesis in primates. *Science (80-.).* **4690,** 16–19 (1985).

8. Ramón y Cajal, S. & May, R. *Degeneration and regeneration of the nervous system*. 750 (Hafner, 1913).

9. Altman, J. & Das, G. D. Autoradiographic and histological evidence of postnatal hippocampal neurogenesis in rats. *J. Comp. Neurol.* **124,** 319–335 (1965).

10. Eriksson, P. S. *et al.* Neurogenesis in the adult human hippocampus. *Nat. Med.* **4,** 1313–7 (1998).

11. Spalding, K. L. *et al.* Dynamics of hippocampal neurogenesis in adult humans. *Cell* **153,** 1219–27 (2013).

12. Ming, G.-L. & Song, H. Adult neurogenesis in the mammalian brain: significant answers and significant questions. *Neuron* **70,** 687–702 (2011).

13. Bergmann, O. & Frisén, J. Neuroscience. Why adults need new brain cells. *Science* **340,** 695–6 (2013).

14. Doetsch, F., Caillé, I., Lim, D. a, García-Verdugo, J. M. & Alvarez-Buylla, a. Subventricular zone astrocytes are neural stem cells in the adult mammalian brain. *Cell* **97,** 703–16 (1999).

15. Alvarez-buylla, A. & Garcı, J. M. Neurogenesis in Adult Subventricular Zone. **22,** 629–634 (2002).

16. Menn, B. *et al.* Origin of oligodendrocytes in the subventricular zone of the adult brain. *J. Neurosci.* **26,** 7907–18 (2006).

17. Lois, C. & Alvarez-Buylla, a. Long-distance neuronal migration in the adult mammalian brain. *Science* **264,** 1145–8 (1994).

18. Lledo, P.-M., Alonso, M. & Grubb, M. S. Adult neurogenesis and functional plasticity in neuronal circuits. *Nat. Rev. Neurosci.* **7,** 179–93 (2006).

19. Bonaguidi, M. a *et al.* In Vivo Clonal Analysis Reveals Self-Renewing and Multipotent Adult Neural Stem Cell Characteristics. *Cell* **145,** 1142–1155 (2011).

20. Zhao, C., Teng, E. M., Summers, R. G., Ming, G. & Gage, F. H. Distinct Morphological Stages of Dentate Granule Neuron Maturation in the Adult Mouse Hippocampus. *J. Neurosci.* **26,** 3–11 (2006).

21. Jessberger, S., Toni, N. & Jr, G. C. Directed differentiation of hippocampal stem/progenitor cells in the adult brain. *Nat. ...* **11,** 888–893 (2008).

22. Duan, X., Kang, E., Liu, C. Y., Ming, G.-L. & Song, H. Development of neural stem cell in the adult brain. *Curr. Opin. Neurobiol.* **18,** 108–15 (2008).

23. Kriegstein, A. & Alvarez-Buylla, A. The glial nature of embryonic and adult neural stem cells. *Annu. Rev. Neurosci.* **32,** 149–184 (2009).

24. Babu, H., Cheung, G., Kettenmann, H., Palmer, T. D. & Kempermann, G. Enriched monolayer precursor cell cultures from micro-dissected adult mouse dentate gyrus yield functional granule cell-like neurons. *PLoS One* **2,** e388 (2007).

25. Palmer, T. D., Markakis, E. a, Willhoite, a R., Safar, F. & Gage, F. H. Fibroblast growth factor-2 activates a latent neurogenic program in neural stem cells from diverse regions of the adult CNS. *J. Neurosci.* **19,** 8487–97 (1999).

26. Kondo, T. Oligodendrocyte Precursor Cells Reprogrammed to Become Multipotential CNS Stem Cells. *Science (80-.).* **289,** 1754–1757 (2000).

27. Gabay, L., Lowell, S., Rubin, L. L. & Anderson, D. J. Deregulation of dorsoventral patterning by FGF confers trilineage differentiation capacity on CNS stem cells in vitro. *Neuron* **40,** 485–99 (2003).

28. Seri, B., Garcia-Verdugo, J. M., McEwen, B. S. & Alvarez-Buylla, A. Astrocytes Give Rise to New Neurons in the Adult Mammalian Hippocampus. *J. Neurosci.* **21,** 7153–7160 (2001).

29. Seri, B., García-Verdugo, J. M., Collado-Morente, L., McEwen, B. S. & Alvarez-Buylla, A. Cell types, lineage, and architecture of the germinal zone in the adult dentate gyrus. *J. Comp. Neurol.* **478,** 359–78 (2004).

30. Ahn, S. & Joyner, A. In vivo analysis of quiescent adult neural stem cells responding to Sonic hedgehog. *Nature* **437,** 1–4 (2005).

31. Lagace, D. C. *et al.* Dynamic contribution of nestin-expressing stem cells to adult neurogenesis. *J. Neurosci.* **27,** 12623–9 (2007).

32. Suh, H. *et al.* In Vivo Fate Analysis Reveals the Multipotent and {Self-Renewal} Capacities of Sox2+ Neural Stem Cells in the Adult Hippocampus. *Cell Stem Cell* **1,** 515–528 (2007).

33. Encinas, J. M. *et al.* Division-coupled astrocytic differentiation and age-related depletion of neural stem cells in the adult hippocampus. *Cell Stem Cell* **8,** 566–579 (2011).

34. Bonaguidi, M. a, Song, J., Ming, G. & Song, H. A unifying hypothesis on mammalian neural stem cell properties in the adult hippocampus. *Curr. Opin. Neurobiol.* **22,** 754–61 (2012).

35. Song, J. *et al.* Neuronal circuitry mechanism regulating adult quiescent neural stem-cell fate decision. *Nature* **489,** 150–4 (2012).

36. Doetsch, F., Petreanu, L., Caille, I., Garcia-Verdugo, J. M. & Alvarez-Buylla, A. EGF converts transit-amplifying neurogenic precursors in the adult brain into multipotent stem cells. *Neuron* **36,** 1021–34 (2002).

37. Jablonska, B. *et al.* Chordin-induced lineage plasticity of adult {SVZ} neuroblasts after demyelination. *Nat. Neurosci.* **13,** 541–550 (2010).

38. Ma, D. K., Bonaguidi, M. A., Ming, G.-L. & Song, H. Adult neural stem cells in the mammalian central nervous system. *Cell Res.* **19,** 672–682 (2009).

39. Kuhn, H. G., Dickinson-Anson, H. & Gage, F. H. Neurogenesis in the dentate gyrus of the adult rat: age-related decrease of neuronal progenitor proliferation. *J. Neurosci. Off. J. Soc. Neurosci.* **16,** 2027–2033 (1996).

40. Seki, T., Namba, T., Mochizuki, H. & Onodera, M. Clustering, migration, and neurite formation of neural precursor cells in the adult rat hippocampus. *J. Comp. Neurol.* **502,** 275–290 (2007).

41. Espósito, M. S. *et al.* Neuronal differentiation in the adult hippocampus recapitulates embryonic development. *J. Neurosci.* **25,** 10074–86 (2005).

42. Ge, S. *et al.* {GABA} regulates synaptic integration of newly generated neurons in the adult brain. *Nature* **439,** 589–593 (2006).

43. Sierra, A. *et al.* Microglia Shape Adult Hippocampal Neurogenesis through {Apoptosis-Coupled} Phagocytosis. *Cell Stem Cell* **7,** 483–495 (2010).

44. Song, J. *et al.* Parvalbumin interneurons mediate neuronal circuitry-neurogenesis coupling in the adult hippocampus. *Nat. Neurosci.* **16,** 1728–30 (2013).

45. Mathews, E. a *et al.* A distinctive layering pattern of mouse dentate granule cells is generated by developmental and adult neurogenesis. *J. Comp. Neurol.* **518,** 4479–90 (2010).

46. Gong, C., Wang, T.-W., Huang, H. S. & Parent, J. M. Reelin regulates neuronal progenitor migration in intact and epileptic hippocampus. *J. Neurosci.* **27,** 1803–11 (2007).

47. Duan, X. *et al.* {Disrupted-In-Schizophrenia} 1 Regulates Integration of Newly Generated Neurons in the Adult Brain. *Cell* **130,** 1146–1158 (2007).

48. Faulkner, R. L. *et al.* Development of hippocampal mossy fiber synaptic outputs by new neurons in the adult brain. *Proc. Natl. Acad. Sci. U. S. A.* **105,** 14157–62 (2008).

49. Toni, N. *et al.* Neurons born in the adult dentate gyrus form functional synapses with target cells. *Nat. Neurosci.* **11,** 901–7 (2008).

50. Gu, Y. *et al.* Optical controlling reveals time-dependent roles for adult-born dentate granule cells. *Nat. Neurosci.* **15,** (2012).

51. Tashiro, A., Makino, H. & Gage, F. H. Experience-specific functional modification of the dentate gyrus through adult neurogenesis: a critical period during an immature stage. *J. Neurosci.* **27,** 3252–9 (2007).

52. Ge, S., Yang, C., Hsu, K., Ming, G. & Song, H. A Critical Period for Enhanced Synaptic Plasticity in Newly Generated Neurons of the Adult Brain. *Neuron* **54,** 559–566 (2007).

53. Marín-Burgin, A., Mongiat, L. a, Pardi, M. B. & Schinder, A. F. Unique processing during a period of high excitation/inhibition balance in adult-born neurons. *Science* **335,** 1238–42 (2012).

54. Kee, N., Teixeira, C. M., Wang, A. H. & Frankland, P. W. Preferential incorporation of adult-generated granule cells into spatial memory networks in the dentate gyrus. *Nat. Neurosci.* **10,** 355–62 (2007).

55. Emmenlauer, M. *et al.* XuvTools: free, fast and reliable stitching of large 3D datasets. *J. Microsc.* **233,** 42–60 (2009).

56. Waddington, C. H. *The Strategy of the Genes; a Discussion of Some Aspects of Theoretical biology*. (Allen & Unwin, 1957).

57. Gage, F. H. Mammalian Neural Stem Cells. *Science (80-.).* **287,** 1433–1438 (2000).

58. Takahashi, K. & Yamanaka, S. Induction of pluripotent stem cells from mouse embryonic and adult fibroblast cultures by defined factors. *Cell* **126,** 663–76 (2006).

59. Blanpain, C. & Fuchs, E. Plasticity of epithelial stem cells in tissue regeneration. *Science (80-.).* **344,** 1242281–1242281 (2014).

60. Holmberg, J. & Perlmann, T. Maintaining differentiated cellular identity. *Nat. Rev. Genet.* **13,** 429–39 (2012).

61. Perrimon, N., Pitsouli, C. & Shilo, B.-Z. Signaling mechanisms controlling cell fate and embryonic patterning. *Cold Spring Harb. Perspect. Biol.* **4,** a005975 (2012).

62. Friedman, J. M., Gutmann, D. H., MacCollin, M. & Riccardi, V. M. *Neurofibromatosis: Phenotype, Natural History, and Pathogenesis*. 15 (Johns Hopkins University Press, 1999).

63. Balordi, F. & Fishell, G. Mosaic Removal of Hedgehog Signaling in the Adult {SVZ} Reveals That the Residual {Wild-Type} Stem Cells Have a Limited Capacity for {Self-Renewal}. *J. Neurosci.* **27,** 14248–14259 (2007).

64. Zhu, Y. *et al.* Ablation of {NF1} function in neurons induces abnormal development of cerebral cortex and reactive gliosis in the brain. *Genes Dev.* **15,** 859–876 (2001).

65. Novak, A., Guo, C., Yang, W., Nagy, A. & Lobe, C. G. {Z/EG}, a double reporter mouse line that expresses enhanced green fluorescent protein upon Cre-mediated excision. *Genes. {(New} York, {N.Y.} 2000)* **28,** 147–155 (2000).

66. Li, Y., McKay, R. M., Riethmacher, D. & Parada, L. F. Neurofibromin Modulates Adult Hippocampal Neurogenesis and Behavioral Effects of Antidepressants. *J. Neurosci.* **32,** 3529–3539 (2012).

67. Liu, C. *et al.* Mosaic Analysis with Double Markers Reveals Tumor Cell of Origin in Glioma. *Cell* **146,** 209–221 (2011).

68. Chetty, S. *et al.* Stress and glucocorticoids promote oligodendrogenesis in the adult hippocampus. *Mol. Psychiatry* 1–9 (2014). doi:10.1038/mp.2013.190

69. Trotter, J., Karram, K. & Nishiyama, A. NG2 cells: Properties, progeny and origin. *Brain Res. Rev.* **63,** 72–82 (2010).

70. Dasgupta, B. & Gutmann, D. H. Neurofibromin Regulates Neural Stem Cell Proliferation , Survival , and Astroglial Differentiation In Vitro and In Vivo. *In Vivo (Brooklyn).* **25,** 5584 –5594 (2005).

71. Joseph, N. M. *et al.* Article The Loss of Nf1 Transiently Promotes Self-Renewal but Not Tumorigenesis by Neural Crest Stem Cells. *Cancer Cell* 129–140 (2008). doi:10.1016/j.ccr.2008.01.003

72. Zhu, Y. *et al.* Inactivation of {NF1} in {CNS} causes increased glial progenitor proliferation and optic glioma formation. *Development* **132,** 5577–5588 (2005).

73. Hegedus, B. *et al.* Neurofibromatosis-1 Regulates Neuronal and Glial Cell Differentiation from Neuroglial Progenitors In Vivo by Both {cAMP-} and {Ras-Dependent} Mechanisms. *Cell Stem Cell* **1,** 443–457 (2007).

74. Lee, D. Y., Yeh, T.-H., Emnett, R. J., White, C. R. & Gutmann, D. H. Neurofibromatosis-1 regulates neuroglial progenitor proliferation and glial differentiation in a brain region-specific manner. *Genes Dev.* (2010). doi:10.1101/gad.1957110

75. Zheng, H. *et al.* Induction of abnormal proliferation by nonmyelinating schwann cells triggers neurofibroma formation. *Cancer Cell* **13,** 117–128 (2008).

76. Daston, M. M. & Ratner, N. Neurofibromin, a predominantly neuronal GTPase activating protein in the adult, is ubiquitously expressed during development. *Dev. Dyn.* **195,** 216–26 (1992).

77. Daston, M. M. *et al.* The protein product of the neurofibromatosis type 1 gene is expressed at highest abundance in neurons, Schwann cells, and oligodendrocytes. *Neuron* **8,** 415–28 (1992).

78. Gonzalez-Perez, O., Romero-Rodriguez, R., Soriano-Navarro, M., Garcia-Verdugo, J. M. & Alvarez-Buylla, A. Epidermal growth factor induces the progeny of subventricular zone type B cells to migrate and differentiate into oligodendrocytes. *Stem Cells* **27,** 2032–43 (2009).

79. Ortega, F. *et al.* Oligodendrogliogenic and neurogenic adult subependymal zone neural stem cells constitute distinct lineages and exhibit differential responsiveness to Wnt signalling. *Nat. Cell Biol.* **15,** 1–14 (2013).

80. Wang, Y. *et al.* ERK Inhibition Rescues Defects in Fate Specification of Nf1-Deficient Neural Progenitors and Brain Abnormalities. *Cell* **150,** 816–830 (2012).

81. Rafalski, V. A. *et al.* Expansion of oligodendrocyte progenitor cells following SIRT1 inactivation in the adult brain. *Nat. Cell Biol.* **15,** 1–13 (2013).

82. Rakic, P. Evolution of the neocortex: a perspective from developmental biology. *Nat. Rev. Neurosci.* **10,** 724–35 (2009).

83. Corbin, J. G., Nery, S. & Fishell, G. Telencephalic cells take a tangent: non-radial migration in the mammalian forebrain. *Nat. Neurosci.* **4 Suppl,** 1177–82 (2001).

84. Walsh, C. & Cepko, C. L. Clonally related cortical cells show several migration patterns. *Science* **241,** 1342–5 (1988).

85. Walsh, C. & Cepko, C. Widespread dispersion of neuronal clones across functional regions of the cerebral cortex. *Science (80-.).* **5043,** (1992).

86. Walsh, C. & Cepko, C. Clonal dispersion in proliferative layers of developing cerebral cortex. *Nature* **362,** 623–635 (1993).

87. O'Rourke, N. a, Sullivan, D. P., Kaznowski, C. E., Jacobs, a a & McConnell, S. K. Tangential migration of neurons in the developing cerebral cortex. *Development* **121,** 2165–76 (1995).

88. Bielle, F. *et al.* Multiple origins of Cajal-Retzius cells at the borders of the developing pallium. *Nat. Neurosci.* **8,** 1002–12 (2005).

89. Britanova, O. *et al.* A novel mode of tangential migration of cortical projection neurons. *Dev. Biol.* **298,** 299–311 (2006).

90. Teissier, A. *et al.* A novel transient glutamatergic population migrating from the pallial-subpallial boundary contributes to neocortical development. *J. Neurosci.* **30,** 10563–74 (2010).

91. Fuentealba, L. C., Obernier, K. & Alvarez-Buylla, A. Adult neural stem cells bridge their niche. *Cell Stem Cell* **10,** 698–708 (2012).

92. Zhao, C., Deng, W. & Gage, F. H. Mechanisms and functional implications of adult neurogenesis. *Cell* **132,** 645–660 (2008).

93. Mirzadeh, Z., Merkle, F. T., Soriano-Navarro, M., Garcia-Verdugo, J. M. & Alvarez-Buylla, A. Neural stem cells confer unique pinwheel architecture to the ventricular surface in neurogenic regions of the adult brain. *Cell Stem Cell* **3,** 265–278 (2008).

94. Shen, Q. *et al.* Adult SVZ Stem Cells Lie in a Vascular Niche: A Quantitative Analysis of Niche Cell-Cell Interactions. *Cell Stem Cell* (2008). doi:10.1016/j.stem.2008.07.026

95. Tavazoie, M. *et al.* A Specialized Vascular Niche for Adult Neural Stem Cells. *Cell Stem Cell* doi:10.1016/j.stem.2008.07.025

96. Palmer, T. D., Willhoite, A. R. & Gage, F. H. Vascular niche for adult hippocampal neurogenesis. *J. Comp. Neurol.* **425,** 479–494 (2000).

97. Kim, E. J., Ables, J. L., Dickel, L. K., Eisch, A. J. & Johnson, J. E. Ascl1 (Mash1) defines cells with long-term neurogenic potential in subgranular and subventricular zones in adult mouse brain. *PLoS One* **6,** e18472 (2011).

98. Encinas, J. M., Vaahtokari, A. & Enikolopov, G. Fluoxetine targets early progenitor cells in the adult brain. *Proc. Natl. Acad. Sci. U. S. A.* **103,** 8233–8 (2006).

99. Ghashghaei, H. T., Lai, C. & Anton, E. S. Neuronal migration in the adult brain: are we there yet? *Nat Rev Neurosci* **8,** 141–151 (2007).

100. Anderson, S. a. Interneuron Migration from Basal Forebrain to Neocortex: Dependence on Dlx Genes. *Science (80-.).* **278,** 474–476 (1997).

101. Marín, O. & Rubenstein, J. L. A long, remarkable journey: tangential migration in the telencephalon. *Nat. Rev. Neurosci.* **2,** 780–90 (2001).

102. Komuro, H., Yacubova, E. & Rakic, P. Mode and tempo of tangential cell migration in the cerebellar external granular layer. *J. Neurosci.* **21,** 527–40 (2001).

103. Leber, S. M. & Sanes, J. R. Migratory paths of neurons and glia in the embryonic chick spinal cord. *J. Neurosci.* **15,** 1236–48 (1995).

104. García-Moreno, F. *et al.* A neuronal migratory pathway crossing from diencephalon to telencephalon populates amygdala nuclei. *Nat. Neurosci.* **13,** 680–9 (2010).

105. Rios, A., Serralbo, O., Salgado, D. & Marcelle, C. Neural crest regulates myogenesis through the transient activation of NOTCH. *Nature* **473,** 532–536 (2011).

106. Teissier, a, Waclaw, R. R., Griveau, a, Campbell, K. & Pierani, a. Tangentially migrating transient glutamatergic neurons control neurogenesis and maintenance of cerebral cortical progenitor pools. *Cereb. Cortex* **22,** 403–16 (2012).

107. Kawaguchi, D., Furutachi, S. & Kawai, H. Dll1 maintains quiescence of adult neural stem cells and segregates asymmetrically during mitosis. *Nat. ...* **4,** 1–12 (2013).

108. Hsu, Y.-C., Li, L. & Fuchs, E. Transit-amplifying cells orchestrate stem cell activity and tissue regeneration. *Cell* **157,** 935–49 (2014).

109. Hsu, Y.-C. & Fuchs, E. A family business: stem cell progeny join the niche to regulate homeostasis. *Nat. Rev. Mol. Cell Biol.* **13,** 103–14 (2012).

110. Snapyan, M. *et al.* Vasculature guides migrating neuronal precursors in the adult mammalian forebrain via brain-derived neurotrophic factor signaling. *J. Neurosci.* **29,** 4172–88 (2009).

111. Whitman, M. C., Fan, W., Rela, L., Rodriguez-Gil, D. J. & Greer, C. A. Blood vessels form a migratory scaffold in the rostral migratory stream. *J. Comp. Neurol.* **516,** 94–104 (2009).

112. Grade, S. *et al.* Brain-derived neurotrophic factor promotes vasculature-associated migration of neuronal precursors toward the ischemic striatum. *PLoS One* **8,** e55039 (2013).

113. Saghatelyan, A. Role of blood vessels in the neuronal migration. *Semin. Cell Dev. Biol.* **20,** 744–50 (2009).

114. Tam, S. J. & Watts, R. J. Connecting vascular and nervous system development: angiogenesis and the blood-brain barrier. *Annu. Rev. Neurosci.* **33,** 379–408 (2010).

115. Schmidt-Hieber, C., Jonas, P. & Bischofberger, J. Enhanced synaptic plasticity in newly generated granule cells of the adult hippocampus. *Nature* **429,** 184–7 (2004).

116. Parent, J. M. *et al.* Dentate granule cell neurogenesis is increased by seizures and contributes to aberrant network reorganization in the adult rat hippocampus. *J. Neurosci.* **17,** 3727–38 (1997).

117. Jessberger, S. *et al.* Seizure-associated, aberrant neurogenesis in adult rats characterized with retrovirus-mediated cell labeling. *J. Neurosci.* **27,** 9400–7 (2007).

118. Ladewig, J., Koch, P. & Brüstle, O. Auto-attraction of neural precursors and their neuronal progeny impairs neuronal migration. *Nat. Neurosci.* **17,** 24–6 (2014).

119. Sahay, A. *et al.* Increasing adult hippocampal neurogenesis is sufficient to improve pattern separation. *Nature* **472,** 466–70 (2011).

120. Aimone, J. B., Deng, W. & Gage, F. H. Resolving new memories: a critical look at the dentate gyrus, adult neurogenesis, and pattern separation. *Neuron* **70,** 589–96 (2011).

121. Tessier-Lavigne, M. & Goodman, C. The molecular biology of axon guidance. *Science (80-.).* **274,** 1123–1133 (1996).

122. Hastings, N. B. & Gould, E. Rapid extension of axons into the CA3 region by adult-generated granule cells. *J. Comp. Neurol.* **413,** 146–54 (1999).

123. Markakis, E. a & Gage, F. H. Adult-generated neurons in the dentate gyrus send axonal projections to field CA3 and are surrounded by synaptic vesicles. *J. Comp. Neurol.* **406,** 449–60 (1999).

124. Luzzati, F., Fasolo, A. & Peretto, P. Combining confocal laser scanning microscopy with serial section reconstruction in the study of adult neurogenesis. *Front. Neurosci.* **5,** 70 (2011).

125. Kron, M. M., Zhang, H. & Parent, J. M. The developmental stage of dentate granule cells dictates their contribution to seizure-induced plasticity. *J. Neurosci.* **30,** 2051–9 (2010).

126. Zhou, M. *et al.* mTOR Inhibition ameliorates cognitive and affective deficits caused by Disc1 knockdown in adult-born dentate granule neurons. *Neuron* **77,** 647–54 (2013).

127. Kim, J. Y. *et al.* Interplay between DISC1 and GABA signaling regulates neurogenesis in mice and risk for schizophrenia. *Cell* **148,** 1051–64 (2012).

128. Bolstad, B. M., Irizarry, R. A., Astrand, M. & Speed, T. P. A comparison of normalization methods for high density oligonucleotide array data based on variance and bias. *Bioinformatics* **19,** 185–193 (2003).

129. Piatti, V. C. *et al.* The timing for neuronal maturation in the adult hippocampus is modulated by local network activity. *J. Neurosci.* **31,** 7715–28 (2011).

130. Claiborne, B. J., Amaral, D. G. & Cowan, W. M. A light and electron microscopic analysis of the mossy fibers of the rat dentate gyrus. *J. Comp. Neurol.* **246,** 435–58 (1986).

131. Henze, D., Urban, N. & Barrionuevo, G. The multifarious hippocampal mossy fiber pathway: a review. *Neuroscience* **98,** 407–427 (2000).

132. Lorente de Nó, R. Studies on the structure of the cerebral cortex. II. Continuation of the study of the Ammonic system. *J Psychol Neurol* **45,** 381–438 (1934).

133. Römer, B. *et al.* Adult hippocampal neurogenesis and plasticity in the infrapyramidal bundle of the mossy fiber projection: I. Co-regulation by activity. *Front. Neurosci.* **5,** 107 (2011).

134. Blackstad, T. W., Brink, K., Hem, J. & Jeune, B. Distribution of hippocampal mossy fibers in the rat. An experimental study with silver impregnation methods. *J. Comp. Neurol.* **138,** 433–49 (1970).

135. Ramón y Cajal, S. Estructura del asta de Ammon fascia dentata. *Am Soc Esp Hist Nat* **22,** 53–114 (1893).

136. McLardy, T. Some cells and fiber peculiarities of uncal hippocampus. *Progr Brain Res* **3,** 71–88 (1963).

137. McLardy, T. & Kilmer, W. L. Hippocampal Circuitry. *Am. Psychol.* **25,** 563–566 (1970).

138. Swanson, L., Wyss, J. M. & Cowan, W. M. An autoradiographic study of the organization of intrahippocampal association pathways in the rat. *J. Comp. Neurol.* **181,** 681–715 (1978).

139. Tamamaki, N. & Nojyo, Y. Crossing fiber arrays in the rat hippocampus as demonstrated by three-dimensional reconstruction. *J. Comp. Neurol.* **303,** 435–42 (1991).

140. Acsády, L., Kamondi, a, Sík, a, Freund, T. & Buzsáki, G. GABAergic cells are the major postsynaptic targets of mossy fibers in the rat hippocampus. *J. Neurosci.* **18,** 3386–403 (1998).

141. Swanson, W. & Wyss, J. M. An Autoradiographic Study of the Organization of lntrahippocampal Association Pathways in the Rat. 681–715 (1978).

142. Ragan, T. *et al.* Serial two-photon tomography for automated ex vivo mouse brain imaging. *Nat. Methods* (2012). doi:10.1038/nmeth.1854

143. Hama, H. *et al.* Scale: a chemical approach for fluorescence imaging and reconstruction of transparent mouse brain. *Nat. Neurosci.* (2011). doi:10.1038/nn.2928

144. Chung, K. *et al.* Structural and molecular interrogation of intact biological systems. *Nature* **1,** (2013).

145. Kuwajima, T. *et al.* ClearT: a detergent- and solvent-free clearing method for neuronal and non-neuronal tissue. *Development* **140,** 1364–1368 (2013).

146. Khalil, A. S. & Collins, J. J. Synthetic biology: applications come of age. *Nat. Rev. Genet.* **11,** 367–79 (2010).

147. *BRAIN 2025: A Scientific Vision, Brain Research through Advancing Innovative Neurotechnologies (BRAIN) Working Group Report to the Advisory Committee to the Director, NIH*. (2014). at <http://www.nih.gov/science/brain/2025/>

148. Morgan, J. L. & Lichtman, J. W. Why not connectomics? *Nat. Methods* **10,** 494–500 (2013).

149. Oh, S. W. *et al.* A mesoscale connectome of the mouse brain. *Nature* **508,** 207–14 (2014).

150. Khatiwala, C., Law, R., Shepherd, B., Dorfman, S. & Csete, M. 3D Cell Bioprinting for Regenerative Medicine Research and Therapies. *Gene Ther. Regul.* **07,** 1230004 (2012).

Curriculum Vitae

Gerald Jan-Yu Sun

(443) 676-0772 | 3100 Saint Paul St. #103

gsun8@jhu.edu; gerrysun@gmail.com | Baltimore, MD 21218

Summary and Career Interest

I am a creative, multidisciplinary, and resourceful Neuroscience Ph.D. candidate who has performed innovative research and obtained breakthroughs in understanding basic cellular mechanisms of neural stem cell fate decisions, newborn neuron migration, and axo-dendritic development and architecture in the mature central nervous system. I have strong passion to make significant contributions to understanding the brain. I am interested in hands-on technical R&D work as well as future management opportunities. One of my long-term goals is to create brain repair or related technologies to benefit mankind.

Education

2008-2014	Ph.D. expected	Department of Neuroscience	Johns Hopkins University School of Medicine
2004-2008	B.S.	Biochemistry	University of Southern California

Research Experience

2008- *Ph.D. Candidate, Johns Hopkins University School of Medicine*

present *Laboratory of Dr. Hongjun Song*

- Discovered for the first time sophisticated axon projections and lamination patterns of adult-born hippocampal granule cells that advanced understanding of mature central nervous system ability to support long-distance axon growth (Cover article, J Neurosci, July 2013)
    - Developed serial end-block imaging technology for seamless large-volume imaging and reconstruction, and performed the first large-scale characterization of adult-born dentate granule cell primary axon development for the discovery above
- Discovered first example and new principle of excitatory neuron tangential migration in adult brain under physiological conditions
- Discovered that a negative regulator of growth factor signaling could inhibit certain neural stem cell fate choices, suggesting a novel, non-canonical paradigm of stem cell regulation via active limitation of stem cell plasticity
- Contributed microscopy, image processing, and programming expertise as coauthor of 3 high-profile peer-reviewed publications
- Led and mentored team of 5 undergraduates, 2 graduate rotation students, 1 high school student, resulting in 5 conference abstracts, 1 peer-reviewed publication, and 2 ongoing research projects nearing completion

2011 Cold Spring Harbor Laboratory Course: Computational Cell Biology

2007-2008 *Undergraduate Research Assistant, University of Southern California*

Laboratory of Dr. Norberto Grzywacz, Dr. Eun-Jin Lee

- Discovered putative regeneration of non-canonical photosensitive neurons during retinal degeneration remodeling, which led to 1 conference abstract and first prize for life sciences in undergraduate research symposium
- Contributed tissue-processing and histological expertise as second author of 1 peer-reviewed publication

2006-2008 *Undergraduate Research Assistant, University of Southern California*

Laboratory of Dr. Bosco Tjan

- Discovered computational mechanism of humans' suboptimal peripheral visual processing and mechanism by which such visual processing can be improved with learning as first author of 1 peer-reviewed publication
- Designed and developed web-based experiment to test image enhancement algorithms for improving visual performance in humans with impaired vision, which contributed to successful award of multi-million dollar NEI R01 grant to Dr. Norberto Grzywacz

Fellowships and Scholarships

2012-2014	Children's Tumor Foundation Young Investigator Award
2012	Richard Goodman Scholars Neurosciences Award
2009	William and Mary Drescher Award for Graduate Medical Research
2008	Dr. Milton Okin Award, USC Biological Sciences Department
2007	USC Provost's Undergraduate Research Fellowship
2007-2008	USC Provost's Undergraduate Research Grant (with Dr. Bosco S. Tjan)
2006-2007	USC College Albert Fischer Scholarship
2005-2006	USC College Haltom Scholarship

Honors and Awards

2008	B.S. Biochemistry, *summa cum laude*
2008	Departmental honors: Biochemistry, Biology
2008	USC 10th Annual Undergraduate Symposium for Scholarly and Creative Work
	First prize, Life Sciences
2007	Elected into Phi Beta Kappa
2004-2008	Thematic Option Honors General Education Program

Teaching Experience

2011-present Mentored Research

Mentored undergraduates

- (2/2011-12/2013) Shiori Ito (now at medical school)
- (11/2011-2/2012) Sang Hyuk Yu
- (1/2012-6/2013) Qasim Mahmood (now at graduate school)

- (8/2013-present) Nikhil Modak (class of 2016)
- (1/2013-present) Nicholas Kawasaki (class of 2015)

Mentored graduate rotation students

- (9/2011-12/2011) Genevieve Stein-O'Brien (lab of Carlo Colantuoni)
- (9/2013-12/2013) Jing Hui Yong (rotating)

2012-2013 River Hill High School Gifted and Talented Education Program

Mentor for independent research for high school student, Deep Singh (now at Dartmouth College)

2013 Keystone Symposia on Molecular and Cellular Biology: Neurogenesis

Conference Assistant

2011 Teaching assistant

Course: Stem Cells: Unit of Development and Unit of Regeneration

2009 Teaching assistant

Course: Neuroscience and Cognition I

Peer-reviewed Publications

Gerald J. Sun*, Yi Zhou*, Ryan P. Stadel*, Jonathan Moss, Jing Hui Adeline Yong, Shiori Ito, Nicholas K. Kawasaki, Randall R. Reed, Nicolas Toni, Hongjun Song, and Guo-li Ming. Tangential migration of adult-born hippocampal neuronal precursors of dentate granule cells. *In submission*.

Michael A. Bonaguidi*, Ryan P. Stadel*, Teresa G. Krieger, Daniel A. Berg, **Gerald J. Sun**, Yoon Namgung, Ji Young E. Park, Steven Park, Jung Jin Oh, Randall R. Reed, Guo-li Ming, Benjamin D. Simons, and Hongjun Song. Different states and discrete populations of neural stem cells in the adult hippocampus. *In revision*.

Gerald J. Sun*, Kurt A. Sailor*, Qasim Mahmood, Nikhil Chavali, Kimberly M. Christian, Hongjun Song, and Guo-li Ming. Seamless reconstruction of intact adult-born neurons by serial end-block imaging reveals complex axonal guidance and development in the adult hippocampus. Journal of Neuroscience. 33: 11400-11 (2013). *Cover article.*

Juan Song, Jiaqi Sun, Jonathan Moss, Zhexing Wen, **Gerald J. Sun**, Derek Hsu, Chun Zhong, Heydar Davoudi, Kimberly M Christian, Nicolas Toni, Guo-li Ming, and Hongjun Song. Parvalbumin interneurons mediate neuronal circuitry–neurogenesis coupling in the adult hippocampus. Nature Neuroscience. 16: 1728-1730 (2013).

Juan Song, Chun Zhong, Michael A. Bonaguidi, **Gerald J. Sun**, Derek Hsu, Yan Gu, Konstantinos Meletis, Z. Josh Huang, Shaoyu Ge, Grigori Enikolopov, Karl Deisseroth, Bernhard Luscher, Kimberly Christian, Guo-li Ming, and Hongjun Song. Neuronal circuitry mechanism regulating adult quiescent neural stem cell fate decision. Nature. 498: 150-154 (2012).

Michael A. Bonaguidi, Michael Wheeler, Jason S. Shapiro, Ryan Stadel, **Gerald J. Sun**, Guo-li Ming, and Hongjun Song. In vivo clonal analysis reveals self-renewing and multipotent adult neural stem cell characteristics. Cell. 145: 1142-55 (2011).

Gerald J. Sun, Susana T.L. Chung, and Bosco S. Tjan. Ideal observer analysis of

crowding and the reduction of crowding through learning. Journal of Vision. 10: 1-14 (2010).

Aditi Ray, **Gerald J. Sun**, Leanne Chan, Norberto M. Grzywacz, James Weiland, and Eun-Jin Lee. Morphological alterations in retinal neurons in the S334ter-line3 transgenic rat. Cell and Tissue Research. 339: 481-491 (2010).

Conference Presentations

Gerald J. Sun, Shiori Ito, Michael. A. Bonaguidi, Yi Zhou, Genevieve Stein-O'Brien, Nicholas Kawasaki, Yuan Zhu, Guo-li Ming, and Hongjun Song. De novo generation of oligodendrocyte progenitor cells from adult hippocampal neural progenitors upon conditional inactivation of neurofibromin 1. Children's Tumor Foundation Annual Neurofibromatosis Conference. 2014.

Gerald J. Sun, Shiori Ito, Michael. A. Bonaguidi, Genevieve Stein-O'Brien, Yuan Zhu, Guo-li Ming, and Hongjun Song. Conditional neurofibromin 1 inactivation leads to oligodendrocyte progenitor cell genesis from multi-potent adult neural stem cells in mouse hippocampus. Society for Neuroscience Annual Meeting. 2013.

Gerald J. Sun, Shiori Ito, Michael. A. Bonaguidi, Genevieve Stein-O'Brien, Yuan Zhu, Guo-li Ming, and Hongjun Song. Neurofibromin 1 and regulation of adult neural stem cell characteristics. Children's Tumor Foundation Annual Neurofibromatosis Conference. 2013. *Awarded as best poster*.

Gerald J. Sun, Shiori Ito, Guo-li Ming, and Hongjun Song. Global adult hippocampal neural progenitor organization and structure. Keystone Symposia on Molecular and Cellular Biology: Neurogenesis. 2013.

Gerald J. Sun, Michael A. Bonaguidi, Yuan Zhu, Guo-li Ming, and Hongjun Song. Exploring cell fate specification and self-renewal with clonal *in vivo* inactivation of neurofibromin 1 in adult neural stem cells. Janelia Conference: Control of Neuronal Identity. 2011.

Gerald J. Sun, Michael A. Bonaguidi, Yuan Zhu, Guo-li Ming, and Hongjun Song. *In vivo* analysis of neurofibromin 1 inactivation in adult neural stem cells. Society for Neuroscience Annual Meeting. 2011.

Gerald J. Sun, Biju B. Thomas, Aditi Ray, Eun-Jin Lee, and Norberto M. Grzywacz. Expression of melanopsin-containing ganglion cells in degenerative retina. The Association for Research in Vision and Ophthalmology Annual Meeting. 2008.

Gerald J. Sun, Susana T.L. Chung, and Bosco S. Tjan. Mechanisms of Crowding and Learning to "Uncrowd". Vision Sciences Society Meeting. 2008.

Invited Seminars

Gerald J. Sun. Tangential migration of excitatory neurons in the normal adult mouse brain. 10th Annual Christopher Reeve 'Hot Topics' in Stem Cell Biology Data Blitz. Society for Neuroscience Annual Meeting. 2013.

Hongjun Song, Kurt A. Sailor, **Gerald J. Sun**. Seamless reconstruction of fine circuitry in brain subregions. Center for Neural Informatics, Neural Structures, and Neural Plasticity: Guest Seminar. George Mason University. 2012.